3D Bioprinting of Human Induced Pluripotent Stem Cells Derived Neural Progenitors using Bioinks containing Drug-releasing Microspheres

by
Ruchi Sharma
M.Sc., Chinese Culture University, Taipei, Taiwan, 2013
B.Sc., Delhi University, Delhi, India, 2006

A Dissertation Submitted in Partial Fulfillment
of the Requirements for the Degree of

DOCTOR OF PHILOSPHY

in the Department of Mechanical Engineering

Supervisory Committee

3D Bioprinting of Human Induced Pluripotent Stem Cells Derived Neural Progenitors using Bioinks containing Drug-releasing Microspheres

by

Ruchi Sharma
M.Sc., Chinese Culture University, Taipei, Taiwan, 2013
B.Sc., Delhi University, Delhi, India, 2006

Supervisory Committee

Dr. Stephanie Michelle Willerth and Department of Mechanical Engineering
Supervisor

Dr. Mohsen Akbari and Department of Mechanical Engineering
Departmental Member

Dr. Katherine Elvira and Department of Chemistry
Outside Member

Abstract

Tissue engineering employs biological and engineering principles to create functional substitutes for damaged tissue by combining biomaterial scaffolds with drug delivery devices. 3D (three-dimensional) bioprinting has grown into a potential manufacturing technology for creating such scaffolds. The key problem with this technology is printing scaffolds while preserving cell viability, functioning, and structural integrity. This dissertation explores the features of bioink formed from the combination of natural biomaterials and their influence on the bioprinting process. This work aims to explain the development of bioprinting processes for producing tissue with neural progenitor cells (NPCs) derived from human induced pluripotent stem cells (hiPSCs) and fibrin-based bioink encapsulated with microspheres for neural tissue engineering applications. Moreover, hiPSCs are stem cells made from skin or blood cells that have been reprogrammed into an embryonic-like pluripotent state, which means they can be used to make any kind of human cell that is needed for therapeutic use. To accomplish these goals, this study pursues three objectives: first, to bioprint healthy hiPSC-derived NPCs with guggulsterone microspheres; second, to examine the physical and mechanical properties of bioink with and without guggulsterone microspheres; and finally, to bioprint Parkinson's disease (PD) patient-specific hiPSC-derived NPCs with guggulsterone microspheres for advanced drug-screening. The RX1 bioprinter from Aspect Biosystems, which is based on microfluidics, was used to manufacture domes of 1 cm in diameter using our fibrin-based bioink containing guggulsterone microspheres and hiPSC-derived NPCs. Bioprinted

healthy brain tissues had over 90% cellular viability one day after printing. Tissues displayed early and mature neuronal markers TUJ1 (15.3%), dopamine marker TH (8.1%), and other genes (NURR1, LMX1B, TH, and PAX6) that expressed in midbrain dopaminergic neurons. The storage and loss modulus, viscosity, and shear rates of bioprinted constructs with and without microspheres were also determined. Physical properties such as microstructure, porosity, swelling, and biodegradability were also studied. According to our findings, the elastic modulus of constructs with microspheres was higher than without microspheres. The integration of microspheres resulted in mechanical strength, indicating their potential for use in neural tissue engineering in the future. A bioprinted model of PD was generated utilising hiPSC-derived NPCs from PD patients. NPCs were differentiated into dopaminergic neurons. These models can efficiently identify viable compounds in the early phases of drug development. Finally, I validated that using a microsphere-laden bioink to bioprint hiPSC-derived NPCs can stimulate neural tissue development.

Table of Contents

List of Tables

List of Figures

Chapter 1

Chapter 2

Chapter 3

Chapter 4

List of Abbreviations

HiPSCs	-	Human induced pluripotent stem cells
TE	-	Tissue engineering
CNS	-	Central nervous system
PNS	-	Peripheral nervous system
ECM	-	Extracellular matrix
ESC	-	Embryonic stem cells
PD	-	Parkinson's disease
2D	-	Two dimensional
NSC	-	Neural stem cells
NPC	-	Neural progenitor cells
OPC	-	Oligodendrocyte progenitor
ESCs	-	Embryonic stem cells
AA	-	Ascorbic acid
AD	-	Alzheimer's disease
Dbc AMP	-	dibutyryl cyclic AMP
HPLC	-	High-performance liquid chromatography
L-DOPA	-	Levodopa
TBS	-	Tris buffered saline
3D	-	Three-dimensional
BDNF	-	Brain-derived neurotrophic factor
SG	-	Soluble guggulsterone
UM	-	Unloaded microsphere
SHH	-	Sonic hedgehog
FGF-8	-	Fibroblast growth factor-8
GDNF	-	Glial cell–derived neurotrophic factor
DNs	-	Dopaminergic neurons
QPCR	-	Quantitative polymerase chain reaction
MRI	-	Magnetic resonance imaging
OCT4	-	Octamer binding transcription factor 4
SOX2	-	Sex determining region Y-box2
KLF4	-	Kruppel-like factor 4
C-MYC	-	Myc proto-oncogene protein homolog
NAS	-	Neural aggregates
NIM	-	Neural induction media
SMAD	-	Mothers against decapentaplegic protein
BMPs	-	Bone morphogenic proteins
TGFβ	-	Transforming growth factor beta
LDN	-	LDN193189
SB	-	SB431542
GABA	-	Gamma-Amino butyric acid

Puro	-	Purmorphamine
RA	-	Retinoic acid
PLGA	-	Poly (lactic-co-glycolic acid)
PEG	-	Poly (ethylene glycol)
PCL	-	Polycaprolactone
Ca^{2+}	-	calcium ions
VEGF	-	Vascular endothelial growth factor
GP	-	Glycerol phosphate
βT-III	-	beta-tubulin class III
GAD	-	Glutamic acid decarboxylase
LOP	-	Lab-on-a-printer
PDMS	-	Polydimethylsiloxane
GFAP	-	Glial fibrillary acidic protein
MAP2	-	Microtubule associated protein
CHAT	-	Choline acetyltransferase
DDS	-	Drug delivery systems
C-AMP	-	Cyclic adenosine monophosphate
BP	-	BrainPhys Neuronal Medium
GDNF	-	Glial derived neurotrophic factor
IGF-1	-	Insulin-like growth factor
AA-L	-	Ascorbic acid
BDNF	-	Brain-derived neurotrophic factor
PSA	-	Penicillin-streptomycin- amphotericin B
NBM	-	Neurobasal™ Medium
SMNS	-	Spinal motor neurons
SSEA1	-	Stage specific embryonic antigen-1
OLIG2	-	Oligodendrocyte transcription factor 2
HB9	-	Homeobox protein 9
ISL-1	-	Islet-1
PFA	-	Paraformaldehyde
NPM	-	Neural Progenitor Medium
PE	-	Phycoerythrin
PerCP	-	Peridinin Chlorophyll Protein complex
ICC	-	Immunocytochemistry
PAX6	-	Paired box protein-6
DAPI	-	(4’,6-diamidino-2-phenylindole)
SEM	-	Scanning electron microscope
FBS	-	Fetal bovine serum
EDTA	-	Ethylenediaminetetraacetic acid
EE	-	Encapsulation efficiency
RA	-	Retinoic Acid
GG	-	Guggulsterone
CNS	-	Central nervous system

SNpc	-	Substantia nigra pars compacta
PCL	-	Polycaprolactone
PLGA	-	Poly (lactic-co-glycolic acid)
NGS	-	Normal goat serum
βT-III	-	β□tubulin III
Olig2	-	Oligodendrocyte marker
VSD	-	Voltage sensitive dye
CAD	-	Computer Added Design
PBS	-	Phosphate buffered saline
PTEN	-	Phosphatase and tensin homologue -induced kinase1 (PINK1)

HHH

Acknowledgments

I would like to express deep gratitude to my advisor, Dr. Stephanie Willerth. Professionally, her attention to detail and work ethic motivate me to strive for excellence in all areas. I am tremendously grateful to her, for helping me to grow as a scientist and discover my interest in biomedical engineering. It has been a privilege to be her student and to have such a fantastic role model who has also served as a mentor to me. Thanks for all of the opportunities to enhance my studies and experience, as well as for constant feedback, support, and, most importantly, her trust. I would like to express my gratitude to my committee members, Dr. Mohsen Akbari and Dr. Katherine Elvira, for their insightful feedback and advice during my PhD studies and dissertation completion.

Thank you to all the Willerth lab members, past and present, that have helped shape me as a researcher, problem solver, and person. The collaborative and interactive nature of this lab is truly unique. Thank you all for being willing to listen and offer suggestions. To all the current members, namely, Nadia Masri, Milena Restan, Kali Scheck, Claire Benwood, Rebecca Kirsch, Christine Wong Chong. To all the former members, namely, Meghan Robinson, Laura De La Vega, Chris Lee, Laila Abelseth, Emily Abelseth, and Imke Smits. Special thanks to Karolina Papera Valente for assisting me in some experiments. Thank you to the wonderful undergraduates and all of the co-op and MITACS students for being a part of and assisting me on my path.

Thank you to the Stem Cell Network, the Canadian Biomaterials Society, BC RegMed, and ICORD for providing me with opportunities to expand my knowledge and skills. Thank you to the CAMTEC staff for instructing me on how to operate some of the equipment. Thank you to Aspect Biosystems for your continued feedback and direction in 3D bioprinting.

Finally, thank you to all my family and friends that have never ceased to believe in me over the years. Especially, my loving and caring son (Viraaj Sharma), who has grown as a Junior Scientist with me, my husband (Manish Sharma) who has been my second half ever since we married and constantly motivating me to do best and fulfil my dream, my younger brother (Nitin Sharma) who has always been supported and there for me ever since childhood, my mother who always inspired me and never let me fall, and my father in law who always supported me with his best advices.

Ruchi Sharma

University of Victoria

April 2022

Dedication

This dissertation is dedicated to my father, who is now in heaven. It was his dream to see me as a doctor. I also dedicate this thesis to everyone impacted by Parkinson's disease. I am hoping that this research will contribute to the development of new medicines.

Chapter 1 Introduction

1.1. Rationale for the research

For several decades, animal testing has been crucial to preclinical drug development. These tests are inconsistent in their ability to predict human responses both in terms of effectiveness and toxicity/safety [1-3]. Animal and tissue-engineered models have been remarkably useful in understanding disease mechanisms and identifying potential therapeutic strategies for disease-modifying solutions, but models that can provide predictive and physiologically relevant results are urgently needed [2, 4, 5]. Recent advances in stem-cell research, notably the generation of human induced pluripotent stem cells (hiPSCs), provide new avenues for overcoming some of the problems involved with disease modeling. HiPSCs are a form of pluripotent stem cell that develops directly from a somatic cell and has the potential to self-renew and specialise into any tissue of the body indefinitely. They have been genetically reprogrammed to an embryonic stem (ES) cell-like state by the forced expression of genes required for preserving ES cell-defining features. Reprogramming of somatic cells into pluripotent stem cells was accomplished in 2006 by adding four transcription factors: SRY (sex determining region Y)-box 2 (Sox2), Octamer-binding transcription factor 3/4 (Oct3/4) , Krüppel-like factor 4 (Klf4), and Myc proto-oncogene protein homolog (c-Myc) [6]. Furthermore, the process of reprogramming allows us to convert any cell in the body into a pluripotent stem cell, which has opened up new potential for disease research and treatment [2, 7].

Tissue engineering (TE) is the study of biological replacements capable of repairing diseased or damaged tissue in humans by transforming fundamental knowledge into practical and effective materials, technologies, and therapeutic methods. It is a rapidly

growing discipline that intends to improve human health and save millions of lives each year [8, 9]. As a result of the advancement of fabrication methods, the novel three dimensional (3D) printed in vitro tissue models can be used for drug screening applications in place of other (two dimensional) 2D and 3D models generated by various tissue engineering approaches [2, 7, 10]. Conventional 2D cultures consists of cells plated directly on a rigid substrate (e.g. polystyrene or glass), which is covered with substrates that imitate extracellular matrix composition, enhance cell adherence, and can support desirable cell behavior such as proliferation or differentiation [2, 7]. Previous studies reported effective production of ventral midbrain dopaminergic neurons (DNs) from hiPSCs in 2D models. They discussed that degeneration of ventral midbrain neurons has been related to movement impairments in PD, and the ability to investigate these cells in vitro is significant for drug screening purposes [11]. Another study, created hiPSCs from individuals with idiopathic PD. Their procedure generated hiPSCs that were devoid of reprogramming factors and more similar to ES cells; these were then developed into DNs [5, 12]. In contrast to 2D models, traditional 3D models were also used. This study were able to differentiate hiPSCs into DNs utilizing a 3D method combining Matrigel^{TM} and phase-guided microfluidics bioreactors. They asserted that 3D model is durable, cost effective, and exhibits biological accuracy, making it suitable for application in PD modeling and drug development [13, 14]. Organoid techniques have also been found to enhance PD modeling in vitro utilizing hiPSCs. These findings demonstrate how more sophisticated techniques, such as 3D cultures, can yield more complicated outcomes for disease modeling, such as structured cell organization and network creation, which better mimic in vivo tissue [5, 15, 16]. Ultimately, 3D bioprinting has the ability to create functioning human tissue that

would be useful for a variety of applications, including drug screening, disease modelling, and, eventually, tissue restoration [17-20]. Human tissues are fundamentally complex and often organised into composite architectures composed of several cell types, extracellular matrix, and other components [10, 21]. The elastic modulus of these tissues varies greatly in several orders of magnitude, ranging from 0.1 – 1 kPa for soft tissues, like the brain, to 10-20 GPa for hard tissues like mature bone [22-24]. Developments in 3D bioprinting have allowed for hiPSCs to be processed through micro extrusion, allowing for the printing of functionally significant neural tissues [25-28]. These tissues can eventually be differentiated into different structures of the brain. These bioprinting approaches are expected to be capable of creating a model for screening potential therapeutic drugs for neurodegenerative disorders. These discoveries suggest that the approach employed to create these tissues might be used for the screening of tailored drugs for several neurodegenerative disorders such as Alzheimer's disease (AD) and PD [10, 13, 17, 18, 26-32]. PD doesn't naturally occur in other animals, however it may be artificially induced, and the results are inapplicable to humans. Testing on animals in the search for a treatment specifically for PD is unreliable, and even dangerous. The goal is to decrease the use of animals by using 3D bioprinting. This can be accomplished by eliminating the use of animals, lowering the number of animals used in each experiment, limiting animal pain and enhancing animal well-being [4, 15, 17, 33-36]. There is presently no cure for PD, and standard-of-care drugs have limited effectiveness, implying that novel therapeutics is urgently needed. Traditional drug development models, on the other hand, frequently lack clinical translatability [4, 16, 37-40]. The ultimate goal of this study is to create 3D bioprinted models for drug screening from PD patients using hiPSCs. This technology

benefit both animals and humans since they are often faster, less costly, and more precise than the present animal experiments [3, 4, 33, 34, 41]. 3D bioprinted models might be used to evaluate the efficacy of drugs and perhaps eliminate animal testing, with the objective of minimizing, and in some cases, reducing animal testing by providing alternative models [10, 18, 29, 32, 36, 42].

1.2 Ongoing research for PD modelling as a drug-screening platform

Neurodegenerative diseases are associated with gradual dysfunctionality, which involves the loss of certain brain regions [2, 43]. PD is a neurodegenerative disease that primarily affects dopamine-producing ("dopaminergic") neurons in the substantia nigra, a region of the midbrain. A significant cause of PD is the loss of dopaminergic neurons (DNs) from the substantia nigra pars compacta (SNpc) and neuronal intracellular Lewy body (LB) inclusions representing in **Figure 1.1** and Lewy neurites (LN) are referred to as Lewy pathology [44]. LB is circular eosinophilic inclusions composed mostly of insoluble -synuclein clumps, ubiquitin, and other proteins. The aggregation of these misfolded proteins has been linked to PD, dementia with LB [45].

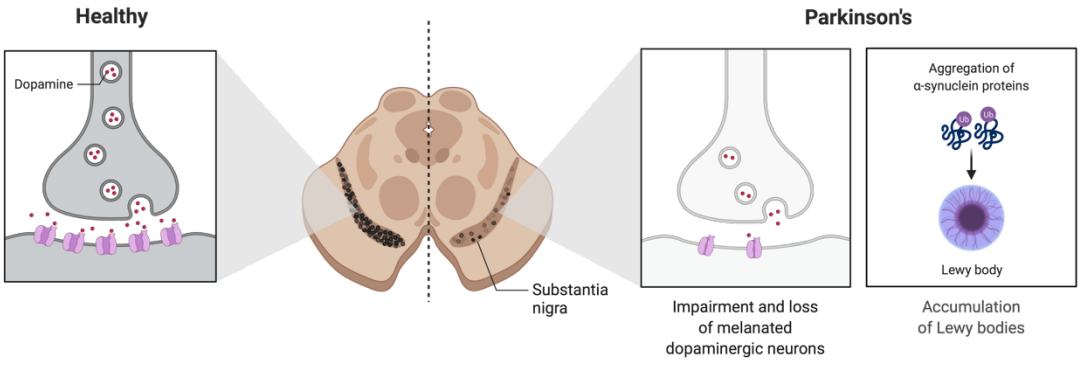

Figure 1.1 Progression of PD in SNpc (Created with BioRender.com)

Late and early onset PD associated with mutations in the Leucine-rich repeat kinase 2 (LRRK2) and Parkin (PRKN) genes, which are responsible for the most common dominant and recessive inherited forms of PD, respectively, have emerged as promising disease examples due to their established role in directing bioenergetics and autophagy balance. Gene mutation and protein aggregation play a main role in the degeneration of DNs. However, the exact aetiology of dopamine degradation is uncertain [16, 37, 39, 46, 47]. Nevertheless, certain rare family types of PD are linked to genetic loci, and the identification of underlying mutations has provided insight into the disease process [48]. People with PD may have tremors, particularly at rest, as well as bradykinesia, limb stiffness, gait difficulty, and balance issues [37]. The main difficulty in treating PD is that no one can predict how the disease would show in different people. The symptoms of PD vary depending on the starting age, the rate of development, and even response to therapies. They are commonly linked to emotional and physical impairment, as well as mortality. Existing pharmacological therapies are insufficient to combat these disorders, which mostly address their symptoms [4, 16, 37, 39, 40, 45, 46, 49]. Researchers studied the effect of embryonic stem cell-derived DNs in a rat model of PD and discovered that the cells enhanced behavioural recovery. Furthermore, rats with 6-OHDA lesions remain the most proven animal model for studying Levodopa (L-DOPA) -induced dyskinesia in the laboratory [34]. However, animal models often used in traditional drug screening may not precisely mimic the pathogenic mechanisms of human disorders, influencing assays and targets that may not adequately address disease causes. Additionally, the present drug development process is not only time-consuming, but also costly, and it is heavily reliant on animal models at the preclinical stage. As a result, a consistent *in vitro* modelling system

is required to explore the processes underlying these disorders and propose therapeutic approaches [4]. However, samples from the early stages of the disease would be most beneficial for understanding the development of pathology or screening for prospective treatments that reduce pathology [2, 33, 46, 50, 51].

PD is an excellent target for cell replacement therapy since it only affects a certain population in a specific region in the brain. Immortalized cell lines of neural origin that can also be exposed to toxin exposure or gene editing, have been frequently utilised to simulate PD [52]. These cell models have shown consistent and reproducible findings. One of their key advantages is that they have a common genetic background, which gives them a high degree of homogeneity. Furthermore, due to their low cost of maintenance and simplicity of editing, they provided broad platforms for disease modelling [52]. One example is the human-derived neuroblastoma cell line SHSY5Y, which may be employed undifferentiated or differentiated to DNs to model PD [53]. However, immortalised cell lines are linked with significant flaws such as the existence of genetic instability or a high rate of glycolytic metabolism, which drives the usage of patient-derived cell models. The majority of PD is caused by an unknown factor, as well as the urgent need to identify novel biomarkers during the prodromal phase, has prompted the development of patient-derived models. The benefits of these patient-derived cell models are that they recreate PD pathogenicity on an individual level, so partially avoiding the shortcomings of animal and established cell line models. In this context, the use of patient-derived cells that preserve patient-specific features has represented a significant advance in the study of PD, given the disease's great complexity and individual variability, which includes unknown genetic and epigenetic factors [48, 54].

Stem cell treatment has been increasingly promising for regenerative medicine in recent years, particularly with the introduction of hiPSCs technology, which presents a new paradigm for drug discovery. Furthermore, hiPSCs can be produced from a variety of patient tissue sources, including skin fibroblasts and blood [6]. Numerous procedures have been devised to differentiate hiPSCs into cells that play important roles in neurodegeneration, such as neurons, microglia, astrocytes, and oligodendrocyte, as well as for the adult onset of neurodegenerative diseases[2, 7, 33, 46, 47, 50, 55, 56]. Some studies on PD have been conducted directly on these stem cells, while others have been conducted by differentiating them into neural precursors or mature neurons. For example, neurosphere models of neural progenitors are commonly used in the study of neuronal development and neurodegenerative diseases [57]. Accessibility to hiPSC-derived neurons from PD patients is expected to shed light on molecular insights into PD pathogenesis and act as a platform for drug screening and early detection. One of the most recent uses of hiPSC is the creation of several brain cell lineages to generate brain organoids that mimic neuronal architecture, self-organization, and cell-to-cell contact in the physiologic brain. They are 3D *in vitro* culture systems that mimic the developmental processes and organisational structure of the growing human brain. Together with other two dimensional (2D) and 3D models such as neurospheres, neural aggregates, neural rosettes, and cortical spheroids, these "mini-brains" provide a physiologically appropriate model for the study of neurological development and disease processes that are unique to the human central nervous system [2]. The advent of hiPSCs for the study of mature-derived neurons has produced a new strategy to simulate PD, allowing researchers to manufacture disease-specific DNs *in vitro*

by reprograming somatic cells from patients with the disease [46]. They are all new and promising models for the study of neurodegenerative disorders [4].

3D bioprinting is a subset of additive manufacturing (AM), which is also known as 3D printing. 3D bioprinting uses layer-by-layer precise positioning of biological materials, biochemicals, and live cells, with spatial control over the placement of functional components, to build 3D structures [17, 25, 36, 58, 59]. 3D bioprinting has the potential to greatly alter and improve the medication screening process for neurodegenerative diseases by recreating the functionalities of brain tissues *in vitro* [10, 17, 18]. Patient-derived hiPSCs may be bioprinted using novel bioink such as ECM and differentiated into mature cell types, allowing researchers to study and monitor disease development, progression, and pharmacological therapies. As a result, employing human-derived cells improves the dependability of tissue-engineered models, which are more relevant than animal models for pharmacological screening and disease monitoring. Finally, drug-screening platforms must mimic human-level physiology in order to accurately predict clinical therapeutic success using reliable preclinical data [3, 5, 16, 46, 54, 60]. Robust, functional human tissue models might be used to supplement or replace existing animal models, which frequently do not fully mimic drug toxicity in humans. The development of a new drug by a pharmaceutical company can take several years and cost up to $billion. It usually starts with tens of thousands of drug candidates being screened [40]. Candidates that pass this step are subsequently tested on animals, with those who pass moving on to clinical trials. Clinical trials provide the most conclusive evidence that a new treatment is both safe and effective. Despite the fact that these trials, which often involve a large number of patients, however many drug treatments tested at this point fail due to lack of clinical efficacy and

unmanageable toxicity. Several medicines that showed promise in animal and early testing have subsequently failed to show clinical benefit, while increasing the risk of serious adverse events among participants [61]. Furthermore, the earliest phases of this process might be accelerated with high-throughput 3D bioprinting technology. It would allow drug developers to rapidly create significant amounts of human tissues on which to test and screen out drug candidates. Finally, inferences established utilising these comprehensive platforms should assist in the advancement of tissue-level, the troubleshooting of failed drugs in the pipeline, and the development of next-generation treatments [5, 10, 15, 31, 38, 62-64].

1.3. 2D/3D neural tissue models using hiPSCs

Many 2D and 3D models based on hiPSCs have been established to better understand the pathogenic processes behind neurodegenerative diseases in order to develop new treatment strategies. HiPSCs have mainly been cultured in 2D systems since they have shown to be extremely beneficial in providing fundamental and low-cost ways for mimicking central nervous system (CNS) disorders. However, 3D models are more advanced in simulating the complexity of the human brain's environment. These models have been proposed as a technique to more accurately replicate *in vivo* the CNS architecture and, as a result, provide more realistic models that could bridge the gap between 2D cell culture and animal models. Indeed, 3D cultures have already been shown to excel 2D in studies of cell-ECM interaction, cell differentiation, cell-cell communications, and electrophysiological network properties [2, 5, 18, 31, 65, 66].

1.4. Protocols for the differentiation of dopaminergic neurons (DNs) from hiPSC-derived neural progenitor cells (NPCs)

HiPSCs can be differentiated into NPCs in a monolayer culture. Following that, NPCs become multipotent and can differentiate into various CNS lineages such as neurons and glial cells (astrocytes and oligodendrocytes) [7, 55, 67]. Thus, hiPSC-based models are effective tools for studying neurodegenerative diseases such as PD. Furthermore, hiPSCs differentiated toward dopa progenitors provide a valuable source for the generation of DNs. However, the current protocols produce a highly variable yield of DNs. Effective cell therapy for PD requires an efficient, well-defined method of DNs generation, in addition to protection from the neuroinflammatory environment during engraftment. Establishing effective methods for the creation of differentiated DNs from pluripotent cells is required for the application of hiPSCs in disease mechanisms research, drug development, and, eventually, cell replacement therapy [33, 38, 44, 50, 68, 69]. Obtaining a high purity population of neuronal cells is essential for the development of cell treatments, disease modelling, and high-throughput drug discovery for PD [21, 55]. Thus, using small molecules to drive pluripotent stem cell development toward a specific linage is a strong method for producing specific cell types with potential therapeutic applications [67, 70]. Several small compounds effectively modulate the SMAD signalling pathway, resulting in an increase in neuroectodermal markers. They cause NPCs to differentiate into DNs, as seen by the expression of tyrosine hydroxylase (TH), dopamine transporter, dopa decarboxylase, and increased dopamine release. They have been shown to boost the ability of hiPSCs to be directed towards neuronal lineage. Furthermore, the anti-cancer drug guggulsterone is an efficient agent for developing both human embryonic stem cells and

hiPSCs into DNs. Robinson et al. proposed that guggulsterone may generate DNs from hiPSC-derived NPCs with comparable efficiency, and that differentiation can occur inside 3D fibrin scaffolds, which could improve cell survival after engraftment. Our group have shown that guggulsterone could be delivered in a controlled manner from microspheres and developed as a method to construct mature brain tissues from hiPSCs [71]. As a result, utilizing reprogrammed hiPSC-derived NPCs in conjunction with small molecules and growth factors provides a technique to boost the yield and functioning of DNs, which produce the neurotransmitter dopamine. Dopamine is released by a neuron into the synapse, where it binds to dopamine receptors on the next neuron [33, 38, 72].

1.5. Microspheres as drug delivery devices

Microspheres are tiny spherical particles, often formed of a biodegradable polymer, in which the drug is distributed throughout the matrix; their diameters range from 1 to 1000 μm. These are frequently referred to as micro particles, and they enable for the effective encapsulation of drug molecules for consistent and sustained therapeutic impact. Furthermore, microspheres are employed for both targeted and extended drug release in affected areas [28, 67, 70, 73-75]. They allow for the precise administration of smaller doses of a potent drug at a lower concentration to a spot other than the target tissue. They may then be combined with stem cell-enriched bioinks to create bioprinted tissues, where they will release the encapsulated drug and facilitate stem cell differentiation into the appropriate mature cell type. Microspheres may be used to encapsulate a wide spectrum of pharmacological agents, including small molecule drugs, DNA, and proteins [70, 74]. The release of contained molecules occurs when the polymer matrix degrades and erodes.

Furthermore, microspheres are employed to manage drug release rates, reducing hazardous side effects and removing the inconvenience of repeated additions. Furthermore, microspheres have the capacity to assimilate relatively high concentrations of the drug. They remain stable for a greater duration of time following synthesis. However, the most important component is biocompatibility of microspheres with regulated biodegradability [73]. Biodegradable polymers such as polycaprolactone (PCL) and poly (lactic-co-glycolic acid) (PLGA) microspheres and nanoparticles have been widely employed in drug delivery [76]. The drug will be delivered at a controlled rate when the polymer degrades. Because of its slow degradation, PCL is a biodegradable polymer that is helpful for long-term implanted devices. Furthermore, PCL is known to degrade more slower than PLGA. PCL is an aliphatic polyester, a semi-crystalline polymer with strong organic solvent solubility and a low melting point. Because of its great permeability to diverse agents, PCL has emerged as a promising choice for the development of drug delivery systems [27, 28, 71, 74].

Microspheres were efficiently produced using a single emulsion approach that utilised an oil-in-water (o/w) emulsion followed by evaporation of the organic solvent as previously reported in protocols [24] and then kept at 20 °C. These drug-loaded microspheres were put to bioink to enable for targeted drug administration, and the encapsulated drugs in those microspheres may improve stem cell development. Incorporating drug-releasing microspheres into our bioinks can increase the efficiency of cell differentiation as well as reduce the amount of time of changing cell culture media on bioprinted constructs. As a result, boosting the distribution of differentiation factors inside the bioinks might increase the quality of our 3D bioprinted constructs. When the qualities

of 3D bioprinted constructs incorporating microspheres were compared to pure bioprinted hydrogels, it was discovered that the integration of microspheres improved cell viability in the 3D constructs [27, 28].

1.6. Bioinks as potential biomaterials for the generation of brain tissue

The properties of the bioink used to create the construct are critical to the success of the tissue model. It is critical that the bioink have the necessary qualities for the creation of an accurate brain tissue. To effectively manufacture 3D printed tissues for drug testing, a suitable bioink that can sustain cell development and differentiation while also printing to the necessary structure and maintaining its integrity during the culture time must be developed [13, 25, 35, 77-80].

Fibrin has been demonstrated to be an effective biomaterial for the growth and maturation of several types of brain cells [66, 78, 81, 82]. Fibrin is a protein present in human blood that plays an important role in coagulation. It consists of 6 polypeptide chains, 2 of each Aa, Bb, and g, all with their N-terminus coming together at a central E node. The C-terminus of the Bb and g chains extends outward from the E node producing two D nodes on either side. The mechanism of fibrin polymerization is initiated by thrombin, an enzyme that first cleaves the Aa chain, allowing non-covalent attachment of the E node on one fibrinogen molecule to the D node on another, resulting in a staggered protofibril double-strand, followed by the Bb chain, which may promote lateral aggregation of the protofibrils. Although any concentration of thrombin is sufficient to induce full polymerization of the fibrinogen, higher concentrations have physiological and structural impacts on clot formation [78]. Fibrin that has been crosslinked by thrombin and $CaCl_2$

tends to last one to two weeks in culture before being destroyed by proteases generated by integrated cells. This restricts the effectiveness of fibrin scaffolds for neural tissue engineering since fully differentiated neural cell types frequently need more than 4 weeks of culture. Soluble protease inhibitors or extra chemical crosslinking can decrease the breakdown of fibrin scaffolds for longer term durability. Furthermore, alginate, a commonly used component of bioinks, polymerizes fast when a divalent cation is added. Other polysaccharides, such as gellan gum, polymerize at comparable rates. However, because these polysaccharides are essentially inert, they have poor cell adhesion [25].

Genipin is a naturally generated tiny molecule formed from geniposide, which is present in fruits. Genipin can be used to covalently crosslink the amine groups of proteins. This helps to stabilise the hydrogel far more, but it can also modify its mechanical characteristics, particularly its stiffness and porosity. The elastic moduli of gels generated with genipin concentrations less than 2.5mM were found to be lower than gels produced without genipin in a study looking at the influence of genipin concentrations on hiPSC neuronal development. Genipin also influenced pore size, with bigger holes in gels containing 1mM-5mM genipin compared to those with none. Alginate is an anionic polysaccharide produced from seaweed [83-85].

Natural polyanionic alginate (M.W. 418.23 g/mol) is a non-immunogenic, non-toxic, and biodegradable polymer. It is a water-soluble polysaccharide comprised of 1–4 linked –L–guluronic acid (GulA; G) and –D–mannuronic acid (ManA; M) residues. Alginates may contain variable lengths of G-blocks, M-blocks, and/or MG/GM-blocks. These multifunctional polymers are structural components of brown microalgae (Phaeophyceae) cell walls and create the intercellular gel matrix. They are found in the form of divalent

salts of alginic acid. Alginate, along with chitin and chitosan, is a popular natural polysaccharide utilised as a biomaterial in tissue engineering. It is one of the most well-known materials with good scaffold-forming characteristics that can be used to treat organ loss or failure. Alginate is often used as a biomaterial because it is biocompatible and biodegradable, and because the polarity of its chains allows it to easily crosslink with Ca2+ ions, resulting in a stable hydrogel. Long-term alginate hydrogel stability is regulated by pH as well as alginate molecular weight. Higher molecular weight results in slower hydrolysis breakdown [13, 86-88].

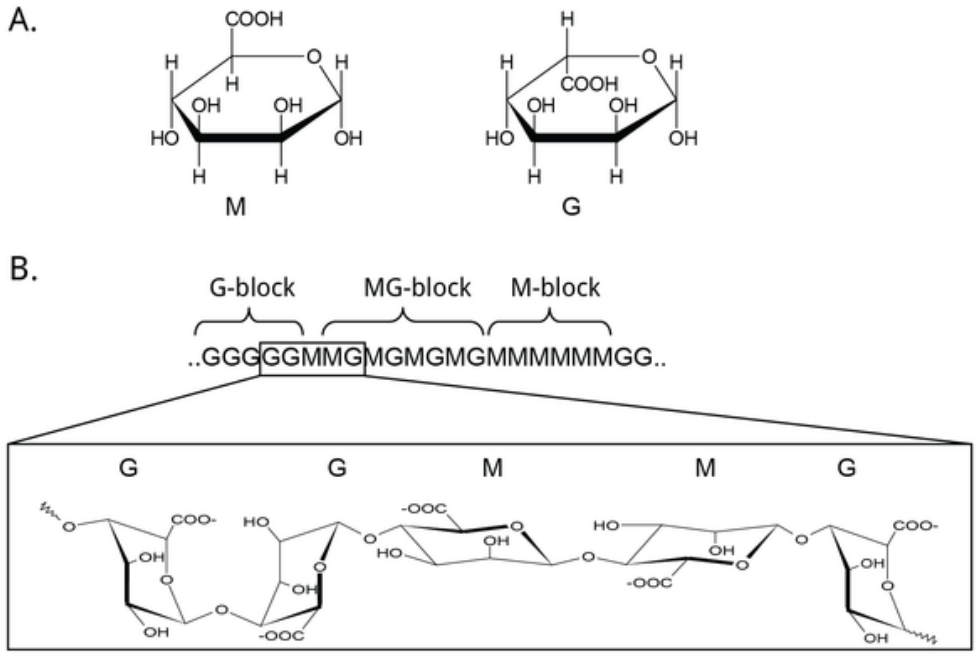

Figure 1.2 Alginate structures showing covalently linked G and M blocks (https://www.cazypedia.org/index.php/Polysaccharide_epimerases)

Chitosan is a cationic polysaccharide derived from crustaceous shells via deacetylation of chitin. Many properties of the biopolymer make it suitable for tissue engineering. They have high biocompatibility and are non-toxic; biodegrade to harmless products; have high protein affinity; and have antibacterial and anti-tumour properties. All of these qualities would be advantageous to tissues created with the polymer. When implanted *in vivo*, chitosan elicits favourable host responses. It has rarely been shown to trigger a foreign body response and fibrous encapsulation within the body [25]. Chitosan (M.W. 1526.5 g/mol) is a non-toxic, biocompatible polycationic polymer. It is a polymer of N–acetyl glucosamine that has been partially deacetylated. It is a natural, water-soluble chitin derivative with specific characteristics. Chitosan is often made from chitin (2 acetamido–2–deoxy–1,4–D–glucan), which may be obtained in a variety of natural sources. Chitosan (14)–linked 2–amino–2–deoxy–b–D–glucan may be synthesised from chitin by alkaline hydrolysis of the N–acetyl groups. It also has biodegradability, antibacterial action, low toxicity, and immunogenicity, all of which are required for scaffolds [13, 83, 89].

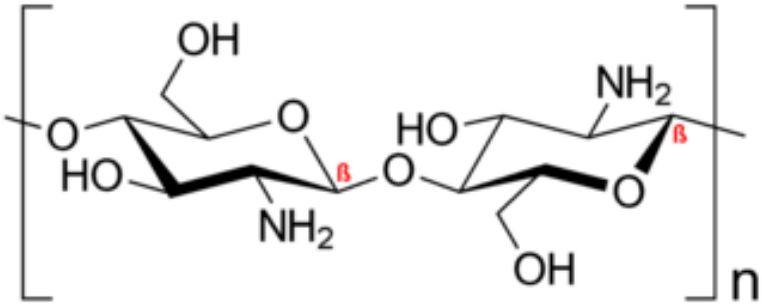

Figure 1.3 Schematic representation of Chitosan (https://en.wikipedia.org/wiki/Chitosan)

There are various aspects to consider while creating a bioink for 3D printing tissues. From the perspective of cell life, the material must be biocompatible and noncytotoxic, allowing it to encapsulate cells without affecting their viability [13, 14, 25, 35, 90, 91].

To facilitate cell attachment, migration, and delivery of differentiation cues, the bioink must be enable cell-material interactions. The bioink must be properly tailored to the printing system with an acceptable viscosity and gelation time in order to be printable. Finally, the printed structures must be able to maintain the cells throughout their differentiation process without degrading prematurely. When designing brain-tissue-like biomaterials for neural tissue engineering, biodegradation times should also be taken into account. Proteins, peptides, sugars, and ions in the brain's fluids interact with and degrade the material implanted. Even though the components of bioink are not chemically identical to those found in brain extracellular matrix, the overall effect is that it boosts proliferative capacity and biological complexity. When cells are integrated with pure extracellular matrix, the components degrade faster. Finally, the bioink solution composed of 20 mg/mL of fibrinogen (341578, Sigma, St. Louis, MO, USA), 0.5% w/v of alginate (120,000–190,000 g/mol, M/G ratio 1.56) (180947, Sigma, St. Louis, MO, USA), and 0.3 mg/mL of Genipin dissolved in de-ionized water (G4796, Sigma, St. Louis, MO, USA) in tris-buffered saline (TBS). The crosslinking solution contained 20 mg/mL of calcium chloride (449709, Sigma, St. Louis, MO, USA), 0.075% w/v of chitosan (C3646, Sigma, St. Louis, MO, USA), and 1.7 U/mL of thrombin (T7009-1KU, Sigma, St. Louis, MO, USA) [25].

1.7. Rheological properties of bioink

Brain tissue is ultra-soft, with a shear modulus of one kilopascal—softer than any other tissue in the human body. The rheology of ultra-soft materials, such as human brain, is extremely sensitive [92, 93]. Understanding the rheology of the brain tissue will help us to better correctly describe brain function throughout development and disease [93]. The

mechanical characteristics of hydrogel affect the activity of brain tissue cells. In this context, in addition to stiffness, viscoelasticity, porosity, and degradability of hydrogels are considered mechanical cues, and outlined here, how these mechanical qualities might impact cell behaviour such as viability, proliferation, differentiation, and spreading [1, 22, 93-98]. The mechanical microenvironment of brain tissue may drive the design of 3D cell culture platforms for neural tissue engineering. Furthermore, matrix stiffness is a critical factor of stem cell differentiation, modulating bioink mechanical characteristics appears to be a practicable technique for spatially regulating stem cell fate inside bioprinted tissues [36, 87, 99-101]. Previous research has indicated that the molecular weight of bioinks, as well as the ionic crosslinker used, may be modified to regulate the mechanical characteristics (Young's Modulus and Degradation Rate) of 3D printed constructions [22, 87, 102-104]. It is feasible to bioprint constructs with spatially changing mechanical microenvironments using the same bioink and crosslinker but modifying the crosslinking ratio. Hydrogel-based 3D culture systems have been widely used to offer cells with a more physiologically appropriate microenvironment. Multiple pioneering studies have found that brain cells are sensitive to changes in the mechanical characteristics of their surroundings. As a result, in the context of neural tissue engineering, the brain-tissue-specific mechanical characteristics of hydrogels must be considered [92, 93, 105].

1.8. Bioprinting of hiPSC-derived NPCs

Traditionally, scientists studied biological and disease pathways using flat 2D cell cultures grown on a plate. 2D cell models are easy to culture and process, as well as inexpensive [2]. However, 3D cell cultures have grown in popularity over the last decade since they are

more physiologically relevant and better resemble in vivo tissue. 3D cell cultures are increasingly being used in fundamental research and drug development. 3D cell culture is a culture environment that allows cells to grow and interact in three dimensions with the surrounding extracellular matrix. This process is in contrast to standard 2D cell cultures, which grow cells in a flat monolayer on a plate. 3D cell cultures may be generated either with or without a scaffold. A 3D microfluidic cell culture chip built to simulate the physiology of an organ is known as an organ-on-a-chip. 3D cells are grown in scaffolds within a microchip's chambers. Tiny channels allow liquid (microliter to picoliter quantities) to pass through them, transporting and distributing nutrients or other substances throughout the cells [2, 7, 43, 55, 106-108].

Furthermore, bioprinting is a new technique with several applications in the creation of functional tissue scaffolds. It is a technique for patterning a cell-encapsulating bioink to generate complex tissue structures. Interestingly, 3D bioprinting allows for the creation of tissues that are more physiologically similar to human tissue. This technology offers a greater throughput than most standard cell culture techniques [10, 18, 42, 61, 90, 109]. Most notably, drug discovery can benefit from these 3D structures since they employ the patient's own cells to create tissue, reducing the danger of the body rejecting it. It is a novel method that offers great reproducibility and exact control over produced structures in an automated setting. The use of 3D bioprinting has had a significant impact on brain tissue engineering research. Furthermore, whereas 2D neural cultures are commonly used to investigate brain cells, 3D cultures can more closely mimic the environment of neural tissues. Bioprinting neural tissue constructs allows for precise microenvironment control

by specifically formulating the bioink for supporting neural tissues and spatially patterning cell types and scaffold characteristics in three dimensions[10, 17, 20, 26-28, 32, 66].

The RX1 printer from Aspect Biosystems is the first of its type — a 3D bioprinter combined with a microfluidic printhead, Lab-on-a-printer (LOP^{TM}). It boasts accurate motion and pressure control, allowing it to achieve micro-scale resolution even at high speeds. Microfluidics' flexibility enables homogeneous cell and material patterning. It contains user-friendly software that allows for the creation of highly customizable structures. Furthermore, the print heads are designed to be compatible with a wide variety of biomaterials. It features a protective coaxial coating that reduces shear stress on cells, preserving cell viability and phenotypic and function. Furthermore, the microfluidic printhead offers versatility, including the capacity to print cell-laden, stacked fibres. Furthermore, with a printer, accurate pressure and valve control allows for consistent changeover between numerous materials as well as precision control over fibre diameter. This method uses a printhead for crosslinking mechanism to print a wide range of materials with great print quality, including low viscosity bioinks to replicate soft tissue microenvironments. The DUO-1 print head features four channels, which include a buffer channel, a crosslinker channel, and two distinct material channels. During the print, the pressure-controlled valve system in the microfluidic channels allows for on-the-fly switching of materials. A bioink must be chemically crosslinked in order to be compatible with the print head. The cross-linking process is begun inside the printhead at the junction point between the bioink and crosslinker channels and takes a few seconds. A crosslinker channel connects with the bioink channels on the print head, causing gelation and allowing the material to escape the print head as a fiber [25-28].

In mammals, the native microenvironment limits the regenerating ability of brain tissues, particularly in the CNS. Thus far, most therapy for neurodegenerative diseases have focused on symptom relief rather than repair of damaged regions. Furthermore, implantation of drug- or cell-laden tissue engineering scaffolds to the damaged site of the CNS may be a possible therapeutic treatment [93, 110]. Recent advances in 3D bioprinting technology hastened the arrival of the era of customised medicine. With diverse printing processes and materials produced, 3D bioprinting offers a wide variety of medical applications, including the fabrication of soft tissue for future clinical use or the formation of tissues in disease models. The key advantages of 3D bioprinting are personalised design and accurate construction, both of which are crucial for tissue engineering. One of the biggest issues with the many 3D printing technologies available, such as inkjet, extrusion, and stereolithography, is the amount of shear stress the cells get when they are extruded, which leads to limited cell viability. Aspect Biosystems RX1 bioprinter has created a unique microfluidic bioprinting technology that has the potential to deliver reduced shear stress to cells and enhance greater and long-term survivability [10, 27, 28, 31].

1.9. Research Objectives

As previously discussed, several research have targeted on establishing models for PD for cell replacement therapies of DNs and patient-specific drug-screening. However, the intricacy of the human brain is one of the hurdles for developing in vitro models. There is still a critical need for complicated 3D models that can provide more accurate and physiologically relevant outcomes in order to develop disease-modifying treatments. The discovery of effective therapeutic targets in preclinical research and customised precision

medicine is constrained by a lack of adequately representative *in vitro* models. PD is a condition for which animal models can not well predict human responses.

The difficulty in replicating the multifactorial complexity of the condition in traditional *in vitro* models, as well as the overreliance on animal models, explain a portion of the unexpectedly high failure rate of novel candidate molecules in clinical trials. As a result, the focus of our study is on developing a complex drug screening platform for PD. The goal of this study is to 3D bioprint healthy and diseased hiPSC-derived NPCs and differentiates them into DNs. It is hypothesized that 3D bioprinted hiPSC-derived NPCs with drug releasing microsphere can be differentiated in to mature and functional neural tissues containing DNs. This work focused on bioprinting hiPSC-derived PD-NPCs from a 63 year old male patient. The diseased NPCs will be bioprinted with fibrin-based bioink and guggulsterone microspheres. Here, the aim is to evaluate whether hiPSCs from PD patients have distinct differentiation potential in bioprinted constructs as compared to 2D and other 3D methods such as organoid development. The final objective of this work is to create a functioning 3D bioprinted PD tissue model from patient-specific hiPSC-derived NPCs that may be utilised for personalised drug screening and disease modelling.

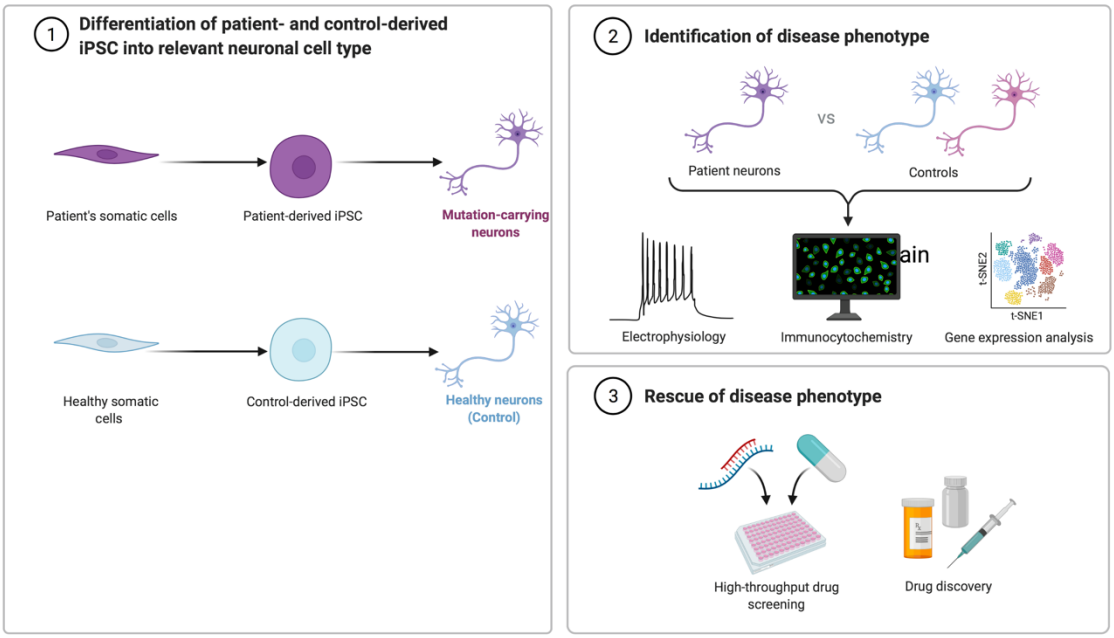

Figure 1.4 Use of hiPSC-based disease modeling of neurodegenerative disorder (Created with BioRender.com)

1.9.1. Research Objective 1

To Bioprint Healthy Human Induced Pluripotent Stem Cells derived Neural Progenitor Cells With Drug-Releasing Microspheres

The hypothesis to be tested in this research is “3D bioprinted hiPSC-derived NPCs with drug releasing microsphere can be differentiated in to mature and functional neural tissues containing DNs.” This work demonstrates how the regulated release of guggulsterone from microspheres can improve the survival and differentiation of NPCs in dome-shaped bioprinted tissues. "Because of its likeness to the human midbrain, a dome-shaped replica must be printed."

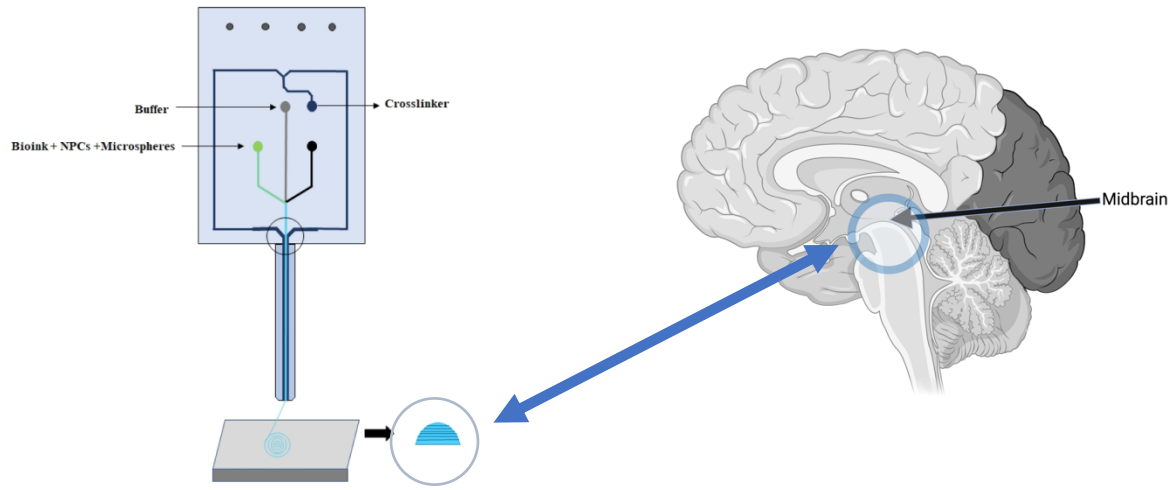

Figure 1.5 Schematic representation of the Aspect Biosystems Duo-1 printhead and 3D bioprinted dome-shaped constructs with mid-brain (Created with BioRender.com)

1.9.2. Research Objective 2

To perform physicomechanical Analysis of Bioink and Bioprinted Constructs With Drug-Releasing Microspheres

This work validates that 3D bioprinting allows for the creation of highly regulated 3D tissue structures. To create tissue constructs, this method employs bioinks, which are specially customised materials that assist in the survival of incorporated cells. To support particular cell types, bioink characteristics like as stiffness and porosity should resemble those present in targeted tissues. Our previous research confirmed soft substrates for neuronal growth utilising neural cells obtained from hiPSCs. It is critical to validate that the mechanical characteristics of these bioprinted tissues are comparable to those of natural neural tissues. In this study, the physical and mechanical characteristics of bioprinted constructs created from our unique bioink-containing microsphere were examined. The

storage and loss modulus, viscosity, and shear rates were all tested as well. Physical parameters including microstructure, porosity, swelling, and biodegradability were also investigated.

1.9.3. Research Objective 3

To Bioprint Parkinson's Patient-Specific Human Induced Pluripotent Stem Cells derived Neural Progenitor Cells With Drug-Releasing Microspheres

This work elaborates 3D printed tissue models using patient-specific hiPSC-derived NPCs with our fibrin-based bioink and encapsulated guggulsterone microspheres for customised drug screening and disease modelling. Here, all the dysfunctionalities such as

of diseased neurons were tested by immunocytochemistry and Hematoxylin and Eosin (H & E) staining.

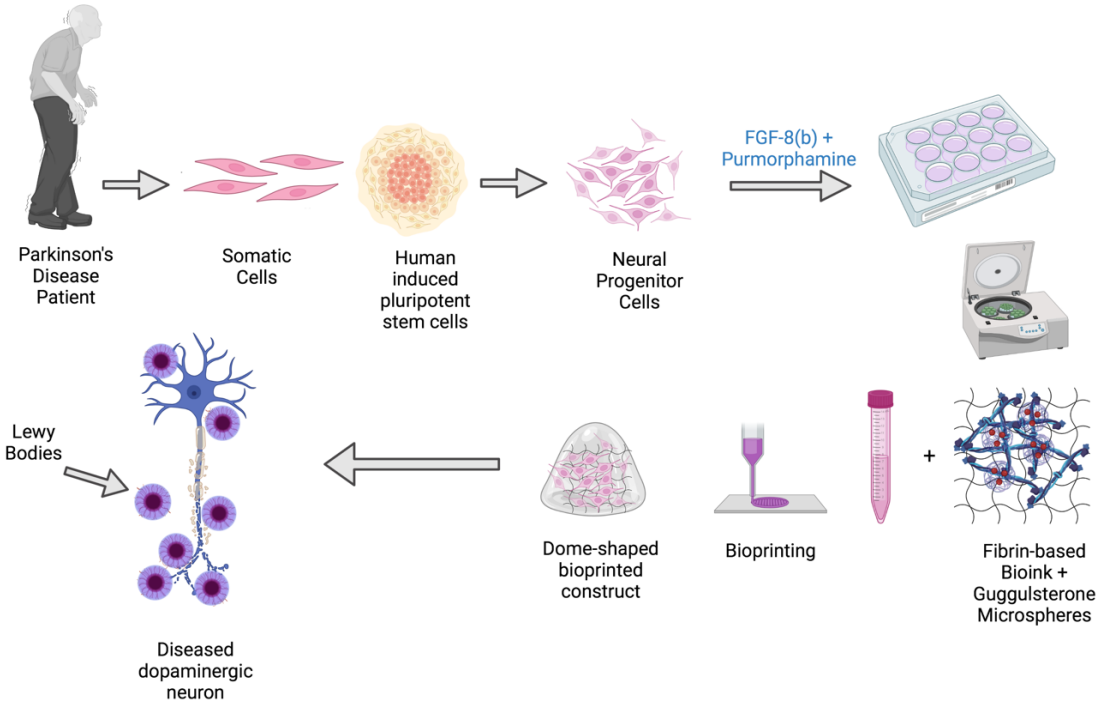

Figure 1.6 Progression of PD in Substantia Nigra Pars Compacta (SNpc) (Created with BioRender.com

Chapter 2 3D Bioprinting Pluripotent Stem Cell Derived Neural Tissues Using a Novel Fibrin Bioink Containing Drug Releasing Microspheres[a]

Ruchi Sharma[1], Imke P. M. Smits[2], Laura De La Vega[1], Christopher Lee[3] and Stephanie M. Willerth[1,2,4*]

[1]Department of Mechanical Engineering, University of Victoria, Victoria, BC, Canada,
[2]Department of Biomedical Engineering, Eindhoven University of Technology, Eindhoven, Netherlands,
[3]Djavad Mowafaghian Centre for Brain Health, The University of British Columbia, Vancouver, BC, Canada,
[4]Division of Medical Sciences, University of Victoria, Victoria, BC, Canada

Keywords:

Tissue engineering, regenerative medicine, small molecules, drug delivery, guggulsterone, stems cells

Author contributions

R.S designed, performed, and supervised experimental procedures and data analysis. She contributed to writing, reviewing, and editing this manuscript. I.P.M.S. assisted on experimental set-up, and data analysis. L.D.L.V. assisted on experimental set-up, and helped with data analysis. C.L. helped in editing manuscripts and figures. S.M.W. provided input into experimental design, provided feedback and supervision on the experimental analysis, as well as writing and editing the manuscript.

[a]The following chapter is from: **Ruchi Sharma,** Imke P. M. Smits, Laura De La Vega, Christopher Lee, Stephanie Michelle Willerth **"3D bioprinting pluripotent stem cell derived neural tissues using a novel fibrin bioink containing drug releasing microspheres"** ***Frontiers in Bioengineering and Biotechnology,*** **section** ***Biomaterials*****. 2020**

2.1. Abstract

3D bioprinting combines cells with a supportive bioink to fabricate multiscale, multi-cellular structures that imitate native tissues. Here, we demonstrate how our novel fibrin-based bioink formulation combined with drug releasing microspheres can serve as a tool for bioprinting tissues using human induced pluripotent stem cell (hiPSC)-derived neural progenitor cells (NPCs). Microspheres, small spherical particles that generate controlled drug release, promote hiPSC differentiation into dopaminergic neurons when used to deliver small molecules like guggulsterone. We used the microfluidics based RX1 bioprinter to generate domes with a 1 cm diameter consisting of our novel fibrin-based bioink containing guggulsterone microspheres and hiPSC-derived NPCs. The resulting tissues exhibited over 90% cellular viability 1 day post printing that then increased to 95% 7 days post printing. The bioprinted tissues expressed the early neuronal marker, TUJ1 and the early midbrain marker, Forkhead Box A2 (FOXA2) after 15 days of culture. These bioprinted neural tissues expressed TUJ1 (15 ± 1.3%), the dopamine marker, tyrosine hydroxylase (TH) (8 ± 1%) and other glial markers such as glial fibrillary acidic protein (GFAP) (15 ± 4%) and oligodendrocyte progenitor marker (O4) (4 ± 1%) after 30 days. Also, quantitative polymerase chain reaction (qPCR) analysis showed these bioprinted tissues expressed *TUJ1, NURR1* (gene expressed in midbrain dopaminergic neurons), *LMX1B*, *TH*, and *PAX6* after 30 days. In conclusion, we have demonstrated that using a microsphere-laden bioink to bioprint hiPSC-derived NPCs can promote the differentiation of neural tissue.

2.2. Introduction

3D bioprinting has become an increasingly popular strategy for engineering tissues as shown in recent reviews [10, 20, 51]. This process combines cells with bioinks, which are optimized to encourage the formation of target tissues, and deposits them into 3D structures based on specifications given in a digital design file. The properties of the bioink will also determine how well the bioprinted tissue replicates the physiology of the target tissue or organ being printed [35, 79, 111]. Bioinks should possess a number of characteristics, including high biocompatibility, printability, and the ability to deliver factors to promote the desired behavior from the cells seeded inside. The properties of these bioinks can be tuned for printing specific tissue types as well as to support specific cell populations. In particular, hydrogels often possess the desired characteristics necessary for bioprinting tissues, in terms of viscosity and dealing with the shear stress generated during printing [112].

Human induced pluripotent stem cells (hiPSCs) were discovered in 2007 when scientists determined that overexpression of certain transcription factors could revert adult human fibroblasts back into stem cells possessing the property of pluripotency [6]. This discovery has enabled the study of many diseases as these stem cell lines can be derived from patients suffering from different diseases and disorders. Using patient derived hiPSCs lines and differentiating them into a target tissue type is a powerful way to study diseases, including those affecting the nervous system – like Alzheimer's and Parkinson's [54]. Often, research on hiPSC models of these diseases is conducted in 2D, despite brain tissue possessing a complex 3D structure. Recent work has examined the necessary conditions for 3D printing neural tissues derived from stem cells using hydrogel-based bioinks. For example, Lozano

et al. (2015) successfully bioprinted brain-like structures utilizing a bioink composed of gellan gum modified with the RGD peptide containing primary cortical neurons. More recent work from the McAlpine group demonstrated that multiple neural cell types, including neural stem cells derived from hiPSCs, could be printed with relatively high levels of viability into structures that resemble the spinal cord [30]. However, most of these bioprinting studies have not attempted to generate structures that resemble the brain.

Neural tissues can be generated using many different types of bioprinting technology, including extrusion-based methods; laser assisted printing, inkjet printing, and drops on demand method [113]. Our lab uses the Aspect Biosystems RX1 printer with its novel microfluidic Lab-on-a-Printer technology due to its ability to protect the cells within the bioink from shear stress during printing – enabling us to maximize cell viability. Our own group developed a novel fibrin-based bioink for printing hiPSC-derived neural aggregates that both maintained their viability and differentiated into mature neural tissues after 46 days of culture [25]. This same formulation was also used to print dissociated hiPSC-derived neural progenitor cells (NPCs) that could be matured into spinal cord-resembling tissues upon treatment with specific small molecules [26]. This bioink formulation supported the generation of ring shaped constructs containing the human glioblastoma cell line where the tissues exhibited high levels of viability and expressed cancer associated protein markers. We also showed that effects of a potential glioblastoma cancer treatment were different in our 3D bioprinted model compared to 2D culture, illustrating the need for such bioprinted models of neural diseases.

One of the challenges when working with hiPSCs is ensuring their differentiation into the desired, mature phenotypes. Neural differentiation of hiPSCs can take months and require

a significant amount of labor and resources [114]. One promising strategy for promoting such differentiation requires treating these hiPSCs with small molecule morphogens [115]. Our lab has extensively explored the use of small molecule morphogens encapsulated in microspheres, which degrade over time to slowly release the drug in a controlled manner, as a means to direct neural differentiation in an autonomous fashion [71, 74]. Guggulsterone, an anti-cancer drug, is a potent agent for differentiating both human embryonic stem cells and hiPSCs into dopaminergic neurons, the cellular population affected by Parkinson's disease [68, 69]. Our recent study demonstrated that we could deliver guggulsterone in a controlled fashion from microspheres as a way to engineer mature neural tissues from hiPSCs [71].

This work now incorporates these novel guggulsterone-releasing microspheres into our fibrin-based bioink as a tool for 3D bioprinting tissues similar to that found in the brain. The goal was to generate neural tissues containing dopaminergic neurons from hiPSCs derived NPCs to model healthy brain tissue in a dish as well as to validate the bioactive properties of our microsphere-containing bioink. In this study, we bioprinted dome shaped constructs containing hiPSC-derived NPCs encapsulated inside of our bioink containing guggulsterone microspheres and characterized their properties. We printed dome shaped structures that were 1 cm in diameter in a layer-by-layer fashion, consisting of six layers. We printed two additional sets of control tissues – (1) tissues containing NPCs and treated with guggulsterone in the media, and (2) tissues containing unloaded microspheres and NPCs. All three sets of constructs were analyzed for cell viability and their expression of markers associated with neural differentiation, in particular dopaminergic neurons.

2.3. Materials and Methods

2.3.1. Expanding Neural Progenitor Cells From hiPSCs for Bioprinting

Experiments using hiPSC-derived NPCs were conducted with the approval of the University of Victoria's Human Ethics Committee – Protocol No. 12-187. NPCs were derived from undifferentiated hiPSCs (1-DL-01 line – male, WiCell Research Institute) as described previously [69]. NPCs were cultured in STEMdiff™ Neural Progenitor Medium (NPM), (STEMCELL™ Technologies, Vancouver, BC, Canada), on cell culture plates coated with poly-L-ornithine (PLO, Sigma, St. Louis, MO, United States) and laminin (Sigma, St. Louis, MO, United States). The NPCs were cultured under standard conditions consisting of 5% CO_2 at 37°C with daily media changes. Cells were cryopreserved in STEMdiff™ Neural Progenitor Freezing Medium (STEMCELL™ Technologies Vancouver, BC, Canada) liquid nitrogen upon reaching 80% confluence.

2.3.2. Preparation of Unloaded and Guggulsterone Microspheres

Microspheres were prepared using an oil-in-water (o/w) emulsion process as previously described [71]. 2% poly (vinyl alcohol) (PVA) (Mw ~ 13,000–23,000, 87%– 89% hydrolyzed) (Sigma-Aldrich, St. Louis, MO, United States) solution was prepared by diluting PVA in de-ionized water for an hour at 85°C with 850 rpm on a magnetic mixer (Corning Life Sciences, Tewksbury, MA 01876, United States) for the water phase. Subsequently, 100 ml of 0.3% (w/v) PVA solution was prepared by dissolving 2% PVA with de-ionized water and kept at 35°C. 500 mg of poly- ε-caprolactone (PCL) (Mn ~ 45,000), was dissolved in 3 ml of dichloromethane (DCM, Fisher Scientific, Ottawa, ON,

Canada) on a magnetic mixer for 15 min at 900 rpm for making the oil phase. Later, 0.3 mg of guggulsterone (Sigma-Aldrich, St. Louis, MO, United States) was dissolved in 100% ethanol then added to the oil phase to make microspheres at a concentration of 0.6 μg/mg (w/w, guggulsterone/PCL) microspheres. Unloaded microspheres were prepared by adding an equal volume of ethanol without the drug to the oil phase. 3 ml of 2% PVA was slowly added to the oil solution to prevent disruption of the boundary layer after removal from the magnetic mixer. Afterward, an emulsion (w/o) was then achieved by vortex mixing (Fisher Scientific) at 3000 rpm for 15 s. This (w/o) emulsion was mixed into the 0.5% PVA water phase and held at 35°C at a mixing speed of 500 rpm for 4 h to evaporate of the organic solvent. Then after mixing, the microspheres were isolated by centrifugation at 4,000 rpm (Eppendorf 5810 R model with swinging bucket rotors) and washed with deionized water. The microspheres were lyophilized for 24 h and stored at −20°C. The microspheres were sterilized by low power air-plasma treatment (Harrick Plasma, Ithaca, NY, United States) for 30 s before being added to our bioink.

2.3.3. Bioprinting of Neural Tissues Consisting of hiPSC-Derived NPCs and Microspheres

Bioink was prepared prior to printing as previously described. NPCs at a concentration of 1 million cells/mL were thawed and resuspended in the bioink composed of 20 mg/mL of fibrinogen (Sigma, St. Louis, MO, United States), 0.5% w/v of alginate (120,000–190,000 g/mol, M/G ratio 1.56) (Sigma, St. Louis, MO, United States), and 0.3 mg/mL of genipin (Sigma, St. Louis, MO, United States) dissolved in dimethyl sulfoxide (DMSO) (Sigma, St. Louis, MO, United States), along with 0.5 mg of microspheres in tris-buffered saline (TBS) with phenol red (Sigma, St. Louis, MO, United States) when appropriate. A 15 mL

conical tube containing NPCs, bioink and when appropriate microspheres was connected to the "Material 1" channel of the Lab-On-The-Printer (LOP^{TM}) printhead (Aspect Biosystems, Vancouver, BC, Canada) shown in **Figure 2.1A**. The crosslinker was comprised of 20 mg/mL of calcium chloride (Sigma, St. Louis, MO, United States), 0.075% w/v of chitosan (Sigma, St. Louis, MO, United States), and 1.7 U/mL of thrombin (Sigma, St. Louis, MO, United States) in a conical connected to the crosslinker channel. Cross-linking occurs at the junction of the bioink and crosslinker channels in the printhead (**Figure 2.1A**). Genipin was included in the bioink solution to avoid cross-linking of the chitosan present in the cross-linker solution before printing. Dome shaped constructs shown in **Figures 2.1D,E** were bioprinted based on the specifications detailed in the relevant CAD file (**Figure 2.1B**) generated using Aspect's studio software (V1.2.59.0, Aspect Biosystems, Vancouver, BC, Canada) using a rectilinear infill pattern in a repeated layer by layer fashion. The resulting constructs consisted of 6 deposited layers of cell laden bioink. Specific pressures are applied to each channel to monitor the flow rate to provide sufficient time for the crosslinking reaction to occur. The printing speed used was 25 mm/s and pressure for bioink, crosslinker and buffer channels were 50 mbar, 60 mbar, and 100 mbar, respectively. The bioprinted groups included constructs containing guggulsterone microspheres constructs containing unloaded microspheres, and control constructs soluble guggulsterone (SG). The bioprinted constructs were transferred to 12 well cell culture plates (Greiner Bio-One GmbH, Kremsmünster, Austria) coated with PLO and laminin and incubated at 37°C in 5% CO_2.

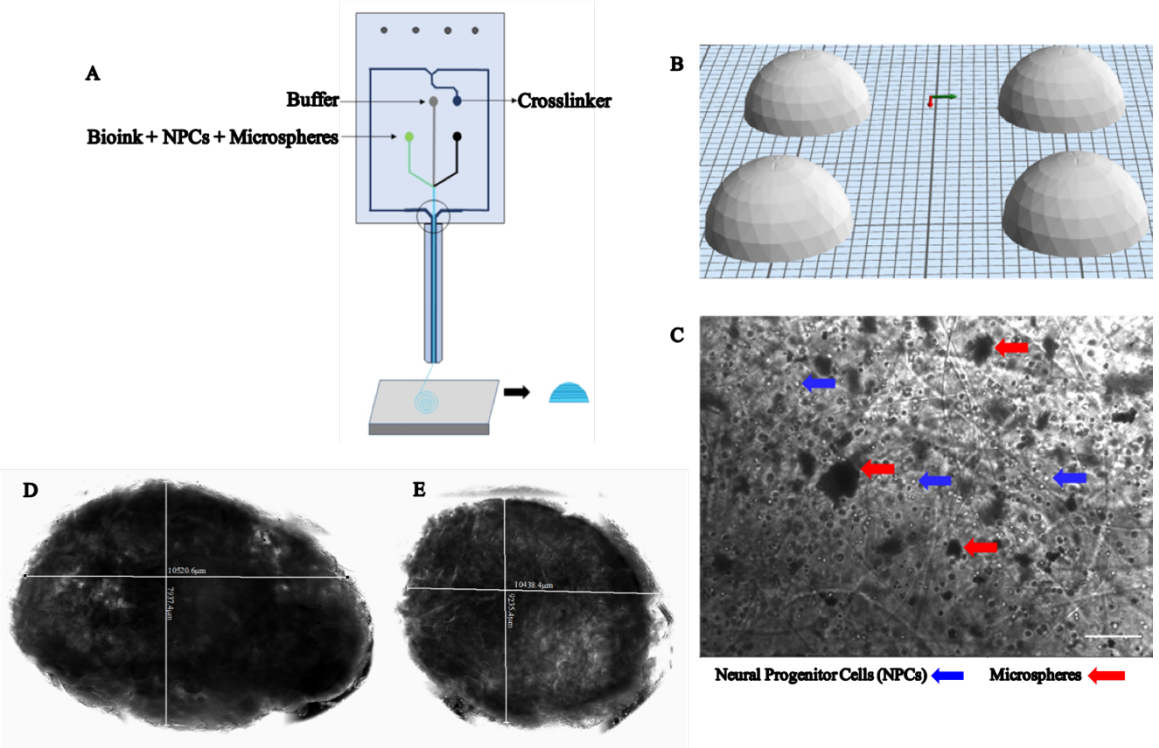

Figure 2.1 The design and printing of a dome-shaped 3D neural tissue structure. **(A)** Schematic representation of Aspect Biosystems' printhead. **(B)** The Computer Aided Design file representing dome structures. **(C)** Phase contrast images of day 0 printed construct showing NPCs and microspheres are dispersed throughout the fibers within the constructs (100 µm). Top-down light microscopy image of bioprinted dome shaped construct consisting of neural progenitor cells (NPCs) with bioink containing encapsulated guggulsterone microsphere **(D)** Image showing the side view of a bioprinted dome and **(E)** showing bottom view of the construct Scale bar for (D, E) represent 10,000 µm.

2.3.4. Culture of Bioprinted Constructs

The bioprinted constructs were initially cultured in STEMdiff™ Neural Progenitor Media (NPM) (STEMCELL™ Technologies, Vancouver, BC, Canada), on cell culture plates

coated with poly-L-ornithine (PLO, Sigma, St. Louis, MO, United States), and laminin (Sigma, St. Louis, MO, United States). with 1% Antibiotic Antimitotic Solution (AAS) (Sigma-Aldrich, St. Louis, Missouri, United States) for the first 10 days after printing. This media contains both epidermal growth factor and basic fibroblast growth factor to promote proliferation of hiPSC- derived NPCs. On day 10, the NPM was replaced by STEMdiff™ Neural Induction Medium [116] (STEMCELL™ Technologies, Vancouver, BC, Canada) with 1% AAS to promote maturation of the hiPSC-derived NPCs toward mature neurons as it contains the small molecules SB431542, LDN193189, and rock inhibitor Y-27632. On day 20, the NIM was replaced by Brain Phys Neuronal Medium (STEMCELL™ Technologies, Vancouver, BC, Canada) for all groups to promote further maturation of these bioprinted tissues. The media changes were performed after every 2 days by replacing 50% of media for the first 30 days of culture. Phase contrast imaging was performed with a Leica DMI3000B (Leica Biosystems, Wetzlar, Germany) microscope a QImaging RETIGA 2000R camera (QImaging, Surrey, BC, Canada) at 10X magnification. Imaging of whole bioprinted construct was performed using the Cytation 5™ Gen5 imager and its associated software version 3.05 (BioTek instruments, Winooski, VT, United States).

2.3.5. Assessment of Cell Viability Post Printing

The bioprinted constructs were degraded using the Neural Tissue Dissociation Kit-Postnatal Neurons (Miltenyi Biotec GmbH, Bergisch Gladbach, Germany) in combination with gentleMACS™ Dissociator (Miltenyi, Biotec GmbH, Bergisch Gladbach, Germany) on day 1 and 7 to obtain single cell suspensions for analysis. This process utilizes an optimized combination of enzymatic and mechanical degradation to obtain single cell

suspensions. The bioprinted constructs were transferred from each group in to gentleMACS C-tube (Miltenyi Biotec GmbH, Bergisch Gladbach, Germany), from 12 well plate and later, wells of plate were washed with 1960 µL of Enzyme Mix 1 and then that enzyme added into the gentleMACS C-tube. Later, a tightly closed C tube was attached upside down on to the sleeve of gentleMACS Dissociator. Subsequently, the optimized, pre-set gentleMACS program m_brain_01 was run twice on Dissociator for 30 sec each and then constructs incubated for 20 min at 37°C. 45 µL of Enzyme Mix 2 was added to C-tubes and the pre-set gentleMACS program m_brain_02 was run twice for 30 sec each and incubated for 20 min at 37°C then finally, pre-set gentleMACS program m_brain_03 was run twice for 1 min each. Lastly, 2 mL of Fetal Bovine Serum (FBS) (Gibco^{TM}, Thermo Fisher Scientific, Waltham, MA, United States) was added to the mixture to quench the enzymatic reaction and then the cell suspension was run through a 37 µm strainer (STEMCELL^{TM} Technologies, Vancouver, BC, Canada) and centrifuged at 300 × *g* to pellet the cells. The supernatant was removed, and the pellet was resuspended in 1 mL of phosphate buffered solution (PBS) (Thermo Fisher, Waltham, MA, United States). 20 µL of the cell suspension was mixed with 380 µL of Guava ViaCount reagent® (Millipore, Burlington, MA, United States). 100 µL of this mixture was added to the individual wells of the 96-well plate and cell viability was determined using the Guava EasyCyte HT flow cytometer (Millipore, Burlington, MA, United States).

2.3.6. Characterization of Bioprinted Constructs by Immunocytochemistry

Immunofluorescent staining was performed to assess the cell markers expressed by the bioprinted constructs on day 15 and 30. The constructs were fixed with 10% formalin at

4°C for 2 h then permeabilized with 0.1% Triton X (Sigma, St. Louis, MO, United States) at 4°C for 45 min and blocked with 5% Normal Goat Serum (Sigma, St. Louis, MO, United States) and incubated at 4°C for 2 h at 2 rpm on the shaker (The Belly Dancer® orbital shaker) (Sigma-Aldrich Canada Co., Oakville, ON, Canada). The constructs then were incubated with the primary antibody FOXA2 (1:400, AbCam, Eugene, OR, United States) and anti- β-tubulin III (TUJ1) (1:400, Sigma-Aldrich Canada Co., Oakville, ON, Canada) after 15 days of culture. For day 30 constructs, the primary antibodies used were tyrosine hydroxylase (TH) (1:400, Pelfreeze, Arkansas, United States) and TUJ1 (1:400, Sigma-Aldrich Canada Co., Oakville, ON, Canada). The constructs were incubated at 4°C overnight at 100 rpm following three washes with PBS for 15 min at 4°C. Secondary antibodies Alexa Fluor 568 Donkey Anti-Mouse (1:500, AbCam, Eugene, OR, United States), and Alexa Fluor 488 Donkey Anti-Rabbit (1:400, AbCam, Eugene, OR, United States) diluted in PBS were added to the constructs. Later, those incubated for an 1 h at room temperature and 3 h at 4°C on the shaker. After incubation with the secondary antibody, cells were washed in PBS three times for 15 min at 2 rpm on the shaker. The cells were counterstained with DAPI (4′,6-diamidino-2-phenylindole) nucleic acid stain (Thermo Fisher Scientific, Waltham, MA, United States). 300 μL of 300-nM DAPI solution in PBS was added to the cultures after the final wash and incubated for 3 min, followed by rinsing with PBS. The bioprinted constructs were then visualized with FIPS – Zeiss Confocal Laser Scanning Microscope ("Objective: 0," Immersion = "Air," Model = "EC Plan-Neofluar 20 × /0.30 M27"; Carl Zeiss Microscopy GmbH, Jena, Germany). The excitation and emission wavelengths used for detecting Alexa Fluor 488 were 479 nm and 519 nm and for detecting Alexa Fluor 588 were 580 nm and 602 nm. The pixel size for 10

× were 1040 × 1040 and 20 × was 710 × 532. The interval used is 10 microns with 20–30 slices in the z stack.

2.3.7. Characterization of Bioprinted Constructs by Flow Cytometry

Bioprinted constructs were analyzed at day 30 using flow cytometry for the following markers: β-tubulin III (βT-III) (TUJ1) (R&D systems, Minneapolis, MN, United States). O4 (oligodendrocytes progenitor marker) (R&D systems, Minneapolis, MN, United States), Anti-Tyrosine Hydroxylase (TH) antibody (AbCam, Eugene, OR, United States), and GFAP (glial fibrillary acidic protein) (AbCam, Eugene, OR, United States) (a mature marker for astrocytes). The bioprinted constructs were degraded and the resulting cell suspension was processed as previously reported in see section "Assessment of Cell Viability Post Printing." Briefly, the cell suspension was washed three times with PBS by centrifuging at 300 *g* for 5 min. The cell suspension was then fixed and stained per the manufacturer's instructions (R&D Systems, Minneapolis, MN, United States). Isotype controls consisted of mouse IgG2A PerCP-conjugated Isotype control (R&D systems, Minneapolis, MN, United States), normal mouse IgM PE-conjugated Control (R&D systems, Minneapolis, MN, United States) and mouse IgG2b, kappa monoclonal [7e10g10] – Isotype control (AbCam, Eugene, OR, United States). The analysis was performed using the Guava EasyCyte HT flow cytometer (Millipore, Burlington, MA, United States).

2.3.8. Characterization of Bioprinted Constructs by Quantitative Reverse Transcriptase Polymerase Chain Reaction (qPCR) Analysis

Total RNA was isolated from the bioprinted constructs using an RNeasy Plus Mini kit according to manufacturer's instructions (Qiagen, Hilden, Germany). RNA content and quality as indicated by the A260/A280 ratio was measured using a NanoVue Plus (GE

Healthcare, Chicago, IL, United States). Only samples with an A260/A280 ratio over 1.8 were used. One step PCR was performed on the isolated RNA as per manufacturer's instructions for the QuantiTect SYBR Green Master Mix (204243, Qiagen, Hilden, Germany). RNA isolated from the bioprinted tissues was added to the individual wells of 96 well plates containing reaction mix. This procedure included a reverse transcriptase step followed by the PCR reaction. PCR reactions were performed in triplicates using the relevant QuantiTect Primer Assay or primers in combination with QuantiTect SYBR Green master mix to determine the levels of gene expression. mRNA levels were quantified using the primers for the following genes: Glyceraldehyde-3-phosphate dehydrogenase (*GAPDH* – served as our housekeeping gene, Eurofins Genomics, Luxembourg City, Luxembourg). β-tubulin III (*Tubb3* – plays important roles in axon guidance and maintenance, Qiagen, Hilden, Germany), tyrosine hydroxylase (*TH* – encodes the enzyme tyrosine hydroxylase, Qiagen, Hilden, Germany), nuclear receptor subfamily 4, group A, member 2 (*Nr4a2* also known as *Nurr1,* – plays a role in the differentiation and maintenance of meso-diencephalic dopaminergic neurons, Qiagen, Hilden, Germany), Paired box protein 6 (*PAX6* – promotes neural stem cell proliferation, Qiagen, Hilden, Germany), *LMX1B* (Qiagen, Hilden, Germany) using an Applied Biosystems StepOnePlus Real-Time PCR System (Foster City, CA, United States). Information on the primer assays used can be founded in **Supplementary Table S1**.

2.3.9. Statistical Analysis

Results are presented as the mean values ± standard deviation. Statistical analysis was performed on viability, flow cytometry and qPCR using the one-way ANOVA followed

by Tukey's *post hoc* analysis using GraphPad prism 5 statistics software with $p < 0.05$ (95% confidence level) indicating minimal significance.

2.4. Results

2.4.1. Generation of Bioprinted Constructs Containing NPCs and Microspheres

Three different types of dome shaped bioprinted constructs containing healthy hiPSC-derived NPCs were printed from the corresponding computer aided design [17] file: NPCs only treated with guggulsterone in the media as a positive control referred to as SG, NPCs along with blank microspheres as a negative control referred to as UM, and NPCs along with guggulsterone releasing microspheres referred to as GM. The constructs showed a homogenous distribution of both NPCs and microspheres after printing (**Figure 2.1C**). Phase microscopy of the whole constructs showed maintenance of the dome shape post-printing. The structure comprised of 1 cm diameter – dome shape with six layers of fibers with an average width of ~1.1 cm and height ~ 0.7 cm (**Figures 2.1D,E**). Further phase microscopy imaging of the construct on day 1 revealed that the cells and microspheres were spread consistently throughout the construct for all culture conditions (**Figure 2.2**). While these images only represent the dispersity throughout the whole construct in the x-y-direction, but we observed similar distributions at various layers using phase microscopy, suggesting an even distribution throughout the construct.

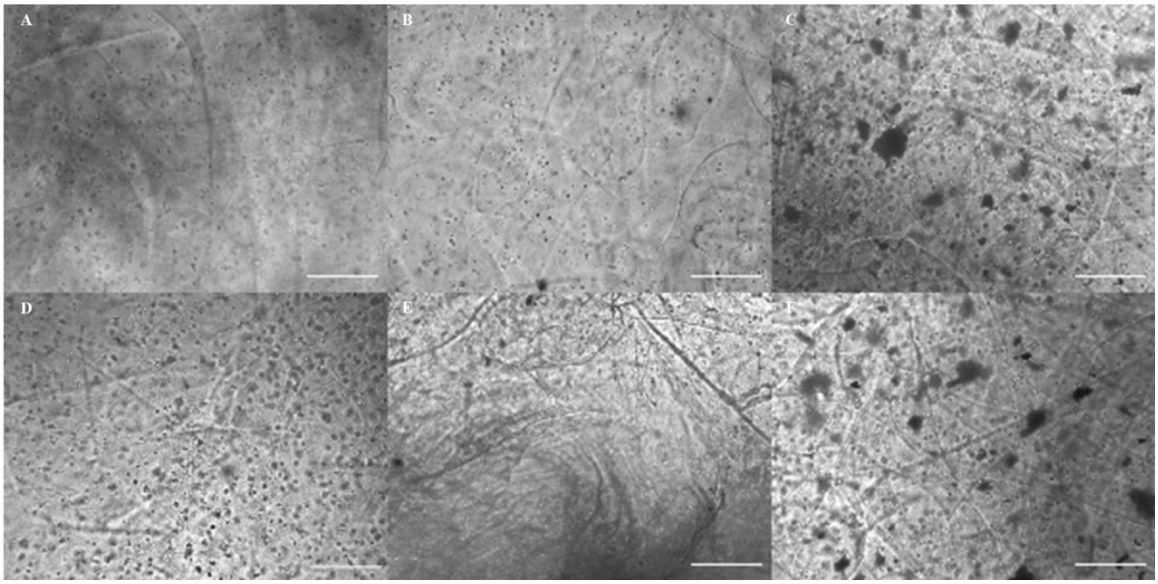

Figure 2.2 Phase contrast imaging of bioprinted constructs treated with soluble guggulsterone (SG) at **(A)** Day One and **(D)** Day 7, bioprinted constructs containing unloaded microspheres (UM) at **(B)** Day 1 and **(E)** Day Seven, and guggulsterone microspheres (GM) at **(C)** Day One and **(F)** Day Seven. Scale bars represent 50 μm.

2.4.2. Cell Viability Analysis of the Bioprinted Tissues

Cell viability of post-printed NPCs was quantified after days 1 and 7 of culture *in vitro* (**Figure 2.3**). Constructs from all groups showed high viability 1-day post-printing: GM (92 ± 3%), UM (78 ± 11%), SG (89 ± 2%), with no statistical significance between groups observed. The GM group exhibited the highest level of viability on day 7 (98 ± 1%) in comparison with the other two groups (UM – 94 ± 2% and SG – 91 ± 2%). Overall, all groups exhibited high levels of viability post printing. The data is reported as the mean ± S.D (∗∗$p < 0.01$ by one-way ANOVA and Tukey post hoc test for significance between samples).

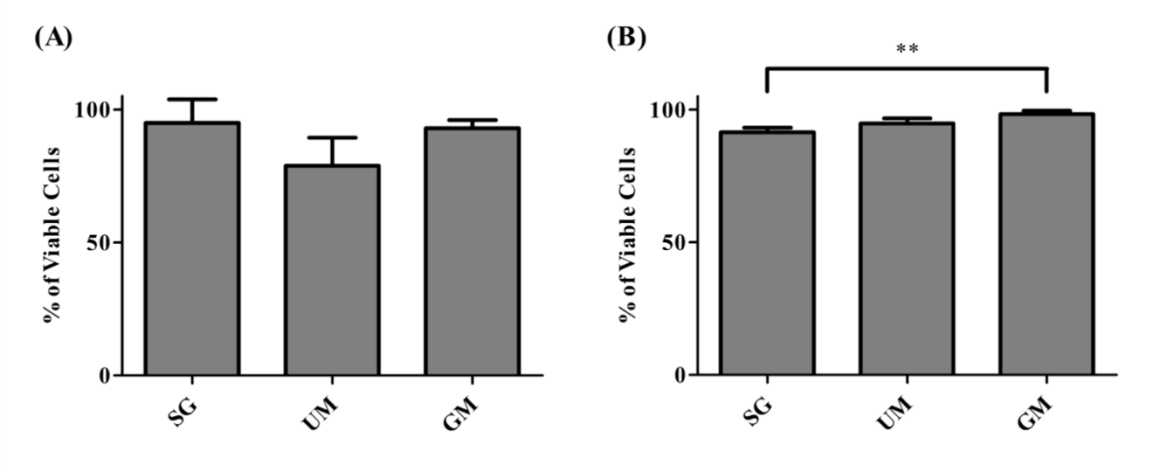

Figure 2.3 Cell viability analysis for all groups, including the bioprinted constructs treated with soluble guggulsterone (SG), constructs containing unloaded microspheres (UM) and constructs containing guggulsterone microspheres (GM) determined at **(A)** Day 1 and **(B)** Day 7 after being bioprinted. Data is reported as the mean ± S.D (n = 3.** = $p < 0.01$ by one-way ANOVA and Tukey post-hoc test for significance between samples).

2.4.3. Immunocytochemistry Analysis of the Bioprinted Tissues

ICC was performed on constructs for all three groups for the cellular markers TUJ1 (an immature neuronal maker) and FOXA2 (a midbrain-type dopamine neuron marker) at day 15 (**Figure 2.4**) and on day 30 for TUJ1 and TH (an enzyme expressed by dopaminergic neurons) (**Figures 2.5, 2.6**). All constructs stained positive for varying levels of TUJ1 and FOXA2 on day 15. Similarly, all constructs expressed TUJ1 on day 30 with the GM and SG tissues expressing TH as well.

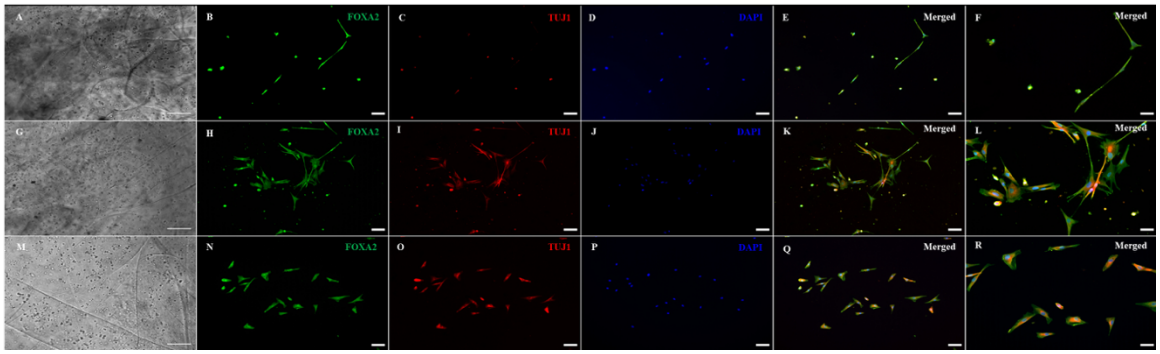

Figure 2.4 Immunocytochemistry was performed after 15 days of culture for the following markers: FoxA2 (a marker expressed by midbrain-type dopamine neurons shown in green), TUJ1 (an early marker for neurons shown in red), and the nuclear stain DAPI, (4',6-diamidino-2-phenylindole shown in blue). **(A–E)** shows bioprinted tissues treated with soluble guggulsterone (SG), **(F–J)** shows bioprinted tissues containing unloaded microspheres (UM), and **(K–O)** shows bioprinted tissues containing guggulsterone microspheres (GM). The scale bar is 100 μm.

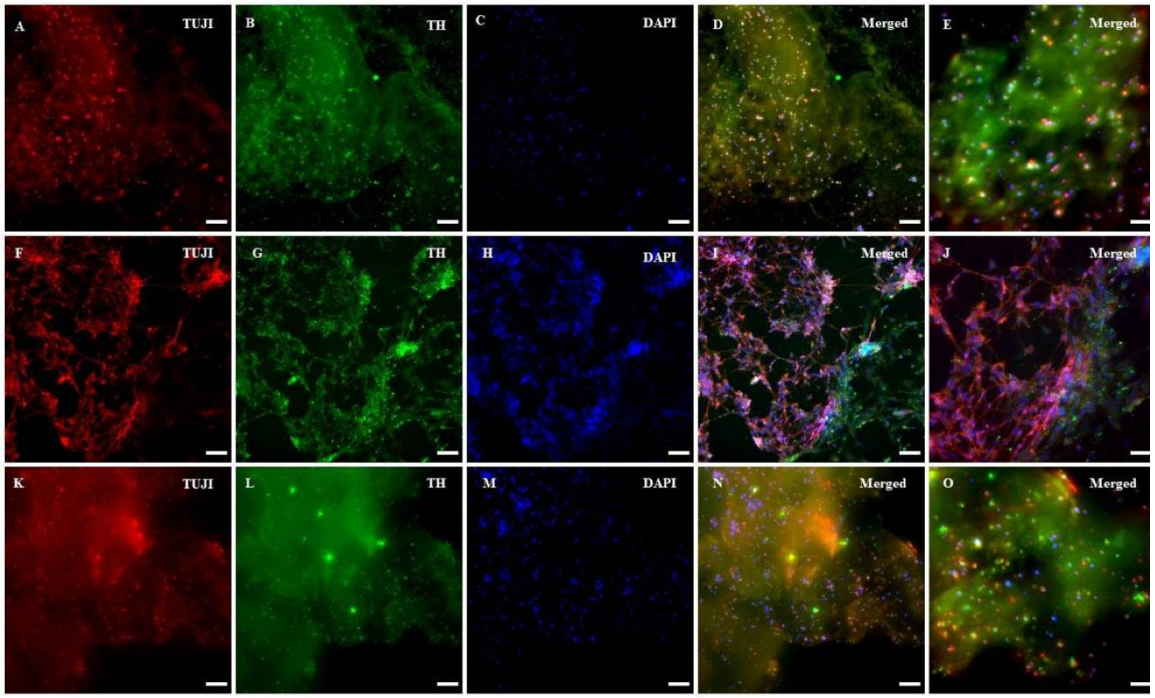

Figure 2.5 Immunocytochemistry was performed after 30 days of culture on cell that migrated out of the bioprinted constructs for the following markers: TUJ1 (an early marker for neurons shown in red), TH (a dopaminergic neuron marker shown in green), and the nuclear stain DAPI shown in blue. **(A–D)** shows bioprinted tissues treated with soluble guggulsterone (SG), **(E–H)** shows bioprinted tissues containing unloaded microspheres (UM), and **(I–L)**

shows bioprinted tissues containing guggulsterone microspheres (GM). The scale bar is 100 μm.

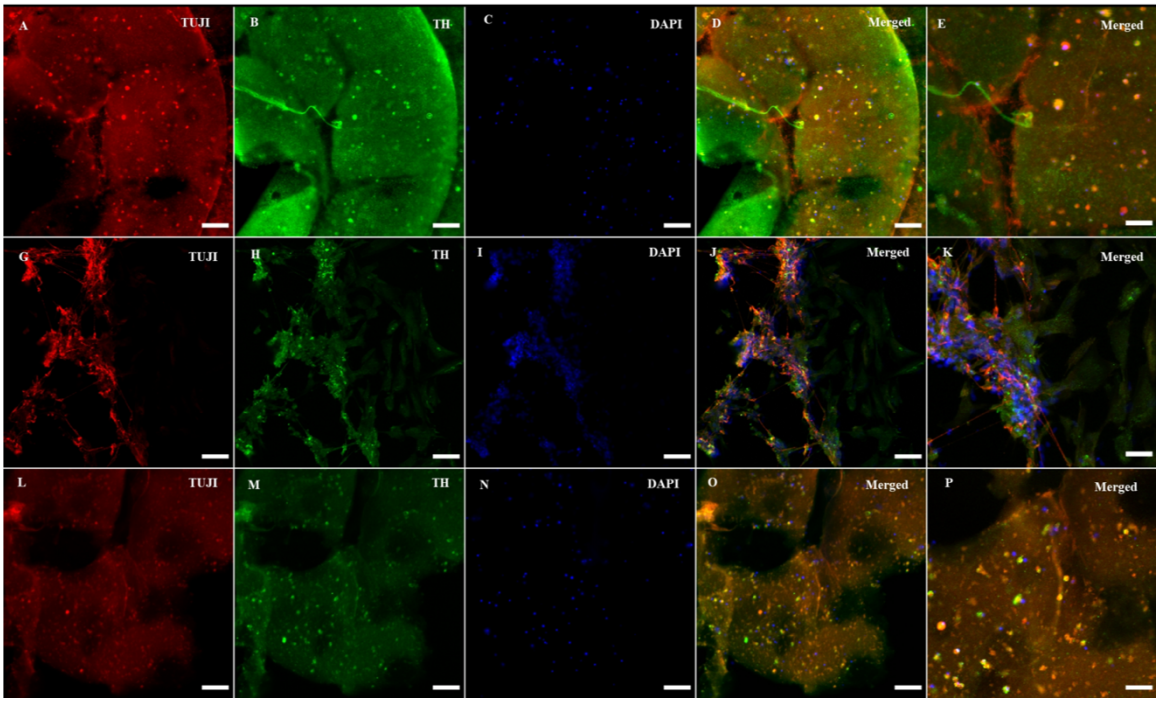

Figure 2.6 Immunocytochemistry was performed after 30 days of culture on the cells embedded in different layers of bioprinted constructs for the following markers: TUJ1 (an early marker for neurons shown in red), TH (a dopaminergic neuron marker shown in green), and the nuclear stain DAPI shown in blue. **(A–D)** shows bioprinted tissues treated with soluble guggulsterone (SG), **(E–H)** shows bioprinted tissues containing unloaded microspheres (UM), and **(I–L)** shows bioprinted tissues containing guggulsterone microspheres (GM). The scale bar is 100 μm.

2.4.4. Flow Cytometry Analysis of the Bioprinted Tissues

Flow cytometry was performed to quantify the percentage of cells expressing the following markers: TUJ1, TH, glial fibrillary acidic protein (GFAP, marker expressed by astrocytes), and O4 (an oligodendrocyte marker) on day 30 (**Figure 2.7**). Expression of TUJ1 was significantly higher for the GM tissues (15 ± 1%), followed UM (4 ± 1%), SG (3 ± 1%). Accordingly, expression of TH was the highest for the GM tissues (8 ± 1%), followed by the SG group (7 ± 1.0%) and then UM group has the lowest expression level (4 ± 1%).

GFAP expression was the highest for the GM group (15 ± 4%) followed by the UM group (6 ± 1%), with the SG group having the lowest expression levels (3 ± 1%). Finally, both the GM and UM groups had similar levels of O4 expression (5 ± 1%) compared to SG (3 ± 1%). Overall, the guggulsterone microspheres promoted more mature differentiation of the bioprinted NPCs seeded inside of our engineered tissues. The data is reported as the mean±SD (n=3;*p<0.05,**p<0.01,***p<0.001by one-way ANOVA and Tukey post hoc test for significance between samples for all groups.

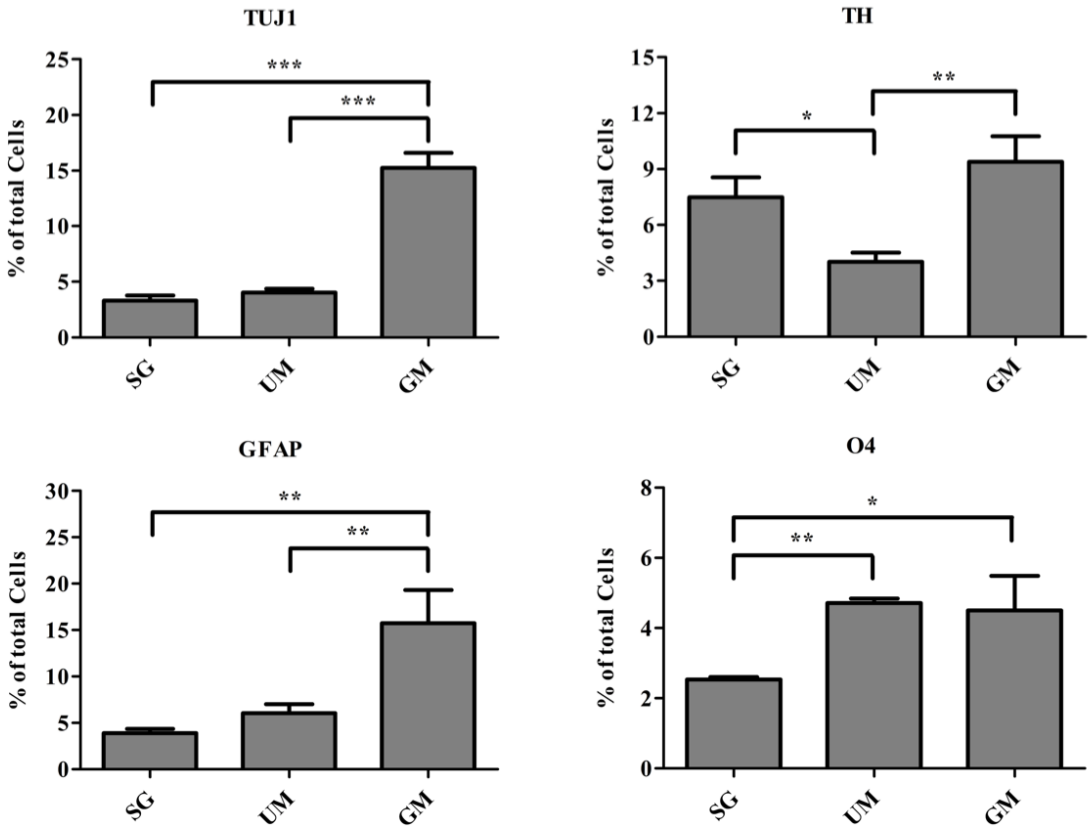

Figure 2.7 Quantitative flow cytometry assessment of the cell types present on day 30 in the bioprinted constructs treated with soluble guggulsterone (SG), bioprinted constructs containing unloaded microspheres (UM), and bioprinted constructs containing guggulsterone microspheres (GM) for the following markers: TUJ1 (an early marker for neurons), tyrosine hydroxylase (TH, a dopaminergic neuronal marker), glial fibrillary acidic protein (GFAP, a protein expressed by astrocytes), O4 (a marker expressed by oligodendrocytes). Data is reported as the mean ± SD (n = 3; *p < 0.05, **p < 0.01,

***p < 0.001 by one-way ANOVA and Tukey post hoc test for significance between samples for all group

2.4.5. QPCR Analysis of the Bioprinted Tissues

Quantitative polymerase chain reaction was performed to analyze the gene expression levels present in our three different groups of bioprinted tissues on day 30 and the gene expression levels were normalized to the positive control – soluble guggulsterone in the media (**Figure 2.8**). Both sets of tissues containing microspheres showed increased levels of *TUBB3* (gene encoding for *TUJ1*) in comparison to the tissues treated with soluble guggulsterone as well reduced levels of *NR4A2* (Nurr1) (dopaminergic neurotransmitter phenotype gene). Interestingly, both the SG and GM groups showed higher levels of TH RNA in comparison to the UM group. The tissues showed decreased LMX1B expression in comparison to the tissues treated with soluble guggulsterone. Finally, the GM group also exhibited the highest levels of PAX6 RNA (a neural progenitor marker).

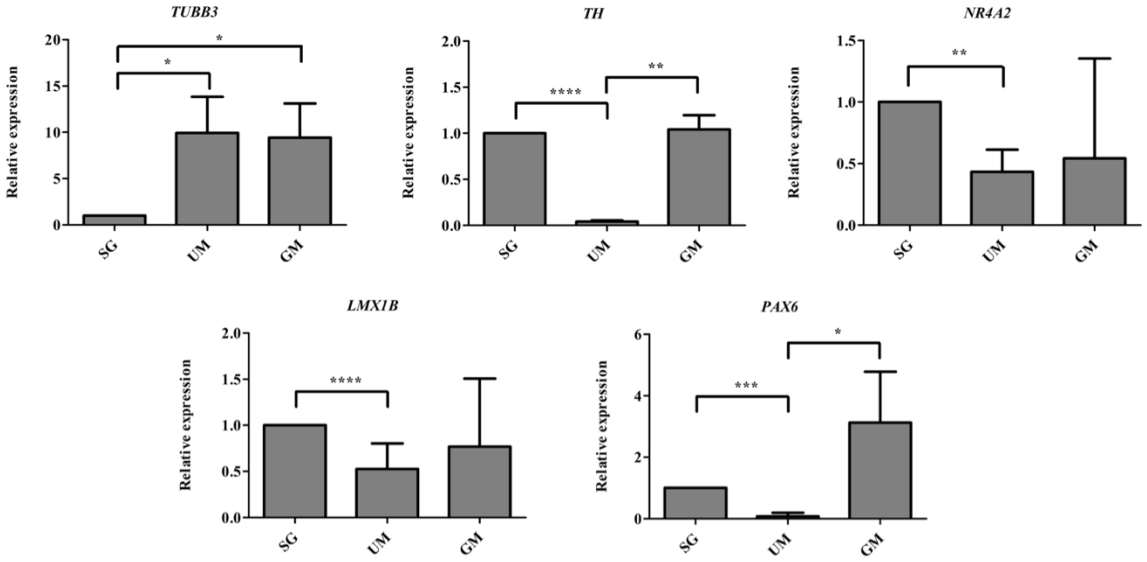

Figure 2.8 qPCR was performed on Day 30 to determine the relative gene expression levels of the following neurodevelopmental genes: b-tubulin III (Tubb3), tyrosine hydroxylase (TH), nuclear receptor subfamily 4, group A, member 2 (Nr4a2 also known as Nurr1), LIM homeobox transcription factor 1b (LMX1B), Paired box protein 6 (PAX6). Gene expression levels were normalized to GAPDH and then to levels expressed the bioprinted constructs treated with soluble guggulsterone (SG). Data is reported as the mean ± SD (n = 3; *p < 0.05, **p < 0.01, ***p < 0.001, ****p < 0.0001 by one-way ANOVA and Tukey post hoc test for significance between samples).

2.5. Discussion

3D bioprinting combines cells with biocompatible materials to create 3D structures with defined micro and macro architectures [18]. In comparison to traditional 2D cultures, 3D bioprinted tissues provide an improved platform for mimicking tissues *in vitro*. In particular, 3D structures can replicate the influence of the microenvironment on cell growth as well as cell-cell and cell-matrix interactions [117]. Such bioprinted microenvironments can promote the differentiation of hiPSC-derived NPCs into mature, electro-physiologically active neurons. Our group has engineered 3D bioprinted hiPSC-derived neural tissue that mimics spinal cord tissue by treating these tissues with a variety of small molecules [26]. While these 3D bioprinted constructs show promise as an *in vitro* neural tissue models, there is still significant room for improvement. Traditional neural differentiation methods require supplementing media with small molecules and growth factors is the conventional technique for inducing neural differentiation. Incorporating drug releasing microspheres in our bioinks can improve the differentiation efficiency of the cells inside while minimizing the number of media changes. As such, our 3D bioprinted constructs could be improved by increasing distribution of differentiation factors within the bioinks. 3D bioprinted constructs containing microspheres and compared their properties to pure bioprinted hydrogels and found incorporation of microspheres enhanced cell viability in the 3D constructs [76]. The goal of this study was to improve functional maturation of 3D printed neural tissue models by incorporating drug releasing microspheres in our bioink. In particular, the incorporation of guggulsterone releasing microspheres in our bioink was evaluated as a method to induce cells to differentiate toward a dopaminergic neuronal fate. 3D printing enables the generation of objects with

geometric structures that would be difficult to produce using traditional tissues engineering methods. In the present study, we have focused on bioprinting of dome-shaped constructs containing NPCs to produce a functional tissue with a homogeneous distribution of cells throughout the construct so they can interact in three dimensions. Additionally, this shape more accurately replicates the microenvironment in the brain compared to cross-hatched structures printed in previous studies [24]. Finally, our dome-shaped constructs possessed a porous structure that enabled transfer of nutrients and oxygen, allowing the long-term culture of cells *in vitro*.

First, we successfully bioprinted NPCs in combination with drug releasing microspheres containing guggulsterone to create a complex tissue model the using Aspect Biosystems RX1 bioprinter. Phase contrast microscopy revealed that post printing cells are homogenously placed with microspheres throughout the fibers in different layers (**Figure 2.1C**). Most of the researchers focused on bioprinting neural stem cells (NSCs) with different biocompatible materials and differentiating them with several factors in to mature neurons and glial cells [18]. While previous research using our bioink showed high cell viability post printing [16, 26], the effect of the addition of microspheres had not been studied. Here we investigated bioprinting NPCs along with guggulsterone releasing microspheres for generating tissues containing mature neurons. The bioprinted tissues containing NPCs showed high levels of viability on both day 1- and 7-day post printing. Cell viability for GM and SG was 92% and 94%, respectively, 1 day post printing while the UM group had 78% cell viability. These percentages are higher than those reported by Gu et al. (2016) where immediately after printing using a bioink made up of alginate, carboxymethyl chitosan and agarose 25% of frontal cortical human NSCs died.

Additionally, Joung et al. (2018) reported the cell viability of spinal NPCs printed in hydrogel matrices consisting of gelatin methacrylate (GelMa) and gelatin mixed with fibrin ranged from 75 to 88% after 3 h and later decreased to 50% after 1 day. Later, bioprinted iPSC-derived spinal NPCs and oligodendrocyte progenitor cells (OPCs) after 4 days remained 75% viable in a 50% Matrigel bioink. Thus, our bioprinting process preserves cell viability at higher levels than previously reported by other groups.

Cell viability was above 90% for all groups, where GM and UM showed the highest levels of cell viability at 98% and 94%, respectively, and SG showed 91% cell viability on day 7. These percentages are higher than those reported by Salaris et al. (2019) where cell viability of NPCs were 71% after 7 days of culture in a bioink comprised of a Matrigel/alginate solution [118]. De La Vega et al. (2018a) reported the cell viability of hiPSC-derived NPCs as >81%. Additionally, Tan et al. (2016) reported the post printing viability of bioprinted mouse fibroblasts L929 cells with poly (D,L-lactic-co-glycolic acid) (PLGA) microspheres was greater than 90% after 2, 7, and 14 days. They reported that microspheres provide a cushion around the cells for preventing shear stress produced during printing process and post printing. This study has demonstrated that these bioprinted constructs containing microspheres provide a suitable 3D environment for different types of cells to grow. Importantly, our work here corroborates that the addition of microspheres does not negatively affect cell viability within the printed constructs. Furthermore, the increased viability on day 7 suggests that cells adapted to the scaffold microenvironment in the presence of microspheres, which enabled the cells to positively proliferate. The microspheres also became less prominent over time, suggesting that they were being degraded by the presence of cells.

Our 3D bioprinted tissues were cultured for 15 and 30 days *in vitro* for analysis of the tissue composition which longer than done in previous studies where ICC staining was performed after 12 days post printing [32]. 3D bioprinted constructs showed positive staining for the TUJ1 and FOXA2 at day 15 and expression of TH at day 30. FOXA2 was positively expressed in SG, GM, and UM. Several studies have suggested that FOXA2 plays an important role in directing NPCs to differentiate into dopaminergic neurons and its expression is critical for phenotype maintenance, function and survival in this neuronal subtype [11, 41]. Its upregulation in all groups indicates that 3D bioprinted environment enabling NPCs toward the dopaminergic neuron fate (**Figure 2.4**). Zhou et al. (2018) cultured their bioprinted constructs for 12 days to assess the potential of 3D (GelMA)-functionalized dopamine (DA) scaffolds to induce neuronal differentiation and demonstrated significant TUJ1 staining was noted on GelMA and GelMA–DA scaffolds over time. In present study, at day 30, TUJ1 was positively expressed by GM and SG in similar way when compared to UM. Upregulation of TUJ1 in all of our bioprinted tissue conditions suggests cells are adopting moving further toward a neuronal fate. In comparison with UM; SG and GM expressed comparatively more of the TH enzyme that synthesizes dopamine [32], and its upregulation in SG and GM imply the adoption of a dopaminergic fate due to the presence of guggulsterone. Interestingly, in Gu et al. (2017), their bioprinted constructs had expressed mature neuronal markers, such as microtubule associated protein 2 (MAP2), gamma- aminobutyric acid (GABA), and Synaptophysin at day 40 though we did not examine these markers in our current study.

Flow cytometry was performed to quantify observed changes in neural marker expression. Previously, Gu et al. (2016) reported low levels expression of TUJ1 (2%) after 21 days of

differentiation for bioprinted hiPSC-derived NPCs. These levels of TUJ1 expression are significantly higher in our studies at day 30. The expression was observed to be higher in GM tissues when compared to UM and SG tissues, implying the delivery of guggulsterone through microspheres provided the best environment for neuronal differentiation. Interestingly, SG tissues had the lowest expression of TUJ1. It may be that soluble drug did not influence differentiation of cells embedded in the bioink to same extent as the delivery of guggulsterone by microspheres. Previous work from our group has shown how such drug releasing microspheres can promote differentiation of hiPSC-derived NPCs into mature neural tissues [71]. Additionally, the UM group expressing higher levels of TUJ1 than SG implies that the presence of the physical presence of the microspheres can influence differentiation. Previous studies also observed similar expression of TUJ1 in tissues treated with GM and SG. The same study showed that TUJ1 expression was the lowest in conditions lacking both guggulsterone and microspheres (Agbay et al., 2018). Here, we also observed that TH expression was higher in GM and SG groups than in tissues containing UM. This result was expected, as guggulsterone works as an effective inducer of pluripotent stem cell-derived neural stem cells into dopaminergic neurons[68, 69]. Interestingly it was observed that the percentage of cells expressing GFAP – a marker for astrocytes – was highest in the GM group. Previous studies have determined guggulsterone to be a potent inhibitor of the signal transducer and activator of transcription 3 (STAT3) pathway, an intracellular pathway responsible for directing neural progenitors toward an astroglial fate [68].

The results of current studies suggest that NPCs react differently to guggulsterone when grown in a 3D environment. Consequently, this microenvironment assists NPCs to

differentiate into glial fate along with TH positive neurons. Additionally, it was found that UM showed the highest percentage of cells expressing O4, suggesting that PCL microspheres preferably assisted in differentiation toward oligodendrocytes rather than neurons and astrocytes. The tissues containing GM also expressed O4, indicating that these tissues possess all three major neural subtypes – neurons, astrocytes, and oligodendrocytes.

We then used qPCR to confirm the transcriptional profile of 3D bioprinted neural tissue after 30 days. Huang et al. (2017) reported expressions of neural-related genes such as nestin, β-tubulin, and GFAP for NSCs in different hydrogel constructs after 3 days by qPCR. Moreover, Salaris et al. (2019) reported bioprinted constructs cultured for 45 days showed expression of neural progenitor markers such as *PAX6, FOXG1*, and *TBR2,* an astrocyte marker GFAP and mature cortical neuron marker TBR1. However, our study demonstrated *TUBB3 (TUJ1)* expression was observed to be higher in GM tissues alongside UM tissues when compared to SG tissues at day 30. It may be that soluble drug did not induce bioprinted NPCs to express this gene while the incorporated microspheres increased expression. A study by Gu et al. (2017) reported gene expression analysis by qRT- PCR supported by flow cytometry and immunofluorescence post printing 3 weeks showing upregulation of *TUJ1, OLIGO2*, and *GFAP*. TUJ1 was upregulated in previous studies when hiPSCs were differentiated with guggulsterone for deriving dopaminergic neurons (Gonzalez et al., 2013). Similar to the results observed using flow cytometry, the UM groups demonstrated a high expression of *TUBB3* suggests that the microspheres strongly influencing differentiation. Previous studies also confirmed PCL microspheres induced the differentiation of hiPSC-derived NPCs into neurons [71]. Thus, it is possible that the particles present in the bioink influence growth and differentiation of cells.

Increased *TH* expression indicated by GM and SG group suggests that guggulsterone is an effective inducer of neural precursors into dopaminergic neurons. Previous studies indicated the importance of *NR4A2 (Nurr1) and LMX1B* in generation of dopaminergic neurons [72, 119]. Two transcription factors that regulate dopaminergic differentiation *NR4A2 (Nurr1)* and *LMX1B* were also more highly expressed in GM and SG groups than UM. These results indicate that guggulsterone is potentially differentiating NPCs into dopaminergic neurons. The UM group expressed lower levels of *NR4A2 (Nurr1)* and *LMX1B,* which indicates the pivotal role of guggulsterone in inducing the dopaminergic fate in these bioprinted tissues.

The transcription factor *PAX6* is known as a neurogenic determinant in adult NPCs during development, is expressed in selectively populated dopaminergic neurons, and plays a significant role in Parkinson's disease [7, 120]. Higher levels of *PAX6* were observed in GM and SG when compared with the UM group. The GM and SG groups expressed *PAX6,* which implies an increased proliferation of NPCs.

TH, *NURR1,* and *LMX1B* mRNAs were upregulated in the guggulsterone containing group, which suggests that bioprinted NPCs possess dopaminergic fate. 3D bioprinted NPCs with GM and SG positively expressed dopaminergic neuron- enriched transcription regulators *NURR1*, *LMX1B*, FOXA2, and TH. These results were similar to other studies that used guggulsterone to derive dopaminergic neurons from hiPSCs [68]. These results also suggest that the bioprinted tissues containing guggulsterone releasing microspheres possess gene and protein expression profiles similar to those for dopaminergic neurons.

Our results suggested that microsphere incorporated scaffolds could potentially generate dopaminergic neurons and a number of committed differentiated neurons. Once optimized, these 3D bioprinted neural tissues could be used to model neurodegenerative diseases using patient-specific hiPSC lines, as currently done in 2D [29, 43]. This study provides an approach to generate 3D neural tissues containing dopaminergic neurons as a clinically relevant model for drug discovery as well as a potential way to generate tissue to replace the lost neurons that die off during Parkinson's disease.

Our work validates that 3D-printed customizable microsphere-based bioinks can play a positive role in promoting neural differentiation into specific neuronal subtypes while maintaining high levels of cell viability. This work suggests that this technique is promising for enhancing tissue corroborated regeneration in the future. Since a major challenge in transplantation is low cell viability, our bioprinted 3D structures could provide an attractive avenue for the regeneration of cell-specific tissues. The results reported here demonstrate how the controlled release of the bioactive small molecule guggulsterone from microspheres can be used for neuronal differentiation toward dopaminergic neurons when used in combination with hiPSC-derived NPCs. Accordingly, further research could focus on increasing the efficiency of dopaminergic neurons in bioprinted neural tissues, as in previously described protocols, For example, additional microspheres delivering retinoic acid and purmorphamine along with these guggulsterone releasing microspheres could further encourage the growth and maturation of tissues [26]. Additionally, the controlled delivery of other signaling factors could be explored to increase the neuronal efficiency and maturation of 3D bioprinted neural tissues.

2.6. Conclusion

Adding drug releasing microspheres to a novel bioink improves cell survival and differentiation, particularly when engineering tissue from stem cells, to indicate their value as a tool for engineering tissues. Here, we show how the controlled release of guggulsterone from microspheres can enhance the survival of NPCs present in bioprinted tissues as well as their differentiation into mature neural tissues. This work lays the groundwork for producing engineered neural tissues from pluripotent stem cells to serve as a potential tool for high- throughput drug screening.

Chapter 2: Author's contribution

I (Ruchi Sharma, the first author) have come up with the scientific idea for this research objective. I designed the experimental plan, performed, supervised all experimental procedures, and data analysis. I wrote the first draft of the whole paper and shared it with other authors and my supervisor for their review, feedback, and comments. Upon receipt of their feedback, I edited and come up with the final draft version for journal publication. Hereunder, I have given more specific details of all the author's contributions towards this publication. I have fully executed the design and printed the dome-shaped 3D neural tissue structure (figure 2.1) on Aspect Biosystems. Phase contrast imaging of bioprinted constructs (figure 2.2) has been done by me and LDLV (the third author) has assisted me in bioprinting of the constructs. Moreover, I have done cell viability analysis for all three groups (figure 2.3). I performed the ICC procedure and Imke P. M. Smits (the second author) assisted and in experimental set-up and final confocal imaging (figures: 2.4, 2.5, and 2.6). The quantitative flow cytometry assessment (figure 2.7) was done by me and Dr. Willerth assisted me in analyzing results. qPCR was performed by me and I supervised the second author for this too (figure 2.8). C. Lee (the fourth author) assisted with manuscript editing and figure captions. Dr. Stephanie Willerth has provided suggestions and input into the experimental design, provided feedback and supervision on the experimental analysis, as well as written and edited the manuscript.

Chapter 3 Physical and Mechanical Characterization of Fibrin-Based Bioprinted Constructs Containing Drug-Releasing Microspheres for Neural Tissue Engineering Applications[b]

Ruchi Sharma [1], Rebecca Kirsch [1], Karolina Papera Valente [1], Milena Restan Perez, [2] and Stephanie Michelle Willerth [1,2,3,4,5,*]

[1]Department of Mechanical Engineering, University of Victoria, Victoria, BC V8W 2Y2, Canada; ruchis0983@gmail.com (R.S.); beckakirsch2@yahoo.co.uk (R.K.); kvalente@uvic.ca (K.P.V.)
[2]Department of Biomedical Engineering, University of Victoria, Victoria, BC V8W 2Y2, Canada; milenarestan@hotmail.com
[3]Division of Medical Sciences, University of Victoria, Victoria, BC V8W 2Y2, Canada
[4]Centre of Biomedical Research, University of Victoria, Victoria, BC V8W 2Y2, Canada
[5]School of Biomedical Engineering, University of British Columbia, Vancouver, BC V6T1Z3, Canada
*Correspondence: willerth@uvic.ca, Tel: +1-250-721-7303; Fax: +1-250-721-6051

Author Contributions:

Conceptualization, R.S. and S.M.W.; Data curation, R.S., K.P.V. and R.K.; Formal analysis, R.S. and M.R.P.; Methodology, R.S. and K.P.V.; Investigation, R.S., R.K. and K.P.V.; Resources, S.M.W.; Supervision, S.M.W.; Validation, S.M.W.; Visualization, R.S.; Writing—original draft, R.S.; Writing—review and editing, R.K., M.R.P. and S.M.W. All authors have read and agreed to the published version of the manuscript.

[b]The following chapter is from: **Ruchi Sharma,** Rebecca Kirsch, Karolina P. Valente, Milena Restan Perez, and Stephanie Michelle Willerth, "**Physical and Mechanical Characterization of Fibrin-Based Bioprinted Constructs Containing Drug-Releasing Microspheres for Neural Tissue Engineering Applications**" ***Processes*** **9, no. 7: 1205**. **2021**

3.1. Abstract

Three-dimensional bioprinting can fabricate precisely controlled 3D tissue constructs. This process uses bioinks—specially tailored materials that support the survival of incorporated cells—to produce tissue constructs. The properties of bioinks, such as stiffness and porosity, should mimic those found in desired tissues to support specialized cell types. Previous studies by our group validated soft substrates for neuronal cultures using neural cells derived from human-induced pluripotent stem cells (hiPSCs). It is important to confirm that these bioprinted tissues possess mechanical properties similar to native neural tissues. Here, we assessed the physical and mechanical properties of bioprinted constructs generated from our novel microsphere containing bioink. We measured the elastic moduli of bioprinted constructs with and without microspheres using a modified Hertz model. The storage and loss modulus, viscosity, and shear rates were also measured. Physical properties such as microstructure, porosity, swelling, and biodegradability were also analyzed. Our results showed that the elastic modulus of constructs with microspheres was 1032 ± 59.7 Pascal (Pa), and without microspheres was 728 ± 47.6 Pa. Mechanical strength and printability were significantly enhanced with the addition of microspheres. Thus, incorporating microspheres provides mechanical reinforcement, which indicates their suitability for future applications in neural tissue engineering

3.2. Introduction

Three-dimensional bioprinting uses cell-laden bioinks to fabricate tissue constructs, often in a layer-by-layer process [66, 106]. The bioprinting system takes the details provided in a digital file to produce the shape and structure of the bioprinted constructs, which can be used for a variety of applications, such as drug screening and regenerative medicine [103, 116]. The bioinks used should have high biocompatibility, slow degradability, and easily tunable mechanical properties [12]. A biocompatible bioink should result in high cell viability, proliferation, adhesion, migration, and differentiation into mature tissues [107]. The mechanical properties of the bioink play an important role in maintaining the desired tissue shape after bioprinting and influence the behavior of cells seeded inside the bioprinted construct [13, 91, 103, 121]. Moreover, achieving the desired print resolution for the bioprinted con- struct depends on the rheological properties of bioinks [93, 122-124]. Therefore, bioinks should possess appropriate rheological, mechanical, biocompatible, and biofunctional properties for the target tissue [107, 125]. Other important properties that need to be considered when choosing bioinks include the material source (natural or synthetic) and required printing conditions [13, 126].

Often, bioinks are produced from hydrogels, which have exceptionally high water retention abilities that allow for elasticity similar to native tissues [63, 103, 127, 128]. The mechanical integrity and stability of engineered tissues depend upon the hydrogel-based bioinks used during fabrication. The adjustable concentration of biomaterials can appropriately tune the mechanical and rheological properties of hydrogels [23]. It is important to understand the effect of mechanical environment on neurite outgrowth for understanding neural tissue regeneration strategies. When Kayal et al. created

physiologically relevant hydrogel substrates with controlled mechanical cues, the neural cell behavior could be analyzed by both the absolute substrate stiffness value and the underlying stiffness gradient [129]. Their results emphasize the importance of considering substrate stiffness in the development of neural tissue-engineered scaffolds [129]. Given that neural tissues have low mechanical stiffness—with Young′s elastic moduli (E) in the order of 0.1 kilopascal (kPa)—compared to other tissues present in the body [8, 22], it is challenging to measure the mechanical proper- ties using standard techniques, such as atomic force microscopy (AFM), impact indentation, and rheometry because these methods are indirect and require several assumptions that lead to variances in data across groups [22, 23, 94-97, 130, 131]. Such methods use mathematical modeling to correlate experimental measurements, such as displacement and load to stress and strain, to evaluate elastic modulus [23]. Alternatively, some researchers have directly measured the rheological properties of white and gray matter using indentation experiments on various regions of the brain, such as the midbrain, cerebrum, and thalamus [1, 132]. They have demonstrated that simple indentation experiments require a much smaller portion of tissue compared to standard rheological tests. The indention method consistently produced robust measurements, which indicated that the white matter tissue was approximately one third stiffer than gray matter tissue. These studies validated the use of indentation methods to interpret the mechanical properties of neural tissues [1, 22, 23, 96, 101, 105, 131-133].

Previous studies suggested that stem cell differentiation is affected by the substrate's elasticity. Additionally, neural stem cells (NSCs) preferentially differentiate into the neural phenotype in soft substrates (~0.1–0.5 kPa), while glial phenotypes are predominant in stiffer substrates (~1–10 kPa) [99, 134, 135]. Sundararaghavan et al. investigated the

mechanical stiffness of neuronal scaffolds in a 3D collagen gel that contained a durotactic gradient. They found that seeded dorsal root ganglion cells responded to their environment by growing longer along the stiffness gradient [85]. Thus, the stiffness of the biomaterial should be tuned to match that of the native tissue to obtain applicable cell activity including cell differentiation, adhesion, proliferation, and migration [87]. Viscoelasticity—a material's elastic and viscous response to stress—is another important parameter to consider when working with bioinks. Living tissues have both elastic and viscous components, and the mechanical behavior of such materials is referred to as viscoelastic. Viscoelasticity can be measured by a rotational rheometer, which gives information about the storage (G′) and loss modulus (G″) [136]. G′ refers to the ability of the hydrogel to store deformation energy in an elastic manner, which gives information about shape retention related to the extent of crosslinking. A higher degree of crosslinking results in a larger G′. G″ represents the hydrogel's viscous flow and ability to dissipate energy [19, 137]. When G″ is greater than G′, the bioink exists in a liquid-like state, which assists its extrusion, but sacrifices print fidelity. When G′ is greater than G″, the material assumes a more solid state, which is favorable for print fidelity but triggers nozzle clogging and nonuniform fibers. Hence, G′ and G″ are important parameters for understanding the properties of the bioink and, accordingly, selecting a bioprinting modality [58].

Another key factor during the printing process is maintaining cell viability, which is influenced by the viscoelasticity and gelation of the bioink [124, 137]. An increase in viscoelasticity and gelation increases shear stress, which can alter the differentiation of stem cells and cell signaling and cause cell death by disrupting membrane integrity [17,

107, 116, 138]. The bioink's viscosity—resistance of a fluid to flow—also plays a significant role in cell viability.

Low viscosity bioinks increase cell viability but often decrease the printed construct's fidelity [123], while bioinks with high viscosity have high structural fidelity but can result in more cell damage and death [139]. The bioink's viscosity can be modified by incorporating biological factors, drug-delivery carriers, nanomaterials, and combinations of biopolymers to improve their mechanical properties [63, 80]. Furthermore, different bioprinters support different bioink viscosities. Efficient bioinks can allow the production of standardized printed constructs with controlled shapes and sizes. These bioinks should also facilitate printing with high fidelity and flexibility to acclimatize the flow and diffusion of nutrients as well as the movement of cells [77]. Additionally, swelling and degradation rates are other important properties of bioinks. An ideal bioink should degrade in a controlled way by creating space for new tissue [109, 128, 140]. Swelling is an intrinsic property of hydrogels as these gels expand due to solvent penetration into void spaces between the polymeric chain network. In the context of 3D bioprinting, the swelling degree also refers to a change in the dimensions of the bioprinted constructs [75, 141, 142]. The swelling ratio is an important parameter which controls the release patterns of drugs from these polymeric networks [75, 143, 144]. Research led by Daikuara et al. found the swelling ratio of bioink at pH 5 (8.2% ± 0.3) and pH 7.4 (8.6% ± 0.5). The swelling capacity of the printed construct was not affected by pH or the addition of platelet lysate, since platelet lysate and gelatin methacryloyl (GelMA) presented almost analogous swelling behaviors. GelMA is a semi-synthetic hydrogel that is similar to the extracellular matrix of

native tissues and made up of gelatin derivatized with methacrylamide and methacrylate groups [145].

Another interesting study discussed the effect of liver decellularized extracellular matrix (dECM), which is an extracellular matrix of tissues from its native environment that has emerged as a biomaterial that preserves a tissue's native environment, promotes cell proliferation, and provides cues for cell differentiation [146]. When the liver dECM was added to GelMA, its swelling ratio notably increased. This research also found that the swelling ratio of GelMA with dECM hydrogel is about 932%, which is much larger than that of GelMA hydrogel (about 644%) [141]. Furthermore, porosity is also an important factor for bioprinted constructs since interconnected pores can facilitate better penetration and migration of cells [8, 88, 103]. Porous constructs are relevant since they enable the diffusion of nutrients and gases as well as the removal of metabolic waste [24, 88, 142]. Mansouri et al. synthesized 3D porous, graphene-polymer scaffolds that have improved stability in aqueous media and neuronal cell interactions using a reducing agent [88]. The stability of a 3D structure depends on the flow behavior of the hydrogel. Hydrogels mostly exhibit a non-Newtonian behavior where they have a nonlinear relationship between their shear stress and rate [58]. Hydrogels are mostly shear-thinning, meaning their viscosity decreases as shear rate increases [19, 58]. The shear-thinning property of a bioink permits easy extrusion from the printing nozzle. Thixotropy is a time-dependent shear-thinning property that allows bioinks to return almost instantly to a gel state [58]. A fast gelation process also facilitates the deposition of layer-upon-layer while preserving the shape of the bioprinted construct for achieving a complex and high resolution structure. Hence, the

optimal composition of the biomaterial should be chosen in consideration of its shear-thinning properties [77, 103, 116].

We have designed and validated our fibrin-based bioink incorporated with drug- releasing microspheres for creating functional neural tissues from hiPSC-derived NPCs in our previous works [27, 28]. hiPSCs are especially relevant to neural tissue engineering since brain cells from patients are rarely available for research. hiPSC-derived neural tissues could become a powerful diagnostic and prognostic tool for drug screening [25, 28, 55]. Additionally, bioinks can efficiently mimic the extracellular matrix found in brain tissue. Our bioink has 20 mg/mL of fibrin 0.5% w/v of alginate (120,000–190,000 g/mol, M/G ratio 1.56), and 0.3 mg/mL of genipin, whereas the crosslinker has 20 mg/mL of calcium chloride, 0.075% w/v of Chitosan, and 1.7 U/mL of thrombin, all of which were purchased from Sigma, St. Louis, MO, United States. Fibrin, a blood-derived biomaterial, supports neural stem cell differentiation and has been widely used in bioinks. However, bioinks that only contain fibrinogen pass through the microfluidic print head too fast to be polymerized, even at the lowest pressure, due to low viscosity. [23, 25, 78]. To overcome this issue, the naturally derived materials alginate and chitosan were added to the bioink to increase its viscosity and gelation speed and, thus, the printability of the ink. Alginate and chitosan are also broadly used as bioink components [13, 25, 104]. The ionic potential differences cause an interaction between alginate and chitosan, in which a polyelectrolyte complex is formed through their interactions. These interactions produce a physically crosslinked film formed at the interface of these two materials. Moreover, alginate and fibrin do not interact with one another but, instead, form an interpenetrating network within the scaffold. Fibrin polymerized by thrombin and crosslinked calcium chloride tends to last one to two weeks

in culture before being degraded by proteases released from incorporated cells. This degradation limits the usefulness of fibrin scaffolds for neural tissue engineering since it often requires more than two weeks of culture to achieve fully differentiated neural cell types. For the long-term stability of fibrin scaffolds, soluble protease inhibitors or additional chemical crosslinking can slow their degradation. Genipin, a naturally derived small molecule that originates from geniposide found in fruits, can be used to covalently crosslink protein amine groups in fibrin and chitosan, which thereby creates a multi-material scaffold. This crosslinking further stabilizes the hydrogel, but can also change the bioink's mechanical properties, mainly its stiffness and porosity. A study that considered the effect of genipin concentrations on hiPSC neural differentiation found that the elastic moduli of gels produced with genipin concentrations lower than 2.5 mM were lower than gels produced without genipin. Additionally, pore size was also affected by genipin, with larger pores in gels made with genipin (1–5 mM) compared to those with no genipin added. Moreover, the porous structure of chitosan allowed cells and nutrients to diffuse and migrate through the structure and can be formed by crosslinking chitosan with a variety of agents [13, 25, 63]. However, to successfully engineer mature bioprinted tissues for drug testing, a bioink should be printed as a desired structure to maintain its integrity over the culture period to support cell growth and differentiation [19, 58, 122]. The bioink must also support cell-material interactions to promote cell attachment and migration and possibly deliver differentiation cues [28, 103, 107, 147]. For printability, the bioink must be precisely tuned to the printing system with an appropriate viscosity and gelation time [136, 137, 148, 149]. Furthermore, the printed structures must support the cells over their differentiation period to prevent premature degradation. Lastly, bioink should also be

degradable yet retain enough mechanical properties for a sufficient time period to support tissue maturation [109, 143].

Microspheres (1–1000 μm in diameter) are drug-delivery particles that release drugs at a controlled rate to overcome localized drug-delivery issues and enhance the therapeutic efficacy of a drug [27, 28, 70, 75]. Our previous work validated that microspheres provide a protective environment around the cells that reduces damage to cells while printing, which enhances cell viability post-printing; additionally, these bioprinted constructs containing microspheres provide an appropriate 3D microenvironment for cells to grow and differentiate [28]. Our group found that drug-releasing microspheres in bioprinted constructs enhanced neuronal differentiation by providing the localized and controlled delivery of morphogens over time. In contrast to procedures that require changing morphogen- containing media frequently, microspheres are a more cost-effective morphogen-delivery method [27, 28].

However, the physical and mechanical properties of these bioprinted neural tissues need to be assessed to determine if their properties are analogous to their corresponding native tissue. This study, in which we manually combined our novel microsphere-containing bioink and crosslinker as well as bioprinted constructs, characterizes the physical and mechanical properties of bioprinted constructs to provide insights into their properties in comparison to the bioink without additives. Here, we adapted two different mechanical characterization techniques to measure the viscoelastic properties of the bioprinted neural tissue comprised of fibrin-based bioink with and without microspheres [22, 23, 116, 150]. Interestingly, many procedures have been used to measure the elastic moduli of soft hydrogel scaffolds since neurons need soft substrates to differentiate and mature. However,

it is challenging to precisely measure the elastic moduli of soft substrates using conventional protocols [23, 99, 104, 116, 151]. Robinson et al. validated a direct method to acquire the elastic moduli of fibrin using a modified Hertz model for thin films. This method involves spherical indenters that are placed on top of the fibrin samples to create an indentation depth that is then correlated with elastic moduli [23]. The indentation method facilitates the elastic modulus of hydrogel samples to be evaluated by combining spherical indenters with fluorescence microscopy [23]. We performed indentation experiments on bioprinted constructs using specific spherical indenters and a modified Hertz model for thin films [23]. Later, we conducted parallel plate rheometry on bioprinted constructs and on manually combined bioink and crosslinker to quantify the frequency-dependent shear elastic moduli [22]. These techniques facilitated a better understanding of the mechanical characterization of bioprinted neural tissue. Lastly, we characterized the physical properties of our bio- printed constructs with and without microspheres, including their microstructure and porosity, since a porous structure improves cell viability, aggregation, and motility as well as biodegradability [24, 88, 109, 128, 140, 142]. Moreover, we have performed these characterization techniques on bioprinted constructs and on manually combined bioink and crosslinker with and without microspheres.

3.3. Materials and Methods

3.3.1. Fabrication of Drug Releasing Microspheres

Microspheres were prepared using an oil-in-water (o/w) emulsion process followed by the evaporation of the organic solvent as previously described [70]. For the water phase, 2% PVA (polyvinyl alcohol (PVA) (Mw ~13,000–23,000, 87–89% hydrolyzed) (Sigma-Aldrich, St. Louis, MO, USA) solution was made by dissolving PVA in de-ionized water for 1 h at 85 ◦C while mixing at a speed of 850 rpm on a Corning PC-420D magnetic mixer. Later, 100 mL of 0.3% (w/v) PVA solution was made by diluting 2% PVA with de-ionized water and held at 35 ◦C. Furthermore, 500 mg of PCL was dissolved in 3 mL of DCM on a magnetic mixer for 15 min at 900 rpm to produce the oil phase. Subsequently, 0.3 mg of the drug (dissolved in 100% ethanol) was added to the oil phase to produce microspheres at a concentration of 0.6 µg mg−1 (w/w, guggulsterone/PCL). After removing from the magnetic mixer, 3 mL of 2% PVA were slowly added to the oil solution to prevent disruption of the boundary layer. An emulsion of the solution (w/o) was then produced by vortex mixing (Fisher Scientific, Waltham, MA, USA) at 3000 rpm for 15 s. This (w/o) emulsion was immediately added to the 0.5% PVA water phase and held at 35 ◦C at a mixing speed of 500 rpm for 4 h to achieve evaporation of the organic solvent. After mixing, the microspheres were isolated by centrifugation at 4000 rpm (Eppendorf 5810 R) and washed with de-ionized water. For long-term storage, the microspheres were lyophilized for 24 h and stored at −20 ◦C. Lastly, the microspheres were sterilized by low power air-plasma treatment (Harrick Plasma, Ithaca, NY, USA) for 30 s before being added to our bioink.

Derivation and Expansion of Neural Progenitor Cells (NPCs) hiPSC-derived NPCs were obtained from the hiPSCs (1-DL-01 line—male, WiCell Research Institute) as described previously [28]. Experiments (rheology and degradation) using hiPSC-derived NPCs were conducted with the approval of the University of Victoria's Human Ethics Committee under protocol number: 12-187. NPCs were cultured in STEMdiffTM Neural Progenitor Medium (NPM), (STEMCELLTM Technologies, Vancouver, BC, Canada) on cell culture plates coated with poly-L-ornithine (PLO, Sigma, St. Louis, MO, USA) and laminin (Sigma, St. Louis, MO, USA). The cultured NPCs were maintained at 37 ◦C with 5% CO2, and media change was performed on a daily basis. Once the cultures reached 80% confluence, the cells were cryopreserved in liquid nitrogen.

3.3.2. Bioprinting Tissue Constructs for Evaluation

The bioink was prepared as previously described [25]. Constructs were bioprinted using Aspect's studio software (V1.2.59.0, Aspect Biosystems, Vancouver, BC, Canada) with and without microspheres using computer aided design [17] files as shown in **Figure 3.1** for analyzing different physical and mechanical properties. Here, **Figure 3.1 a,c** shows dome-shaped and **Figure 3.1 b,d** shows disc-shaped CAD files. Furthermore, **Figure 3.2 a,b** shows that bioink is depositing layer after layer on the platform to form the final structure. Microsphere-laden constructs (1% w/v microspheres in bioink) were printed with previously prepared microspheres. As shown in **Figure 3.3a**, a dome-shaped constructs with ~10 mm diameter, 40% rectilinear infill, and 7 layers were bioprinted using the RX1 bio- printer (Aspect Biosystems, Vancouver, BC, Canada) for analyzing mechanical properties such as elastic modulus with indentation method as well as physical properties

such as porosity, microstructure, and degradation process. Disc-shaped constructs in **Figure 3.3b** with ~30 mm diameter with 40% rectilinear infill were bioprinted using the RX1 bioprinter (Aspect Biosystems, Vancouver, BC, Canada) with 14 layers for measuring viscoelastic properties with an Anton Paar MCR 302 Rheometer (Anton Paar, Ostfildern-Scharnhausen, Germany). The size of the construct should match or be slightly wider than the diameter of the parallel plate (25 mm). Constructs were also bioprinted with varying densities of hiPSC-derived NPCs, such as 1, 2.5, and 5 million cells per 1 mL of bioink, to analyze viscoelastic properties. NPCs were mixed with bioink as in previously described protocols, and bioprinted constructs were fixed with paraformaldehyde before analyzing [26-28]. The printing speed was 25 mm/s, and channel pressures consisted of 60 mbar for the bioink, 50 mbar for the crosslinker, and 100 mbar for buffer solution. After bioprinting, the constructs were gently transferred to 6- and 12-well culture plates with 2 mL of tris-buffered saline (TBS).

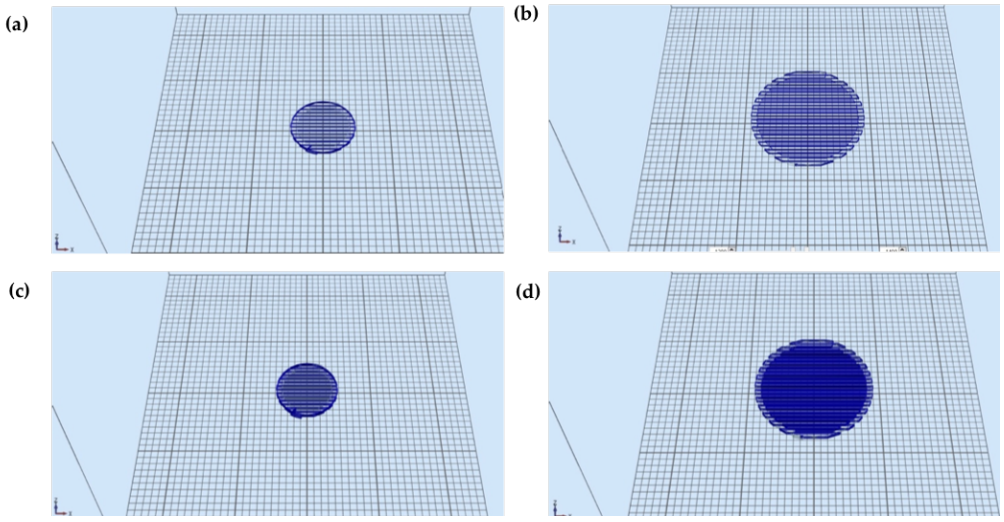

Figure 3.1 CAD file representing rectilinear infill pattern: **(a,c)** dome-shaped (~10 mm in diameter); **(b,d)** disc-shaped (~30 mm in diameter)

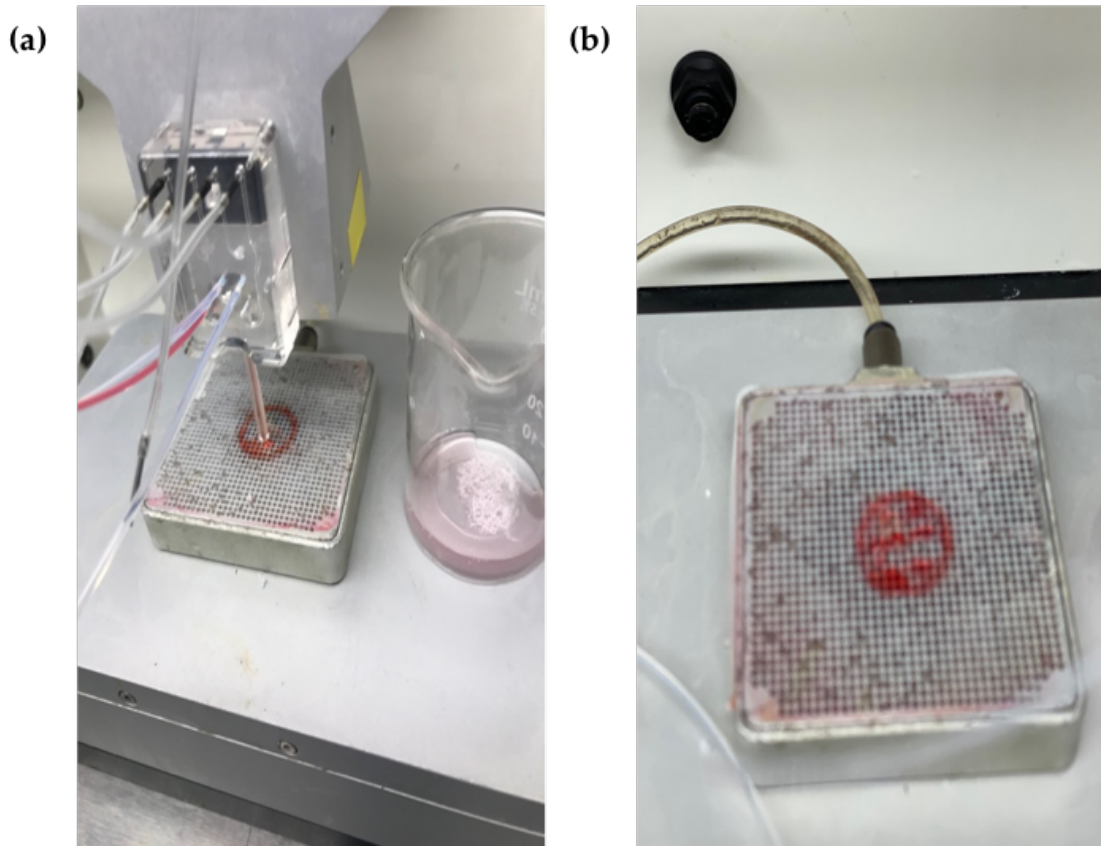

Figure 3.2 Bioprinted constructs consisting of fibrin-based bioink with phenol red (P3532, Sigma-Aldrich). **(a)** Aspect Biosystems duo-1 printhead printing a construct. **(b)** Bioprinted construct on nylon sheet plated on vacuum chuck showing first few layers of dome-shaped structure.

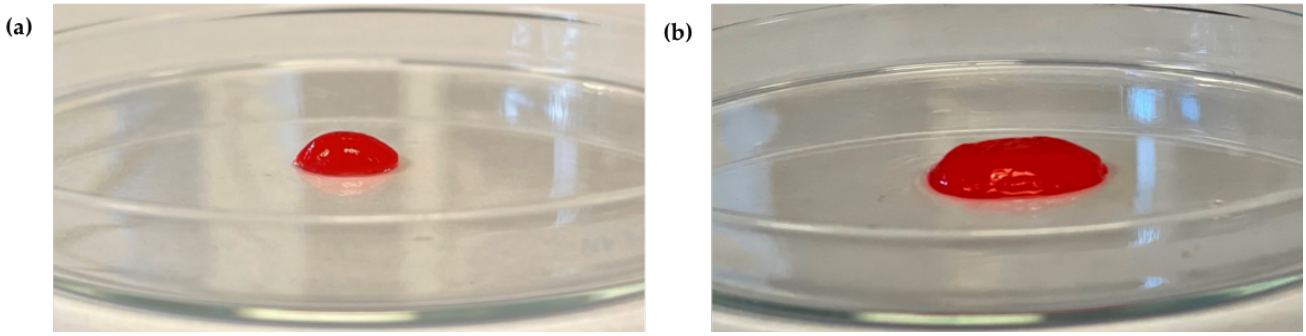

Figure 3.3 Bioprinted constructs of fibrin-based bioink with phenol red. **(a)** A dome-shaped (~10mm in diameter) construct within a glass Petri dish. **(b)** A disc-shaped (~30 mm in diameter) construct within a glass Petri dish.

3.3.3. Mechanical Properties of Bioprinted Constructs as Well as Manually Combined Bioink and Crosslinker with Microspheres

3.3.3.1. Indentation Method

Elastic moduli of the bioprinted constructs were determined using the modified version of the indentation method for hydrogels [23, 101, 133, 152, 153]. Dome-shaped constructs were printed with fibrin-based bioink with and without microsphere and transferred to a 24-well plate. After the 3D printing process, the constructs were incubated with 3 mL of a 50 μM fluorescein sodium salt solution prepared in a phosphate buffer solution (PBS) for 2 h. This solution penetrated the constructs, fluorescently staining them. This staining allowed visualization of the construct under the laser scanning microscope (LSM 880 Zeiss). After incubation with fluorescein sodium salt, the 3D-printed constructs were rinsed three times with fresh PBS to remove the excess fluorescein dye. To clearly define the hydrogel surface during the imagining of the indentation process, 3 mL of a solution containing red fluorescent polystyrene particles in water was deposited in the wells of the constructs. The well plate was then moved to the sample stage of the LSM and left undisturbed for 1 h to allow deposition of the fluorescent particles on the hydrogel surface. Two different types of spherical indenters were used during the measurements of elastic modulus. For the bioprinted constructs in absence of microspheres, a 3/16” zirconium dioxide indenter was carefully positioned on the surface of each sample, creating an indentation without permanent damage. For the constructs, which contained microspheres, a 3/16” stainless steel 302 indenter was used. After carefully positioning the indenter on the surface of the bioprinted samples, fluorescent images were acquired in the LSM. Images were obtained using a 10× objective lens (EC Plan-Neofluar 10×/0.30M27) and

two excitation sources (488 nm and 543 nm). A 488 nm argon laser was used to excite the fluorescein sodium salt molecules embedded in the samples, in which emission was collected from 500 nm to 550 nm. A 543 nm helium–neon laser was used to excite red fluorescent polystyrene particles, with emission from 560 nm to 700 nm. The indentation depth created by the indenter on the surface of the bioprinted constructs was measured by collecting Z-stack images with a layer height of 1 μm and a refractive index of 1.33. The indenter and samples were submerged in the water supernatant from the polystyrene solution. After collecting Z-stack images, cross-section images (XZ and YZ) of the layers were obtained using the Zeiss Zen 2.3 software to measure the total height of the hydro-gel samples and the deformation created at the surface of the samples by the indenter. All the indentation experiments and imaging were performed in triplicates and at room temperature (25 ± 2 ◦C).

As our group previously showed [23], the elastic moduli of the samples were obtained based on the modified Hertz model equation for thin films [140], by maintaining the indentation depth (δ), hydrogel thickness (h), and indenter radius ® in the range of $\delta/h \leq \min(0.6, R/h)$, and $0.3 \leq R/h \leq 12.7$ [154].

3.3.3.2. Rheology with Rotational Rheometer (Anton Paar Rheometer)

Testing was performed on bioprinted constructs with and without microspheres as well as on manually combined bioink (alginate, fibrin, and genipin) and crosslinker (chitosan, calcium chloride, and thrombin). Aspect Biosystems' RX1 bioprinting system employs a microfluidic print head to limit the harsh shear stress to cells as compared to conventional extruder-based printers, and this printhead requires chemically crosslinkable bioinks when

printing. The crosslinker channel on the print head intersects with the bioink channel where it initiates gelation so the print head can extrude a continuous fiber. Here, the rheological tests were done on both bioink and crosslinker to understand the gelation as well as stiffness of crosslinked bioprinted constructs using a rheometer equipped with sandblasted parallel-plate fixtures (PP25/S, 3997) of diameter 25 mm with a gap width of 1 mm [74]. To determine the shear moduli of the bioink formulation, the bioink was loaded in its solution phase onto the plate (25 ± 2 ◦C), and the crosslinker solution was added on top of the bioink; then, the measuring plate was lowered into position. To determine the modulus of bioprinted constructs, approximately 30 mm diameter disc-shaped constructs were loaded on the rheometer. The frequency sweep was conducted from 0.1 to 100 rad/s at a 0.5% strain to measure frequency-dependent G′ and G″. The viscosity was measured at shear rates from 0.01 to 90 s−1 to understand the deformation properties of a material. All the data were collected using Anton Paar Rheocompass software.

3.3.4. Microstructure of Bioprinted Constructs with and without Microspheres

The microstructure of bioprinted constructs with and without microspheres was assessed by scanning electron microscopy (SEM, Hitachi S-4800) [142]. The bioprinted constructs were freeze-dried in a lyophilizer (VirTis Freezemobile 12EL −85 ◦C Freeze Dryer Lyophilizer w/16-Port Tree Manifold) for 24 h and cut into thin slices using a razor blade, then stored in their desiccated form at −20 ◦C until analysis. SEM was used to characterize scaffolds, and the fact that it is a dry vacuum system means it cannot be used to examine wet specimens. Accordingly, bioprinted scaffolds were lyophilized before analysis, making the process of drying wet samples unavoidable, particularly for obtaining high resolution

images. After lyophilization, samples were then sputter coated with gold–palladium (The Anatech Hummer VI, Au/Pd) before scanning. SEM analysis was done on three samples in three independent replicates for constructs with and without microspheres. The SEM images were captured using Hitachi S-4800 software and diameters were measured using Quartz-PCI Image Management Systems® software (Quartz Systems, Vancouver, BC, Canada).

3.3.5. Porosity of Bioprinted Constructs with and without Microspheres

The bioprinted constructs were freeze-dried in a Lyophilizer for 24 h prior to the porosity analysis. The porosity rate of bioprinted constructs with and without microspheres was calculated using Equation (1) as described previously [142]. V1 was defined as the initial volume of dehydrated alcohol used to submerge the freeze-dried bioink sample, V2 the total volume of the system when the sample was immersed in the dehydrated alcohol, and V3 the volume of the residual liquid after impregnating the sample. Three samples were recorded in three independent replicates for both microspheres and no microspheres groups.

$$\textbf{Porosity} = (V1 - V3)/(V2 - V3) \times 100\% \quad (1)$$

3.3.6. Swelling Ratio of Bioprinted Constructs with and without Microspheres

The swelling ratio of bioprinted constructs with and without microspheres was measured by weighing the swollen and lyophilized bioprinted samples. The bioprinted samples were incubated in PBS at 37 ◦C for 24 h. Then, the samples were removed from

the PBS, and the wet weight [86] of the samples was determined. Then, samples were lyophilized for 24 h and the dry weight (Wd) was determined [141, 145]. The swelling ratios of the hydro- gels were calculated by Equation (2). Three samples were recorded in three independent replicates for both the microspheres and no microspheres groups.

Swelling ratio = (Ws − Wd)/Wd **(2)**

3.3.7. Biodegradation of Bioprinted Constructs with and without Microspheres

The degradation rate *in vitro* of bioprinted constructs was detected by quantifying the decrease in weight. Briefly, freshly bioprinted construct samples were weighed [25] and incubated in NPC medium at 37 ◦C for 14 days. At predetermined time points (t), bioprinted constructs were air dried and weighed (Wt). The degradation rate of the construct was calculated by Equation (3) [142]. Three samples were recorded in three independent replicates for both the microspheres and no microspheres groups.

Degradation rate = (WO − Wt)/WO × 100% **(3)**

3.4. Statistical Analysis

All data were expressed as mean ± standard deviation (n = 3 for all). Statistical analysis for the elastic modulus, porosity, and swelling ratio was carried out using an unpaired, two-tailed Student's t-test with 95% confidence level. A one-way ANOVA analysis of variance with a Tukey post hoc analysis, with 95% confidence, was carried out for the degradation results. A value of $p < 0.05$ was considered statistically significant. All statistical analysis was carried out using the GraphPad Prism 5 statistics software.

3.5. Results

3.5.1 Mechanical Properties of Bioprinted Constructs as Well as Manually Combined Bioink and Crosslinker with and without Microspheres

3.5.1.1 Measuring Elastic Modulus of Bioprinted Constructs with Indentation Method

The elastic modulus of the dome-shaped bioprinted constructs with a 1 cm diameter and 0.7 cm height was measured using the modified Hertz model for hydrogels [149]. As shown in **Figure 3.4**, hydrogel samples were fluorescently stained with green fluorescein sodium salt, while red fluorescent polystyrene particles were deposited on the surface of the samples. The indentation depth caused by the mass of the indenter was determined by XZ- and YZ-cross-section images of the constructs.

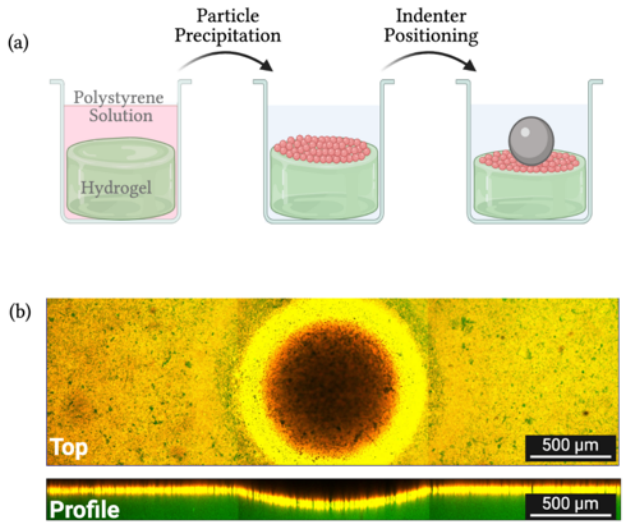

Figure 3.4 Setup for indentation experiment **(a)** Bioprinted constructs were labeled with fluorescein sodium salt, while red polystyrene red particles were deposited in its surface. Spherical ceramic indenters were positioned on the surface of the constructs, generating an indentation depth. **(b)** Indentation depth were measures by visualizing images obtained by the gel indentation surface. Scale bar represents 500 µm

Measurements of elastic moduli of the bioprinted constructs in absence of microspheres were performed using a 3/16" zirconium dioxide spherical indenter, with a density of 5.680 g/cm3. For the 3D printed samples with microspheres, the zirconium dioxide indenter was not sufficient to display a significant indentation depth on the surface of the hydrogels. In this case, a 3/16" stainless steel 302 spherical indenter with a density of 7.860 g/cm3 was selected. The difference in the indenters as long as the values obtained are in the range appropriate according to the modified Hertz model **(Table 1.1)**. The bioprinted samples containing microspheres displayed a higher stiffness values than without microspheres. The use of 3/16'' zirconium oxide indenter on the surface of the bioprinted samples with microspheres did not create an indentation depth that could be measured with confidence. Therefore, in order to create an indentation that could be measure with confocal microscope, a heavier indenter was used (stainless steel 302). Considering that the result for the heavier indenter still obeys the limits of the modified Hertz model for the thin films ($\delta/h \leq \min(0.6, R/h)$, and $0.3 \leq R/h \leq 12.7$), Young's moduli values with different indenters can be compared. **Table 1.1** displays the indentation parameters and elastic moduli values obtained for the 3D-printed samples. As expected, **Figure 3.5** shows that the bioprinted constructs containing microspheres displayed a higher elastic modulus, which could be attributed to the incorporation of microspheres making it more mechanically and structurally stable. The incorporation of microspheres did not drastically increase the concentration of the bioink since the same printing pressures were used with the bioprinted constructs with and without microspheres. However, the increased concentration of microspheres greatly enhanced the stiffness of the bioprinted construct.

Table 3.1 Indentation parameters and elastic moduli values obtained for bioink with and without microspheres

Indentation Results	Without microspheres	With microspheres
$0.3 \leq R/h \leq 12.7$	1.32 ± 0.12	1.43 ± 0.17
$\delta/h \leq \min(0.6, R/h)$	0.33 ± 0.02	0.33 ± 0.02
EHertz	2025.9 ± 170.7	3096.8 ± 356.3
Emodified Hertz	728.4 ± 47.6	1032.6 ± 59.8

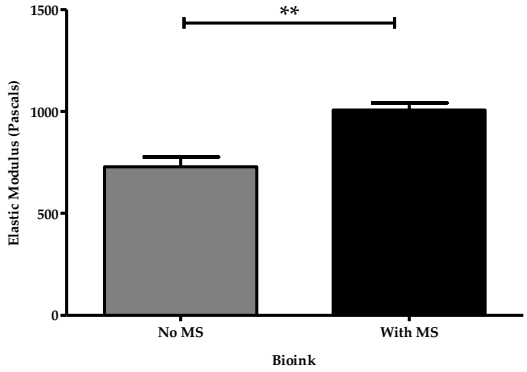

Figure 3.5 Elastic moduli values obtained from modified Hertz model for thin films. Data is presented as the average and standard deviation of three sample replicates. (MS - Microspheres). **indicates that the elastic modulus are statistically different. *P<0.05*

3.5.1.2. Rheology with Rotational Rheometer (Anton-Paar Rheometer)

The viscosity and frequency sweep of the manually combined bioink and crosslinker solution, as well as bioprinted constructs with cells and microspheres, were measured using an Anton Paar Rheometer [155]. The probability of extruding the hydrogel depends upon its viscosity. NPCs were printed in concentrations of 1, 2.5, and 5 million per 1 mL of bioink to test the effects these concentrations have on the mechanical strength of the

bioprinted constructs. The viscosity was analyzed by regression analysis using the Carreau-Yasuda method with shear rate from 0.01 to 90 s−1. **Figure 3.6 (a-c)** shows that the viscosity dependence on shear rate. The log of the shear rate and viscosity was taken to better understand the relationship between them. Here, the viscosity of 1, 2.5. and 5 million cells indicate that there is a decrease in viscosity with an increase of shear rate. Here, the viscosity measurement shows the shear-shinning property of the bioink. Shear thinning is important as it protects the cells during the printing process [103, 116].

G' is associated with the elastic component of the viscoelastic behavior of a material or the more solid-state behavior of a material. In this study, the elastic component was tested on three different concentrations of cells in the bioink: 1, 2.5, and 5 million/mL. **Figure 3.7 a-c** shows that G' increased when the angular frequency increased. At concentrations of 1 , 2.5 and 5 million/mL, G' was represented in logarithmic scale to better understand the relation between storage and loss modulus with angular frequency. Hence, the addition of cells resulted in an increase in G'.

Figure 3.8a shows that the viscosity of the bioprinted constructs with and without microspheres decreases while shear rates increase. Similarly, **Figure 3.8b** representing the viscosity of the manually combined bioink and crosslinker with and without microspheres showed that the viscosity increased with shear rate. **Figure 3.9a,b** shows that G' increases with angular frequency in bioprinted constructs; however, G'' slightly increases as compared to G'. **Figure 3.9c,d** shows a slight difference as bioink and crosslinker with microspheres take slightly longer to crosslink on the Rheometer's platform as compared to bioink and crosslinker without microspheres. The overall increase in G' indicates that the

elastic behavior becomes more dominant. However, G'' is a more liquid-like property. If G'' is greater than G', then applied mechanical force overtakes the inter-particles forces and the material starts to flow[156, 157].

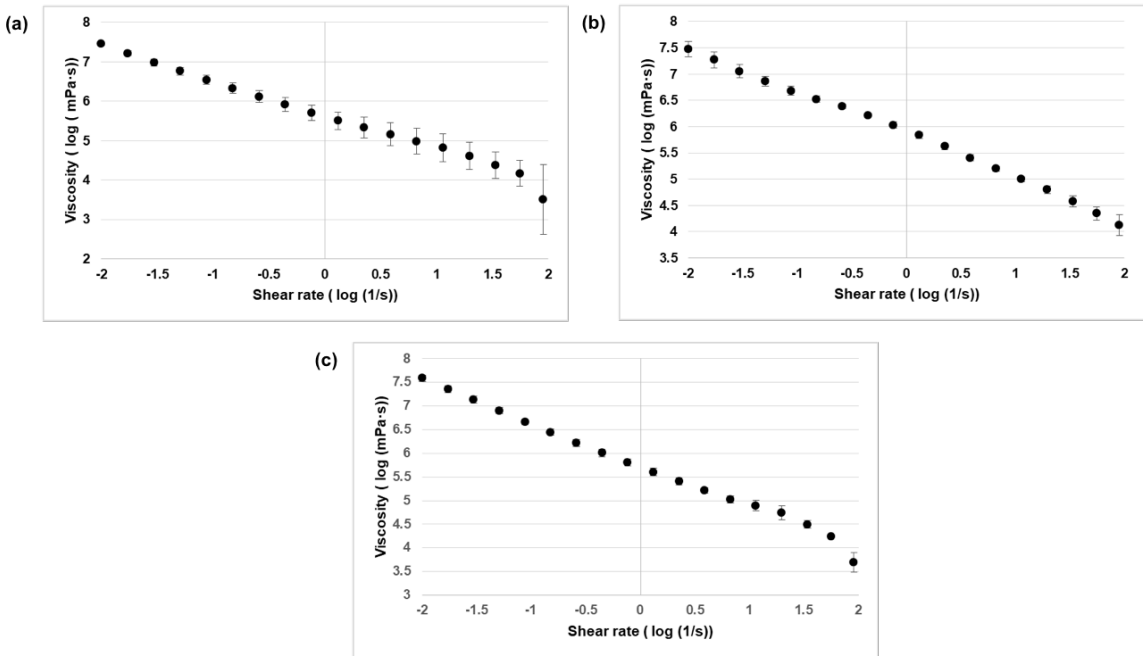

Figure 3.6 Rheological properties. **(a)** Viscosity/shear rate curve of bioprinted constructs with 1 million NPCs and microspheres. **(b)** Viscosity/shear rate curve of bioprinted constructs with 2.5 million NPCs and microspheres. **(c)** Viscosity/shear rate curve of bioprinted constructs with 5 million NPCs and microspheres.

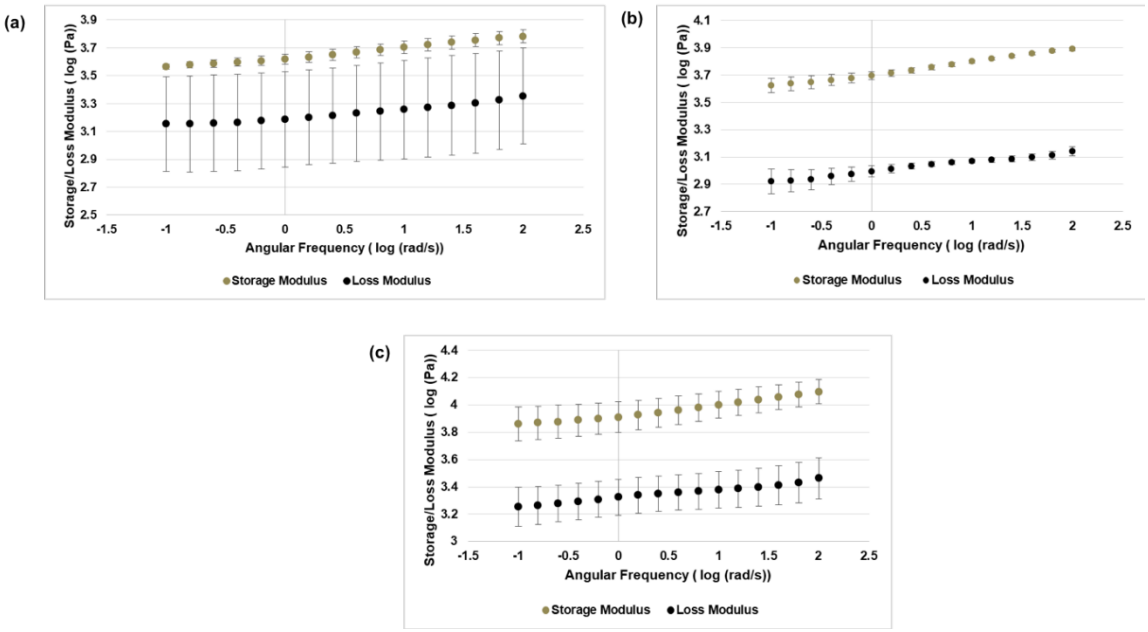

Figure 3.7 Rheological properties. **(a)** Storage/loss modulus of bioprinted constructs with 1 million NPCs and microspheres. **(b)** Storage/loss modulus of bioprinted constructs with 2.5 million NPCs and microspheres. **(c)** Storage/loss modulus of bioprinted constructs with 5 million NPCs and microspheres.

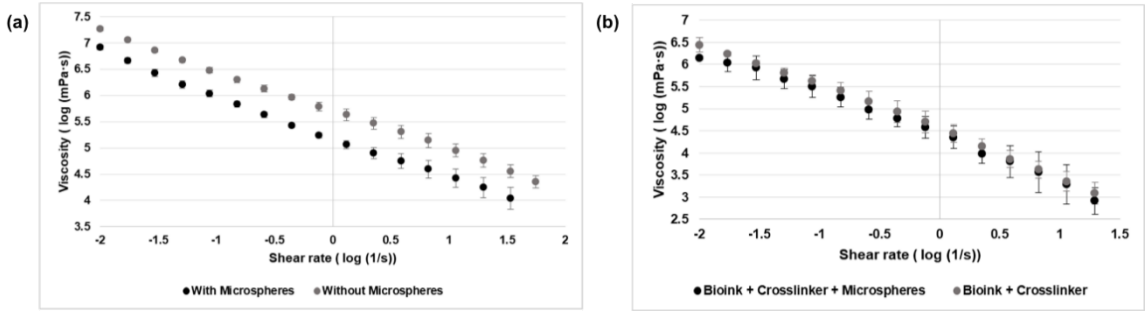

Figure 3.8 Rheological properties. **(a)** Viscosity/shear rate curve of bioprinted constructs with and without microspheres. **(b)** Viscosity/shear rate curve of manually combined bioink and crosslinker printed constructs with and without microspheres.

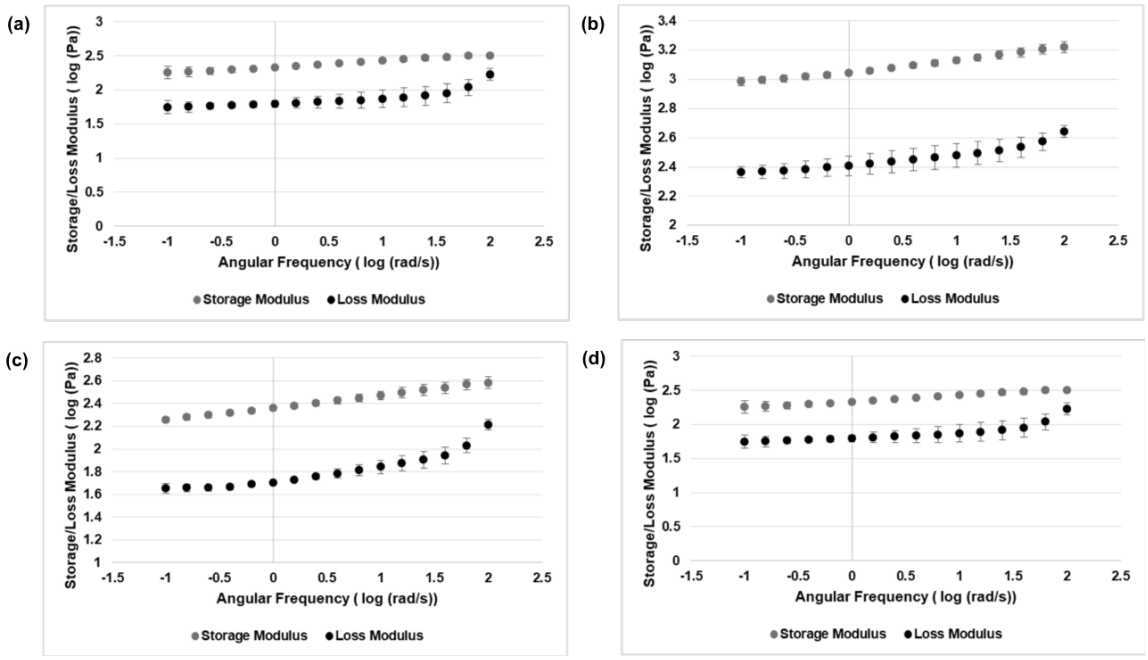

Figure 3.9 (a) Storage/loss modulus of bioprinted constructs with microspheres. **(b)** Storage/loss modulus of bioprinted constructs without microspheres. **(c)** Storage/loss modulus of manually combined bioink and crosslinker. **(d)** Storage/loss modulus of manually combined bioink and crosslinker with microspheres.

3.5.2. Microstructure of bioink with and without microspheres

Freeze-dried constructs were characterized using SEM to investigate the microstructure and the distribution of microspheres. **Figure 3.10a–h** shows the 3D homogenous, macroporous structure with interconnected porosity observed in both groups with the pore sizes ranging from 0.11 to 0.31 um. **Figure 3.10e–h** shows that microspheres were uniformly distributed in the porous structure. These microspheres were smaller in size (1–10 um) and were found to be uniformly distributed in the porous structure.

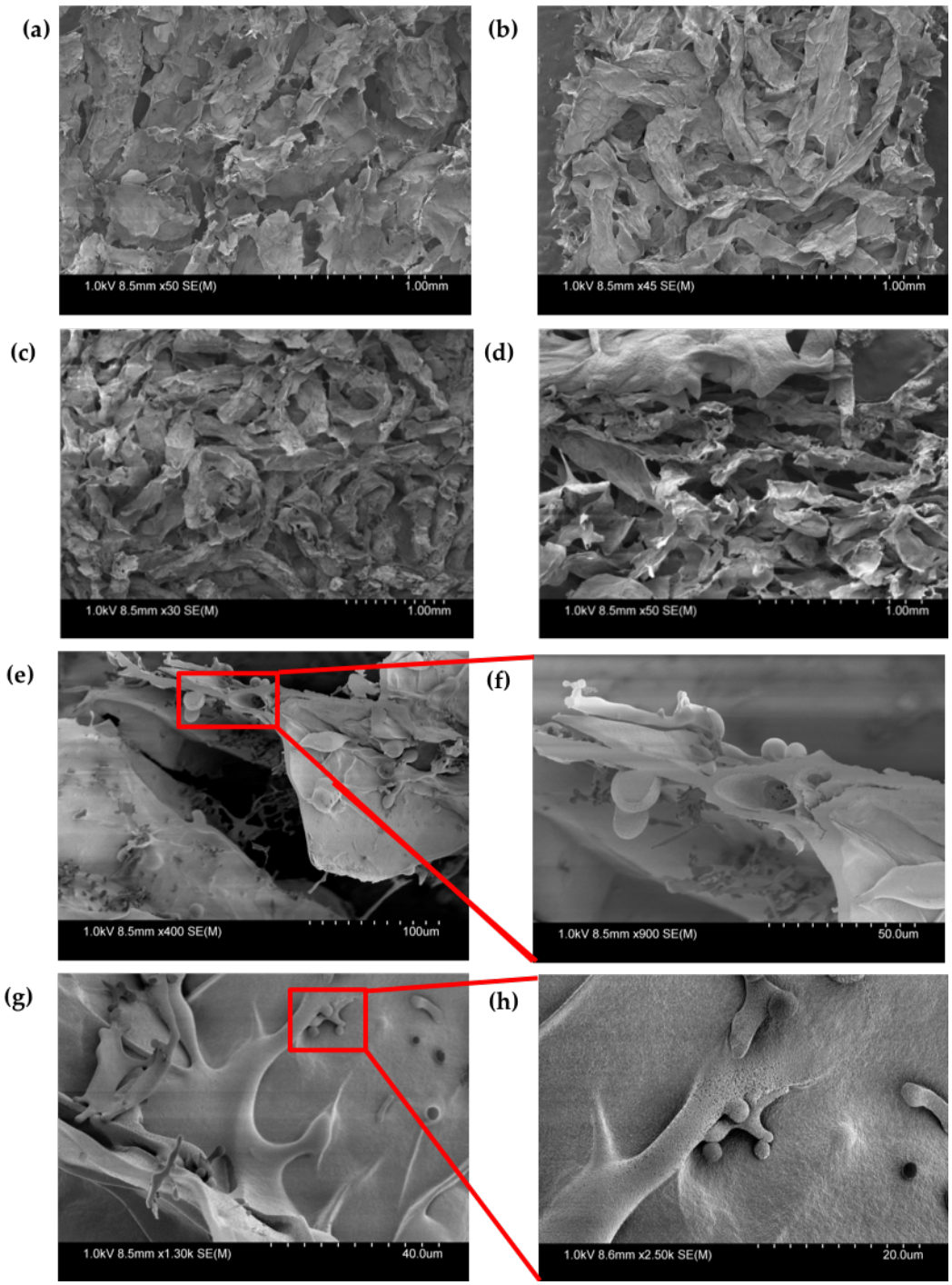

Figure 3.10 SEM images revealed morphological characteristics and interconnectivity of pores of bioprinted constructs **(a)** Horizontal section of bioprinted constructs without microspheres. **(b)** Vertical section of bioprinted constructs without microspheres. **(c)** Horizontal section of bioprinted constructs with microspheres. **(d)** Vertical section of bioprinted constructs with microspheres. **(e)** At 100 um, horizontal section of bioprinted constructs showing microspheres are embedded in the bioprinted construct. **(f)** At 50um,

horizontal section of bioprinted constructs showing microspheres are embedded in the bioprinted construct. **(g)** At 40 um, vertical section of bioprinted constructs showing microspheres are embedded in the bioprinted construct. **(h)** At 20 um, vertical section of bioprinted constructs showing microspheres are embedded in the bioprinted construct.

3.5.3. Porosity of bioink with and without microspheres

The bioprinted constructs with and without microspheres are lyophilized and the level of porosity measured. **Figure 3.11** bioprinted constructs with microspheres and without microspheres had a porosity of 69.33 ± 3.1% and 66.11± 3.2%, respectively. However, after performing a two-tailed Student's t-test, there was no significant difference between the two groups. As from **Figure 3.6**, SEM images also presented that microspheres were homogenously distributed the porous structure, without any large effect on porosity, due to their small size (1-10 um).

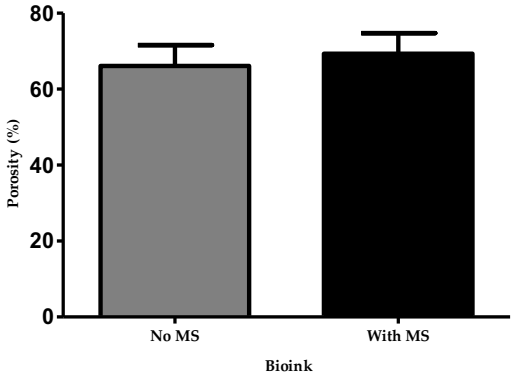

Figure 3.11 Porosity rate of bioprinted constructs with and without microspheres

3.5.3. Swelling ratio of the bioink with and without microspheres

An efficiently printed construct should swell after being placed in culture media and maintain its fluid in the 3D network. Mild swelling was observed in the constructs with and without microspheres after 24 h of incubation. **Figure 3.12** shows the swelling ratio of bioprinted constructs with and without microspheres to be 24.3 ± 0.1 and 25.6 ± 1.3, respectively. There was no statistical difference between the two groups. Moreover, microspheres did not reduce water absorption, and both groups exhibited swelling without dissolving, which is critical for cell growth and differentiation.

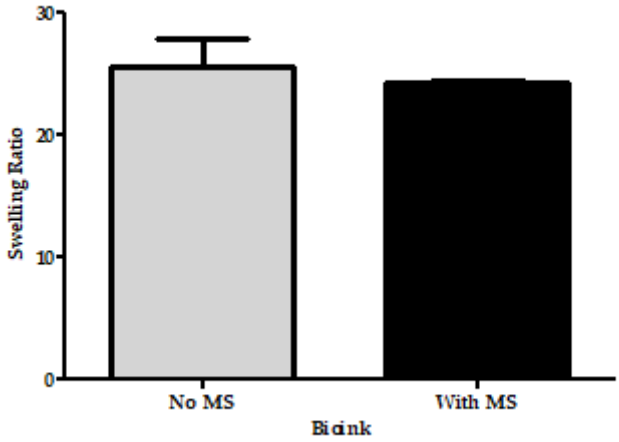

Figure 3.12 Swelling ratio of bioprinted construct with and without microspheres

3.5.4. Biodegradation of bioink with and without microspheres

After culturing under standard conditions at 5% CO2 and 37 °C for 14 days, bioprinted constructs with cells and microspheres had the highest mechanical strength and lowest rate of degradation after 14 days. On the other hand, the bioprinted constructs containing microspheres but no cells had an intermediate mechanical strength and showed less degradation than the constructs with no microspheres or cells since they had a low mechanical strength and a maximum degradation. **Figure 3.13** shows that there is a

significant difference in all three groups, between microspheres and no microspheres, and between microspheres and microspheres and cells.

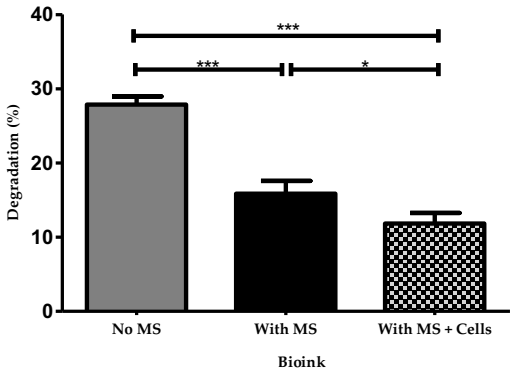

Figure 3.13 Biodegradation rate of bioprinted construct with cells and microspheres, with microspheres, and without microspheres. *** and * indicates statistical differences between the three different groups.

3.6. Discussion

The differentiation of NPCs to mature phenotypes in bioprinted constructs depends on several factors, including the stiffness and porosity of the bioink that comprises the microenvironment. Our group has previously established that fibrin-based bioink printed with and without microspheres enables neuronal survival, proliferation, differentiation, and maturation [25-28, 70]. In this study, we have determined the physicomechanical properties of bioprinted constructs as well as manually combined bioink and crosslink for tissue engineering applications.

In this study, dome-shaped structures were printed to analyze the microstructure, porosity, degradation, and elastic moduli using an indentation method. However, for the mechanical properties, due to the geometry of parallel plate on the rheometer, a uniform structure had to be used. Therefore, for these experiments, a disc-shaped structure used instead of dome-shaped structure. To better understand our fibrin-based bioink, optimization and validation of several physical and mechanical properties were determined. Here, we analyzed the elastic moduli of the fibrin-based bioprinted constructs with and without microspheres. It was hypothesized that the elastic moduli of fibrin-based bioink that contained microspheres would be higher than the 30 mg/mL fibrin, which was previously evaluated by our group [23, 25]. The elastic modulus was previously determined here, we analyzed the elastic moduli of the fibrin-based bioprinted constructs with and for fibrin-concentrations of 10, 20, and 30 mg/mL to be 262.7 ± 5.7, 590.9 ± 23.5, and 719.0 ± 58.3 Pa, respectively [23]. The indentation method used in this study combines spherical indenters and fluorescence microscopy, which allows the direct analysis of the elastic moduli of hydrogel samples. We determined the elastic moduli of bioprinted constructs with and without microspheres

and found their moduli to be 1032 ± 59.8 and 728 ± 47.6 Pa, respectively. It was found that the constructs with microspheres were stiffer than the ones without microspheres. The Hertz theory displayed a high elastic modulus for a stiffer construct. These results showed that the incorporation of microspheres has a significant effect on stiffness, which can overcome the issue of faster degradation of bioprinted constructs; hence, stiffness will help in long-term culture and, ultimately, maturation of bioprinted neural tissues. Additionally, the elastic moduli of bioprinted constructs with microspheres was ~1 kPa, which is similar to the optimal stiffness for neuronal differentiation shown in previous studies [92, 104]. The elastic moduli values obtained by indentation corresponded to the values acquired by rheometry. In addition to the elastic moduli, the viscoelastic properties were determined, since extrusion through the bioprinter's nozzle depends on its viscosity. A useful printing solution should shear-thin under pressure, which implies that it should pass easily through the print nozzle and hold the printed shape once pressure is released [93]. If the viscosity is higher, then a higher pressure is required for extrusion [92]. High pressure creates high shear stress, which ultimately affects cell death. This facilitates the printing of high-fidelity structures; nevertheless, covalent crosslinking is required to attain a mechanically strong structure for long-term stability [103]. Our results showed that bioprinted constructs with and without microspheres, with cells and microspheres, and in a bioink and crosslinker solution exhibited shear-thinning behavior. Our bioink showed high viscosity at low applied shear stresses, exhibiting solid-like behavior. Moreover, the frequency sweep measurements showed that the G′ increased with higher concentrations of cells for bioprinted groups with microspheres, which indicates that bioprinted constructs store deformation energy in an elastic manner and make an increasingly stable structure with the

addition of cells. G′ exceeded G″ over the whole angular frequency range (G′ > G″), and both moduli were dependent on frequency, which signified a standard gel structure under these conditions. In general, G′ is more sensitive to any changes in the microstructure of viscoelastic systems in a frequency sweep test, and information about rigidity of samples can be obtained by G′.

Interestingly, several previous studies have discussed the effect of substrate elasticity on neural precursors [23, 99, 104, 151, 157]. Neurons have also shown sensitivity to rigidity. Neurites have been reported to grow faster on matrices from 0.1 to 1 kPa compared to stiffer substrates [151]. Saha et al. validated that the hippocampus-derived NSC differentiation was favorable on softer substrates (E = 0.1–0.5 kPa) compared to stiffer substrates (E = 1–10 kPa) [135]. Moreover, Leipzig et al. demonstrated that forebrain-derived stem cells differentiated into mature neurons on substrates with a Young′s modulus <1 kPa; however, the proliferation of stem cells was ideal on 3.5 kPa substrates (E in the range of <1–7 kPa) [104], and lastly, Previtera et al. validated that stiffer substrates facilitated the increase in branching relative to neurons grown on softer substrates at the same cell number [157]. Together, these studies showed that neuronal differentiation is optimal on 1 kPa substrates, while stem cell proliferation is optimal on stiffer substrates [23, 99, 104, 151]. Furthermore, the porosity of 3D-printed constructs plays a critical role in tissue engineering. A highly porous scaffold has large area for cell attachment and also enables the diffusion of nutrients and gases due to the removal of metabolic waste [88]. The incorporation of micro- spheres did not affect the porous structure of the bioprinted constructs. Bioprinted constructs with and without microspheres showed similar

macroporous structures with interconnected pores and similar pore sizes between constructs with and without microspheres.

Swelling and degradation are relevant for bioprinted constructs, as these physical properties affect cell viability, proliferation, migration, and the creation of new tissue. The swelling properties can significantly affect the bioprinted tissue. Swelling means that the hydrogel does not dissolve in the solvent but rather increases in volume [143]. During our swelling studies, PBS was changed after 24 h. As PBS was replaced, free chains were removed from the bioprinted samples, thereby reducing their swollen weights [75]. The swelling ratio of bioprinted constructs with and without microspheres was 24.3 ± 0.1 and 25.6 ± 1.3, respectively. Here, bioprinted constructs without microspheres showed similar swelling behavior as with microspheres due to the greater crosslinking. The observed swelling ratio was a balance between the uptake of water and the degradation rate of the constructs. Furthermore, the degradation time should match with the time required for desired tissue regeneration. Here, our bioprinted structure suffered the least amount of degradation when microspheres were incorporated into bioink. A significant difference was found among the groups. Thus, a controlled degradation rate is desired to achieve in tissue engineering. Here, degradation rate and mechanical properties can be tuned by incorporating microspheres, which have a greater influence on hydrogel degradation and swelling. Slow degradation kinetics is important to control the release of therapeutic molecules over a longer period of time [109]. These results showed that microspheres did not have a significant effect on the swelling and porosity of bioprinted constructs. However, our results showed that there is a possibility of specific physical interactions such as chemical bonding between the polymeric chains of biomaterials and microspheres. This

results in an enhancement of the crosslinking density and, thus, in the increased strength and mechanical stability of the bioprinted constructs.

3.7. Conclusions

Here, we have demonstrated a set of methods for measuring the elastic moduli, viscoelasticity, and other physical properties of bioprinted constructs with and without microspheres. In general, the results showed our microsphere incorporated bioink behaved as a composite hydrogel, which could incorporate drugs to regulate cell fates, additional extracellular matrix elements to improve mechanical properties, and biomolecules to improve biological activities. In conclusion, the incorporation of microspheres in bioink enhanced the mechanical strength, lowered the degradation rate, and increased the elastic modulus of bioprinted tissues, thus making bioinks containing these particles highly suitable for neural tissue engineering applications.

Chapter 3: Author's contribution

I (Ruchi Sharma, first author) came up with the scientific concept for the research objective 2. I devised the experimental strategy, carried out all of the procedures, and supervised the data analysis throughout the process. To begin with, I wrote the first version of the whole manuscript and shared it among the other authors and my supervisor for their consideration, opinions, and suggestions. As a result of receiving their input, I have modified and finalised the final draft for publishing in the journal. I have included additional specific information about each author's contribution to this publication. I have prepared the CAD file representing the rectilinear infill pattern (figure 3.1) and bioprinted constructs consisting of fibrin-based bioink with the help of Aspect Biosystems (figure 3.2 and 3.3). For figure 3.4, I have fully prepared all the constructs and after added fluorescein. Later, Karolina Papera Valente (the third author) assisted me to setup for an indentation experiment and (figure 3.4 and table 3.1). She assisted me with the data and I have done elastic moduli (figure 3.5). All rheological properties (3.6, 3.7, 3.8, and 3.9) with Rheometer have done by me. I have prepared all the samples for SEM images and Rebecca Kirsch (the second author) has assisted with imaging and porosity rate of bioprinted constructs (figure 3.11). I have calculated both the swelling ratio of bioprinted constructs (figure 3.12) and the biodegradation rate of bioprinted constructs (figure 3.13) myself. At all stages of this experiment, Dr. Stephanie Willerth has provided suggestions and input into the experimental design, provided feedback and supervision on the experimental analysis, as well as written and edited the manuscript.

Chapter 4 3D Bioprinting Human Models of Parkinson's Disease[c]

Ruchi Sharma[1], Milena Restan Perez[2], Kali Scheck[3] and Stephanie Michelle Willerth[1,2,3*]

[1]Department of Mechanical Engineering, University of Victoria, Victoria, BC, Canada;
[2]Department of Biomedical Engineering, University of Victoria, Victoria, BC, Canada;
[3]Division of Medical Sciences, University of Victoria, Victoria, BC, Canada

* Manuscript to be submitted at Biomaterials

Keywords:

Human induced pluripotent stem cells (hiPSCs); Parkinson's disease; 3D bioprinting; Bioink; Microspheres

Author contribution:

Sharma R. designed, set-up and performed most of the experimental procedures, analysis and preparation of manuscript. Perez Restan M. assisted on tissue culture, bioprinting, and editing of the manuscript. Scheck K. assisted on preparation of the bioink and bioprinting. Willerth S.M. provided feedback on the experimental analysis and editing of the manuscript.

[c]*Sharma R*, Perez Restan M, Willerth S.M. **3D bioprinting human models of Parkinson's Disease.** To be submitted at Biomaterials, 2022.

4.1. Abstract

Somatic cells (skin or blood cells) from Parkinson's disease (PD) patients with mutations may be reprogrammed using transcription factors to human induced pluripotent stem cells (hiPSCs). These patient-derived hiPSC lines can subsequently be differentiated into dopaminergic neurons to model PD. These PD models can be further used as drug-screening applications. 3D bioprinting can be used to achieve hiPSC-based engineered tissues. In this work, 3D structures were bioprinted using PD patient-specific neural progenitor cells (NPCs) encased within a bioink containing drug-releasing microspheres. These constructs were then cultured, and their characteristics were studied, including their morphology, cell death, and alpha-synuclein aggregation. Prior to printing, hiPSC-derived NPCs were primed for 7 days with FGF-8 (100ng/ml) and Purmorphamine (2uM). These NPCs were printed with bioink containing guggulsterone encapsulated microspheres. Furthermore, bioprinted NPCs were differentiated using neural induction medium for 20 days before being supplemented with BrainPhys media for another 10 days of maturation. The generated tissues had over 88.2 ± 1.5% cellular viability one day after printing, which increased to 96.7 ± 1.8% on day seven. After 20 days, tissues were stained for early neuronal markers such FOXA2 (Forkhead box protein A2) and TUJ1 (beta-tubulin III). The adult neural markers MAP2 (Microtubule Associated Protein 2), TH (Tyrosine Hydroxylase), DDC (Dopa decarboxylase), and NURR1 (Nuclear receptor related 1) were then investigated (Nuclear receptor related 1 protein). Aside from alpha-synuclein, DJ-1 (Protein deglycase DJ-1) (a protein which in humans is encoded by the PARK7 gene), and LRRK2 (Leucine Rich Repeat Kinase 2) have been identified as markers of PD. To analyze Lewy body formations, hematoxylin and eosin staining was used. These bioprinted

humanized models of PD may be investigated to better understand the disease's pathophysiology. Our findings indicate that 3D Bioprinting is required to create a complex 3D models.To that aim, the key cellular hallmarks of PD in patient-derived cells must be replicated in order to drive personalised medicine approaches.

4.2. Introduction

PD, the world's second most common neurodegenerative disease after Alzheimer's disease (AD), has no known cause, and its prevalence is predicted to climb significantly over the next decade [37, 39, 72]. Nonmotor symptoms such as constipation, anosmia, rapid eye movement sleep behaviour disorder, and depression may arise years before motor symptoms during PD progression. PD is still clinically diagnosed based on motor symptoms and signs. When deciding on treatments for PD; systems severity, degree of functional impairment and patient preferences are all considered. However, levodopa (L-Dopa) is still considered the gold standard therapy for PD motor symptoms. PD does not develop naturally in animals rather it is artificially generated in animals by inducing a brain injury using neurotoxins [34]. Although these procedures may give an animal brain with PD-like symptoms, their start, action, and development are not inherently analogous to those of the human brain. The disease's limited clinical translatability in animal and *in vitro* culture models contributes to the lack of effective disease-modifying medications [4, 34]. Although two-dimensional (2D) cultures of hiPSC-derived neurons have been shown to be efficient for understanding the human brain, the stiffness of culture substrates does not mimic the physiological properties of native organs. Furthermore, the activity of neurons created in a 2D microenvironment differs from that seen *in vivo* owing to unnatural transport kinetics of released hormones, oxygen, and nutrients, as well as unrealistic neural network density, design, connectivity, and cell functioning [2, 7, 43]. Since hiPSCs may be differentiated into any cell type found in the body, they are widely used for disease modelling. As a result, by reprogramming their somatic cells (skin or blood cells) into hiPSCs, patient-specific models may be created. However, due to their relative

inflexibility, 2D models are restricted for investigating cellular functions and do not offer precise drug responses. 2D models are not physiologically relevant to mimic the real brain to understand the pathogenic mechanisms behind neurodegenerative disorders. Biomimetic 3D culturing methods and organoids that better imitate healthy and pathological brain characteristics have been developed to address these inadequacies [2, 7, 43, 55]. This has provided fresh insights into cytoskeletal dynamics and protein deposition in AD, as well as aberrant electrophysiology and synaptic transmission in PD. Biomaterials offer numerous advantages for engineering 3D human brain models, including the ability to include multiple brain cell types with different functions (e.g., neurons, astrocytes, endothelial cells) and from different germ layers (e.g., ectoderm derived neurons, mesoderm derived microglia) to study cell–cell interactions in healthy and disease states [3, 5, 16, 37-39, 45-47, 60]. Manipulation of extracellular cues also enables researchers to examine the functions of extracellular matrix components in brain development and function. While organoid cultures adequately reproduce *in vivo* development, the absence of a necrotic core makes biofabricated 3D tissues excellent long-term culture tools for modelling the fundamentally delayed genesis and evolution of neurodegenerative disorders [5, 16, 17, 55]. Furthermore, 3D models have garnered a lot of interest for drug screening and therapeutic purposes. The 3D platform enabled the formation of dense dopamine neural network topologies as well as biological profiles that were both equivalent and distinct from 2D culture systems in healthy and PD lines. Previous study showed that PD cells grown on 3D platforms had more alpha-synuclein and had changed purine metabolite profiles [3, 45, 46]. In addition, computational network analysis of transcriptome networks revealed a plethora of novel molecular connections in neurons from patients with LRRK2

and GBA mutations [16, 47, 48, 54]. Given this, tailored physiologically relevant disease-specific tissues may be created utilising hiPSC obtained from PD patients and used to assess prospective treatments. 3D bioprinting, which involves the layer-by-layer deposition of biomaterials, is an advantageous technology for producing highly biomimetic and reliable *in vitro* models. The combination of 3D printing with patient-derived hiPSCs has the potential to generate neurological disease models for more accurate drug target screening [25-28, 66, 118, 158].

Our lab employs the Aspect Biosystems RX1 printer since it protects the cells inside the bioink from shear stress during printing, allowing us to optimise cell viability. Our fibrin-based bioink was created for printing hiPSC-derived neural aggregates that were viable and differentiated into mature neural tissues after 46 days of culture. In addition, hiPSC-derived neural progenitor cells (NPCs) were printed and treated with certain small molecules to develop into spinal cord-like tissues [27]. This bioink formulation enabled the creation of ring-shaped structures with high viability human glioblastoma cell lines that expressed cancer related protein markers. This study also demonstrated the necessity for 3D bioprinted models of neurological diseases. Working with hiPSCs has a number of hurdles, including achieving phenotypic maturation. The neural development of hiPSCs may take months and efforts. Small molecule morphogens are one intriguing method for inducing differentiation in hiPSCs. Our team has studied the use of tiny molecule morphogens encapsulated in microspheres that progressively breakdown to release the drug as a technique to drive neuronal development autonomously. Human embryonic stem cells and hiPSCs can be differentiated into dopaminergic neurons, the neuronal type afflicted by PD. Our previous work showed that microspheres might administer

guggulsterone to hiPSCs to construct mature brain tissues. Sharma et al. validated that these unique guggulsterone-releasing microspheres are now included into our fibrin-based bioink as a tool for 3D bioprinting brain tissues [28]. They replicated healthy brain tissue using hiPSC-derived NPCs and tested the bioactive capabilities of our microsphere-based bioink. Following those studies, this goal for this study was to create patient-specific neural tissues containing dopaminergic neurons from hiPSCs derived NPCs to model diseased brain tissue. Here, used layer-by-layer printing to create dome-shaped structures with a diameter of 1 cm and bioprinted three different groups such as NPCs with soluble guggulsterone (SG), guggulsterone microspheres (GM) and exclusively NPCs as a control (C) to analyze the characteristics of patient-specific neural tissues. Cell viability and the expression of markers that demonstrate how diseased dopaminergic neurons develop were examined on all three sets of constructs.

4.1. Material and Methods

4.1.1. Expansion of PD-NPCs

NPCs (ATCC-DYS0530 PD) (Catalog No. ACS-5001TM) produced from hiPSCs of a 63-year-old male patient were grown on a 12-well plate pre-coated with Cell Matrix Basement Membrane in this work (ATCC ACS-3035). The complete growth media for the expansion of NPCs used is DMEM:F12 (ATCC 30-2006) supplemented with a Growth Kit (ATCC ACS-3003) containing 5 mL L-Alanyl-L-Glutamine, 5 mL Non-Essential Amino Acids, 10 mL NPC Growth Kit Component A, 5 mL NPC Growth Kit Component B, 1 mL NPC Growth Kit Component C. When the cells achieved ~95% confluence, they were reseeded at 40,000 viable cells/cm2, and they were cryopreserved in stem cell freezing medium (ACS-3020).

4.1.2. Microspheres Preparation and Characterization

Using an oil-in-water (o/w) emulsion technique as previously described, microspheres were created [63]. To create the 2% poly (vinyl alcohol) (PVA) (Mw ~ 13,000–23,000, 87%– 89% hydrolyzed) (Sigma-Aldrich, St. Louis, MO, United States) solution, PVA was diluted in de-ionized water for an hour at 85°C with 850 rpm on a magnetic mixer (Corning Life Sciences, Tewksbury, MA 01876, USA). 2% PVA was then dissolved in de-ionized water to make 100 ml 0.3 percent (w/v) PVA solution. The oil phase was made by mixing 500 mg PCL (Mn 45,000) in 3 ml DCM (Fischer Scientific, Ottawa, ON, Canada) for 15 minutes at 900 rpm. Guggulsterone (Sigma-Aldrich, St Louis, MO, USA) 0.3 mg/mL (w/w, guggulsterone/PCL) microspheres were then made by dissolving it in 100% ethanol and adding it to the oil phase. After removing the magnetic mixer, 3 ml of 2% PVA was

progressively added to the oil solution to avoid boundary layer disturbance. Then, for 15 seconds, vortex mixing (Fisher Scientific) produced an emulsion (w/o). Soluble emulsion was put into 0.5% PVA water phase and kept at 35°C for 4 hours to evaporate the organic solvent. Then, it is centrifuged at 4,000 rpm (Eppendorf 5810 R type with swinging bucket rotors) and cleaned them with deionized water. Lyophilized for 24 hours and kept at 20°C. Prior to printing, microspheres were disinfected for 30 seconds using low power air-plasma (Harrick Plasma, Ithaca, NY, USA).

4.1.3. Bioink Preparation and Printing Procedure

In accordance with our previous protocol, the fibrin-based low viscosity alginate bioink, crosslinker, and buffer solution was created [25]. Priming agents such as purmorphamine and FGF8 (b) (100 ng/mL each, PeproTech, R&D Systems) were used to prime hiPSC-derived PD NPCs in Neural Induction Medium (NIM, Cat. No. 05835, STEMCELL Technologies) while the cells were grown to 70-80% confluency. Accutase was used to dissociate the primed PD-NPCs. Following that, 1 million PD-NPCs per millilitre of bioink were bioprinted into a 6-layer dome-shaped construct under sterile circumstances using the Aspect Biosystems RX1 Bioprinter at a speed of 25mm/s with and without microspheres. The bioprinter's system had a pressure of 1700 mbar, whereas the bioink, crosslinker, and buffer had pressures of 70 mbar, 80 mbar, and 500 mbar, respectively. Finally, the bioprinted constructs were transferred to a 12-well cell culture plate that had been pre-coated with Cell-Matrix Basement Membrane comprising NIM and 1% Penicillin-Streptomycin (P/S, Sigma-Aldrich Cat. No. P4333). After that, three replicates for each of the three experimental groups were printed.

4.1.4. Culturing of Bioprinted Constructs

The three experimental groups are soluble guggulsterone (SG), guggulsterone microspheres (GM), and a control (C) group consisting exclusively of NPCs. While the three groups share NIM and 1% Penicillin-Streptomycin ((P/S), Cat. No. P4333, Sigma-Aldrich), the soluble group varies in that it contains soluble guggulsterone. On day 21, however, NIM is substituted with BrainPhys in all experimental groups.

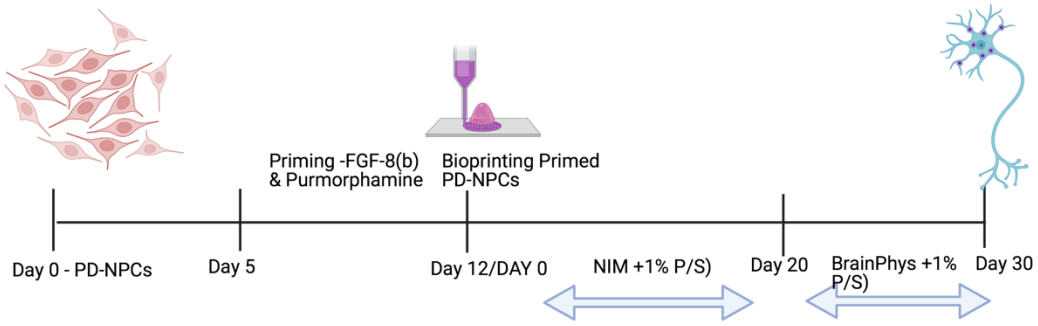

Figure 4.1 Schematic representation of culture, bioprinting, and maturation of PD-NPCs (Created with BioRender.com)

4.1.5. Cell Viability

In this research, a LIVE/DEAD^{TM} Viability/Cytotoxicity kit (Cat. No. L3224, Thermo Fisher) was used to assess cell viability on 3D bioprinted constructs on all the experimental days (1, 20, and 30). To that end, the culture medium was removed and bioprinted 3D constructs and 2D culture were washed with DPBS. Then, as per the manufacturer's instructions, 2D and 3D cultures were treated with 0.05% Calcein AM and 0.2% Ethidium Homodimer-1 in DPBS. After that, 2D and 3D cultures were incubated at 37 $^{\circ}$C with 5% CO2 for 30 minutes and 45 minutes respectively, followed by imaging using a Leica DMI300 B microscope with an X-Cite Series 120Q fluorescent light source (Excelitas

Technologies) and a QImaging RETIGA 2000R camera at 10x magnification. Finally, images were captured using the MicroManager imager. For 3D constructs, cell viability was quantified by imaging one spot on the construct and taking 15 images in varying Z-planes. A Z-projection was then created using ImageJ V1.52a, and the number of live and dead cells were counted to determine the viability throughout the construct.

4.1.6. Tissue Sectioning and Immunocytochemistry

Staining was performed on 3D constructs on day 20 and 30 to visualize the early neuronal markers and mature neuronal markers. On 3D cultures, the media was removed, and the cells were washed twice with PBS, fixed with 4% paraformaldehyde, and incubated at room temperature for 10 minutes. Then, paraformaldehyde was removed, the cultures were washed with PBS twice, permeabilized with 0.1% Triton-X, and incubated at room temperature for 10 minutes. Following this, Triton-X was removed and the cultures were blocked with 5% NGS and incubated for 1-2 hours at room temperature. Additionally, 3D constructs were washed with PBS before being fixed in 4% paraformaldehyde in PBS and cryoprotected in a 30% sucrose solution overnight. These 3D constructs were sectioned at 15–20 mm using a vibratome (*Leica* VT1000 S *vibratome)* and collected on glass microscope slides. After that, both 2D and 3D cultures were immunostained according to standard protocols using the following primary antibodies. Recombinant Anti-Tyrosine Hydroxylase antibody [EP1532Y] (Cat. No. ab137869, abcam) at 1:500 dilution and Anti-beta III Tubulin antibody [5G8] (Cat. No. ab231084, abcam) were added for day 20. Then, they were stained with appropriate fluorescent secondary antibodies and treated with DAPI. Recombinant Anti-MAP2 antibody [AA5] (ab254143, abcam) at 1:100 dilution and NURR1, alpha synuclein, LRRK2, DJ-1 were added on day 30 in 5% NGS.

These antibodies were incubated at 4°C overnight while shaking at 100rpm and washed 3 times with PBS after incubation. Then, the secondary antibodies of Goat anti-Mouse IgG (H+L) Highly Cross-Adsorbed Secondary Antibody (Alexa Fluor 488 (Cat. No. A-11029, ThermoFisher)) and goat anti-rabbit (Alexa Fluor® 568) (Cat. No. A11011, ThermoFisher) were added at a 1:200 dilution in 5% NGS. Following this, they were incubated for 2 hours at room temperature with shaking at 100 rpm. Finally, 2D and 3D cultures were washed twice with PBS and stained with 300 nM of DAPI (Cat. No. D1306, ThermoFisher) diluted in PBS. Afterwards, these cultures were incubated for five minutes at room temperature before being washed twice with PBS. Then, these cultures were imaged using the FIPS-Zeiss Confocal Laser Scanning Microscope.

4.1.7. Histological Studies - Lewy bodies (Hematoxylin & Eosin) Staining:

Constructs were sectioned at 50 μm with a vibratome and incubated with Hematoxylin and Eosin staining kit (Cat. No. ab245880, abcam) according to the protocol. Hematoxylin (Mayer's (Lillie's Modification)) was added to the 3D construct and incubated for 5 minutes to thoroughly coat it. The slides were then cleaned twice in distilled water to remove any remaining stain. The construct was then thoroughly covered with bluing reagent and incubated for 10-15 seconds. The slides were washed in distilled water twice more. Following that, the slides were immersed in 100% alcohol and the excess alcohol was wiped out. The construct was then thoroughly covered with Eosin Y Solution (modified alcoholic) and incubated for 2-3 minutes. The slides were washed in absolute alcohol once again. Finally, the slides were dehydrated in absolute alcohol three times before being cleaned and mounted in synthetic resin. After then, pictures were acquired using the

Cytation 5TM Gen5 imager and its related software version 3.05. (BioTek instruments, Winooski, VT, United States).

4.1.8. Statistics

For cell viability and electrophysiology experiments, a one-way ANOVA and Tukey post-hoc analysis was conducted, using a confidence level of 95% ($p < 0.05$). All statistical analyses were conducted on the Prism 5 (GraphPad) statistical software.

4.4 Results

4.4.1. Cell expansion and Priming

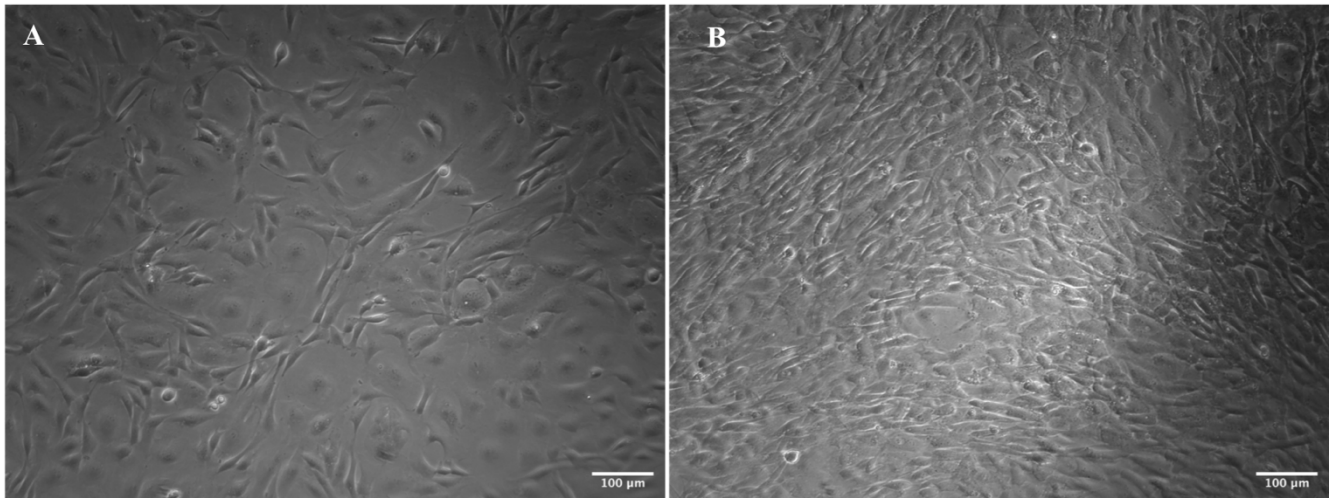

Figure 4.2 PD NPCs **(a)** Prior to Priming, and **(b)** After Priming with FGF-8(b) and Purmorphamine for seven days

To understand the growth and morphology of PD NPCs, the phase contrast images were obtained on the following days: day 0 (when the PD NPCs were 70-80% confluent) **Figure 4.1 (a),** and day 7 after priming with FGF-8(b) and Purmorphamine **(b)** at 10X magnification.

4.4.2. Microspheres Characterization

Guggulsterone-containing microspheres were manufactured with a single emulsion process and examined with a SEM to assess their shape and size distribution **Figure 4.2** the microspheres were spherical with smooth surfaces, but their sizes were not consistent. In comparison, single emulsion unloaded microspheres had a similar architecture but a significantly more consistent size distribution and average diameter. The average diameter

of dried guggulsterone microspheres was 2.133 ± 0.533 μm. The drug encapsulation efficiency of guggulsterone inside the microspheres was 45.09% ±5.693% of the total guggulsterone added throughout the manufacturing process.

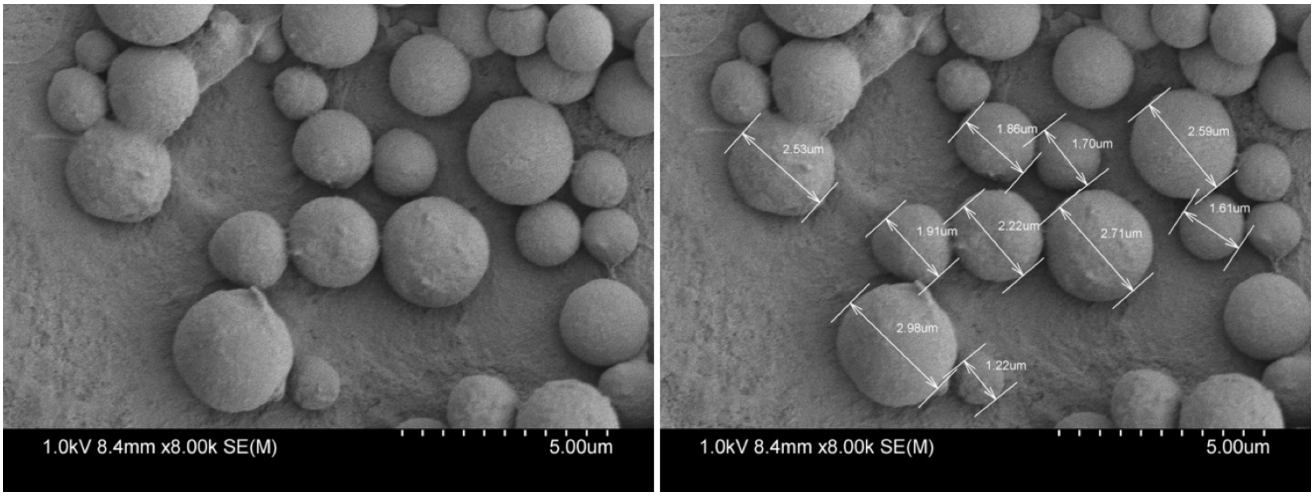

Figure 4.3 Characterization of PCL-based guggulsterone-encapsulated microspheres. SEM images showing morphology and the size of dried guggulsterone microspheres. Scale 5 μm. An accelerating voltage of 1.0 kV and working distances of 8.4 mm were used to capture the images[d].

[d]The Figure **4.3** is from: **Ruchi Sharma,** Claire Benwood, and Stephanie Michelle Willerth **"Drug-releasing microspheres for stem cell differentiation" Current Protocols 2021**

4.4.3. Cell Viability

Figures 4.3, 4.4, 4.5, and **4.6** show images and quantifiable data for bioprinted and cultured PD NPCs treated with soluble guggulsterone, guggulsterone microspheres, and a control group stained for viability on days 1, 20, and 30. On day 1, viability was assessed after 24 hours, on day 20, before to the addition of Brain Phys maturation medium, and lastly on day 30.

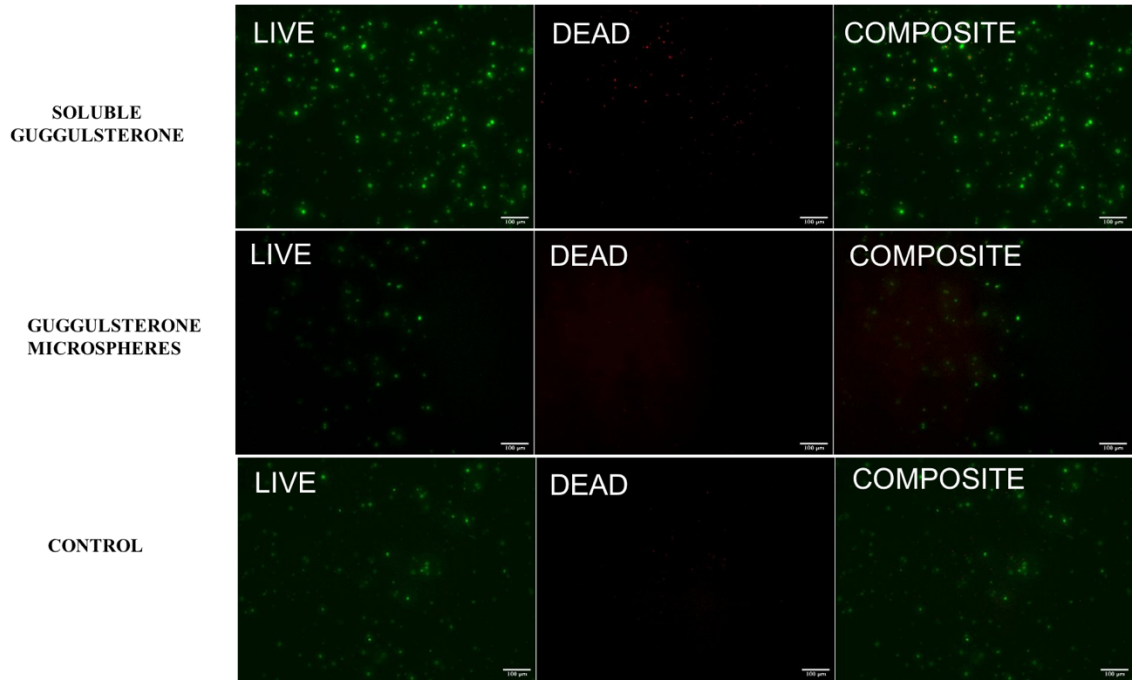

Figure 4.4 Cell viability images using live and dead staining on bioprinted hiPSC-derived NPCs with soluble guggulsterone, guggulsterone microspheres, and control on day 1 (Scale: 100um)

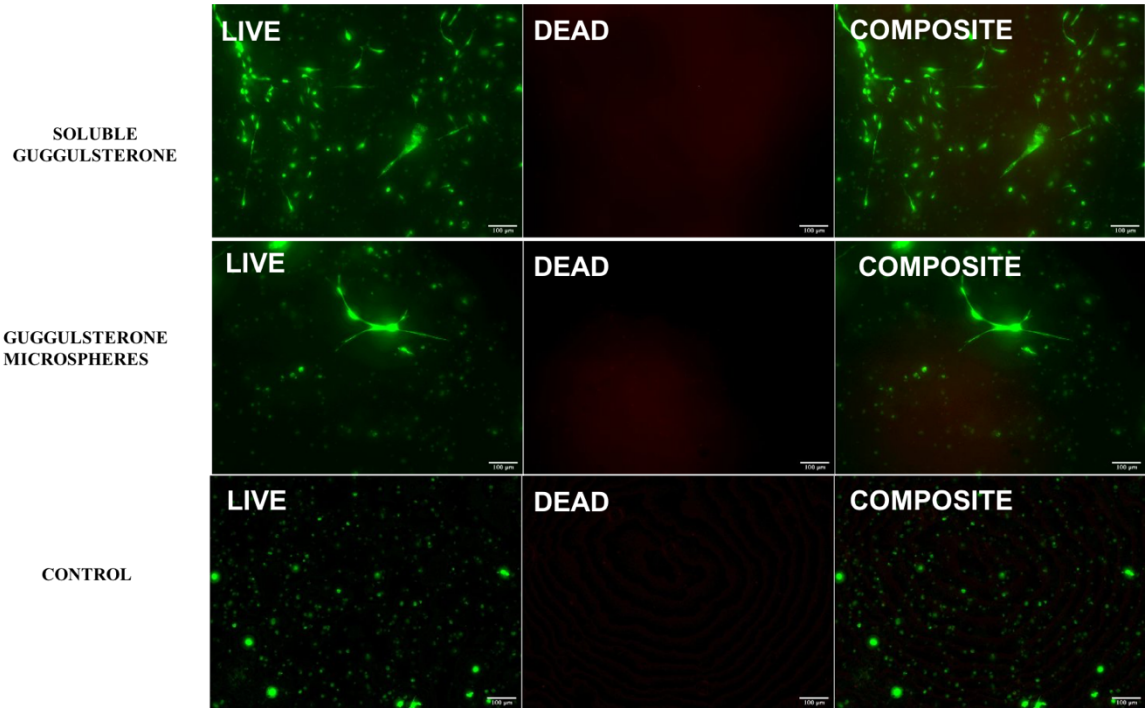

Figure 4.5 Cell viability images using live and dead staining on bioprinted hiPSC-derived NPCs with soluble guggulsterone, guggulsterone microspheres, and control on day 20 (Scale: 100um)

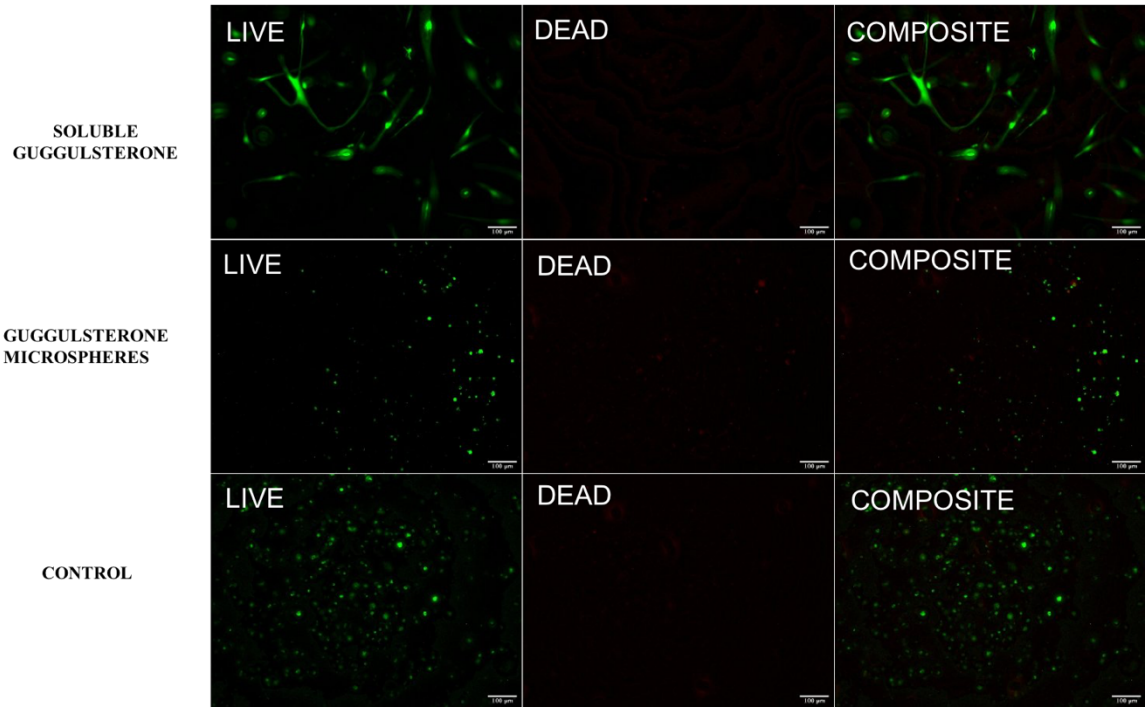

Figure 4.6 Cell viability images using live and dead staining on bioprinted hiPSC-derived NPCs with soluble guggulsterone, guggulsterone microspheres, and control on day 30 (Scale: 100um)

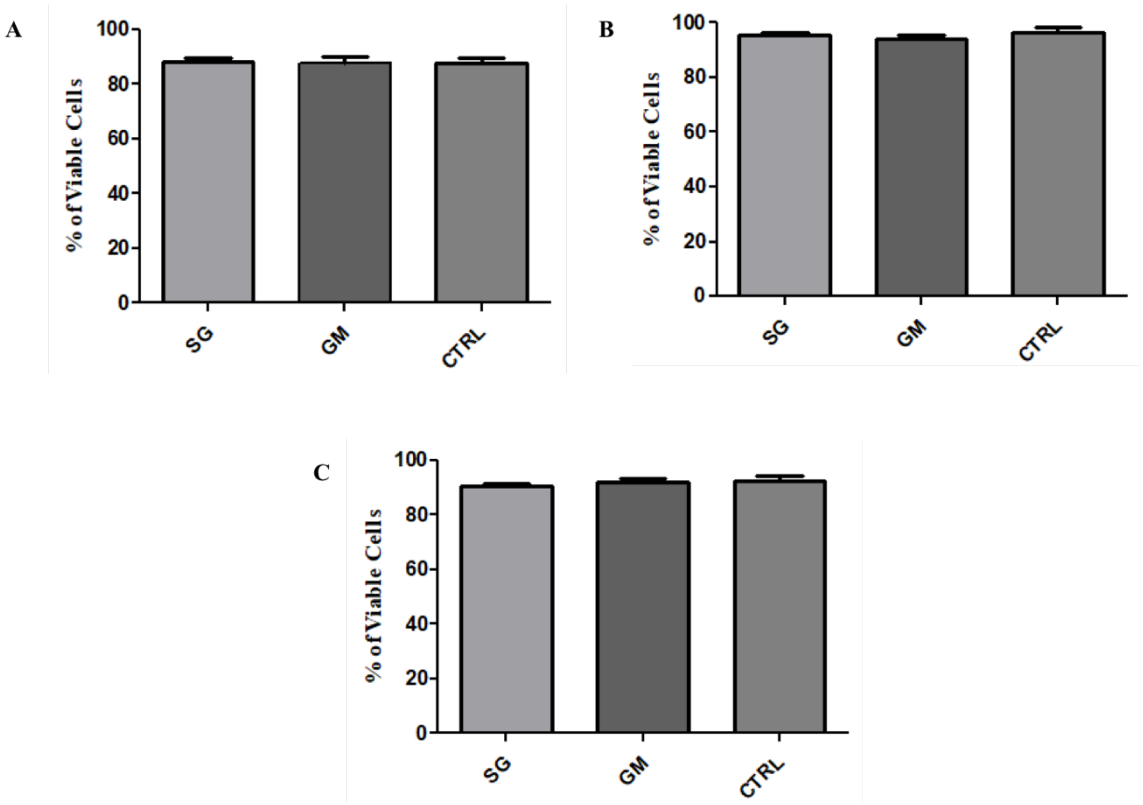

Figure 4.7 Cell viability images using live and dead assay were quantified and values are given as average ± standard deviation on bioprinted hiPSC-derived NPCs with soluble guggulsterone (SG), guggulsterone microspheres (GM), and control (CTRL) on day 30 (Scale: 100um) ($P<0.05$, no statistical difference observed between the groups)

4.4.4. Histological Studies - Lewy bodies H & E Staining

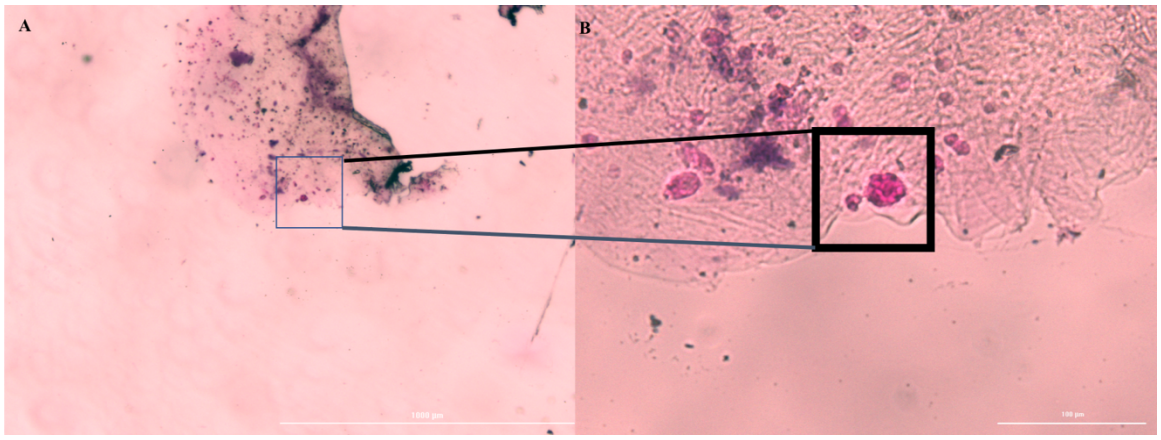

Figure 4.8 H and E staining showing Lewy body formation on bioprinted hiPSC-derived NPCs with guggulsterone microspheres on day 30 (Scale: 1000um)

4.4.5. Immunocytochemistry (ICC)

ICC was performed on constructs for all three groups: soluble guggulsterone, guggulsterone microspheres, and control for the cellular markers TUJ1 (an immature neuronal maker), FOXA2 (a midbrain-type dopamine neuron marker) and TH (an enzyme expressed by dopaminergic neurons) at day 20. (**Figure 4.8, 4.9**) and on day 30 for, FOXA2, TUJ1, TH, NURR1, LRRK2, alpha synuclein (α-Synuclein), DDC, and PARK7/DJ-1(**Figures 4.10-4.14**). All constructs stained positive for varying levels of TUJ1 and FOXA2 on day 20. Constructs at day 30 expressed on LRRK2, alpha synuclein (α-Synuclein) more in the group with microspheres.

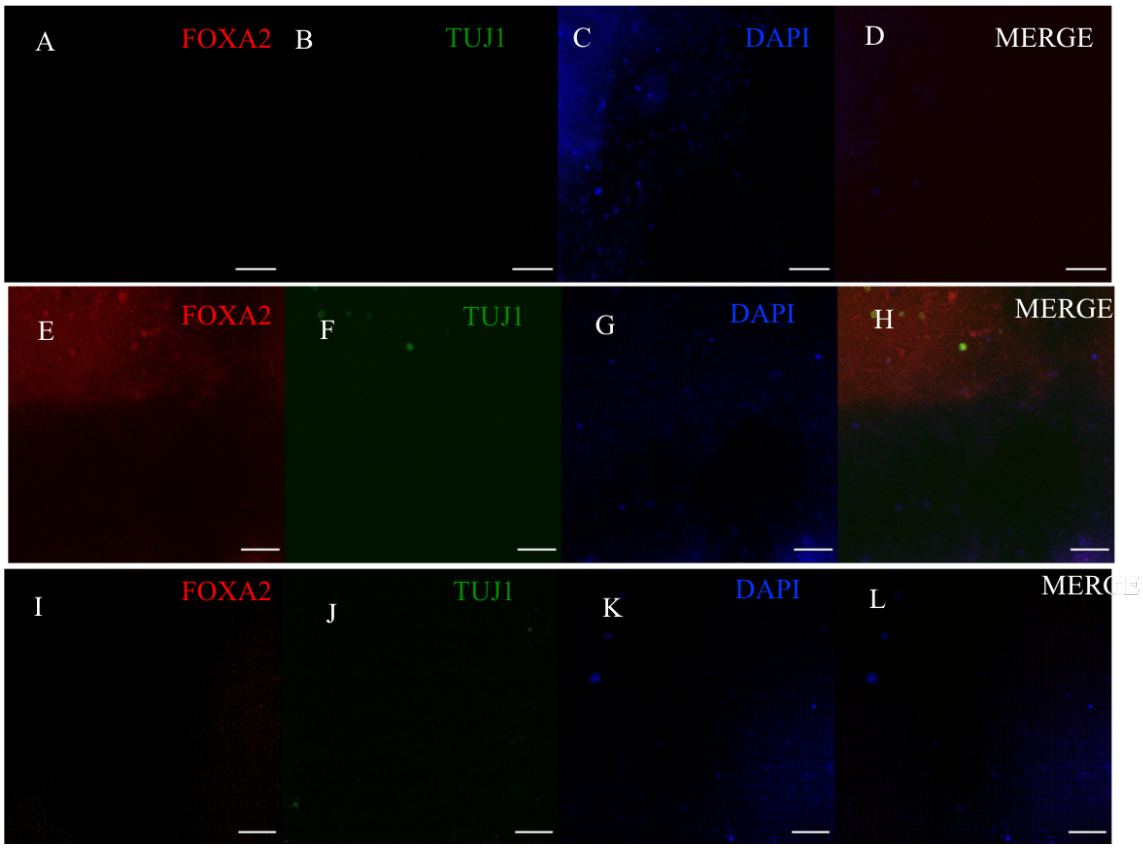

Figure 4.9 Immunocytochemistry of 3D bioprinted hiPSC-derived NPCs with soluble guggulsterone (A-D), guggulsterone microspheres (E-H), and control (I-L) stained for Forkhead Box A2 (FOXA2), TUJ1, and 4′,6-diamidino-2-phenylindole (DAPI) on day 20 (Scale: 100um)

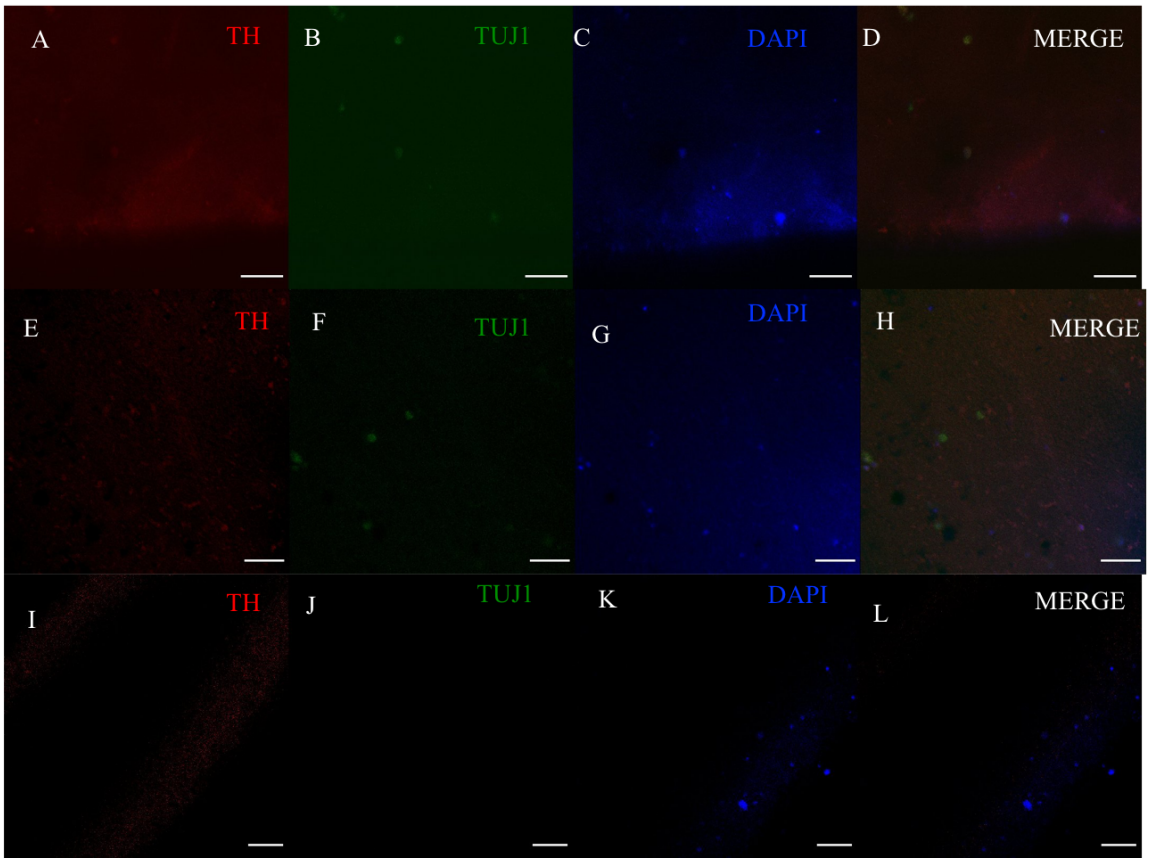

Figure 4.10 Immunocytochemistry of 3D bioprinted hiPSC-derived NPCs with soluble guggulsterone (A-D), guggulsterone microspheres (E-H), and control (I-L) stained for Tyrosine Hydroxylase (TH), TUJ1, and 4′,6-diamidino-2-phenylindole (DAPI)on day 20 (Scale: 100um)

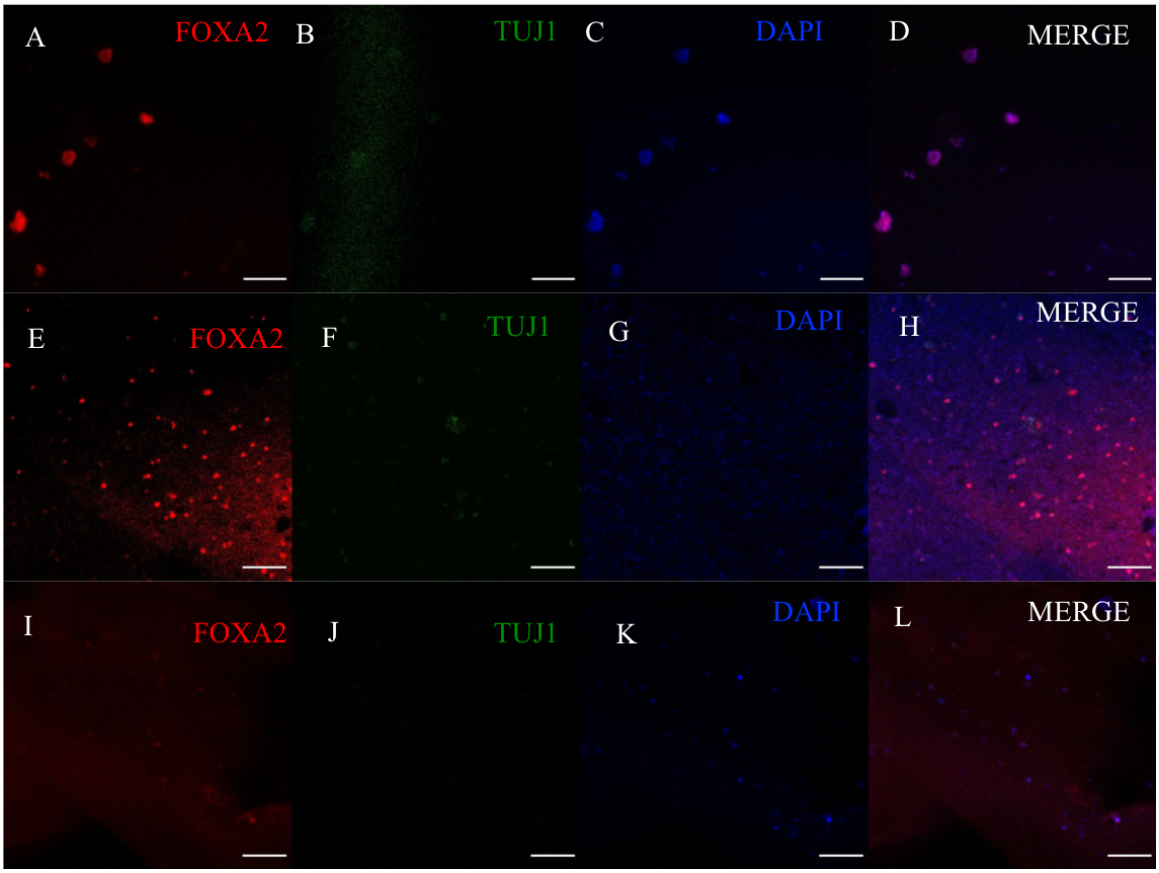

Figure 4.11 Immunocytochemistry of 3D bioprinted hiPSC-derived NPCs with soluble guggulsterone (A-D), guggulsterone microspheres (E-H), and control (I-L) stained for Forkhead Box A2 (FOXA2), TUJ1, and 4′,6-diamidino-2-phenylindole (DAPI) on day 30 (Scale: 100um)

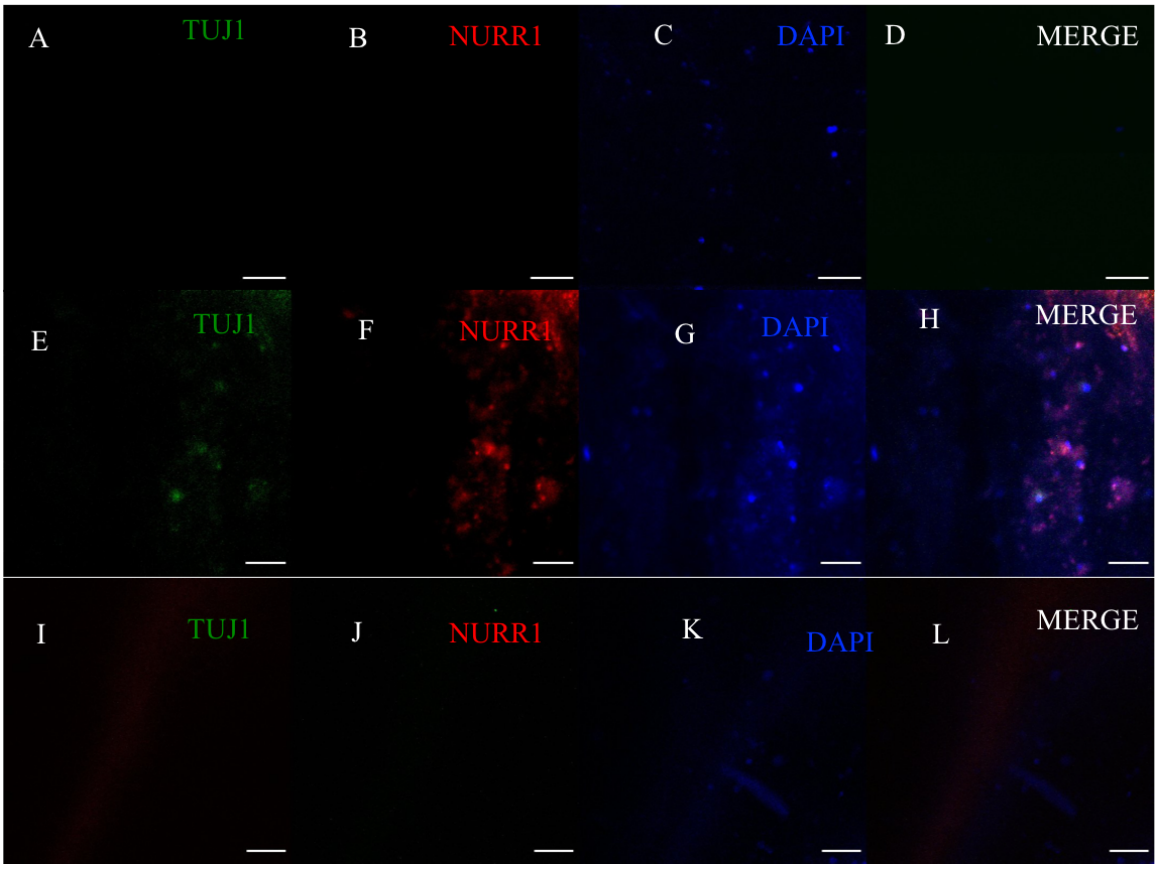

Figure 4.12 Immunocytochemistry of 3D bioprinted hiPSC-derived NPCs with soluble guggulsterone (A-D), guggulsterone microspheres (E-H), and control (I-L) stained for (TUJ1), Nuclear receptor related 1 (NURR1), and 4′,6-diamidino-2-phenylindole (DAPI)on day 30 (Scale: 100um)

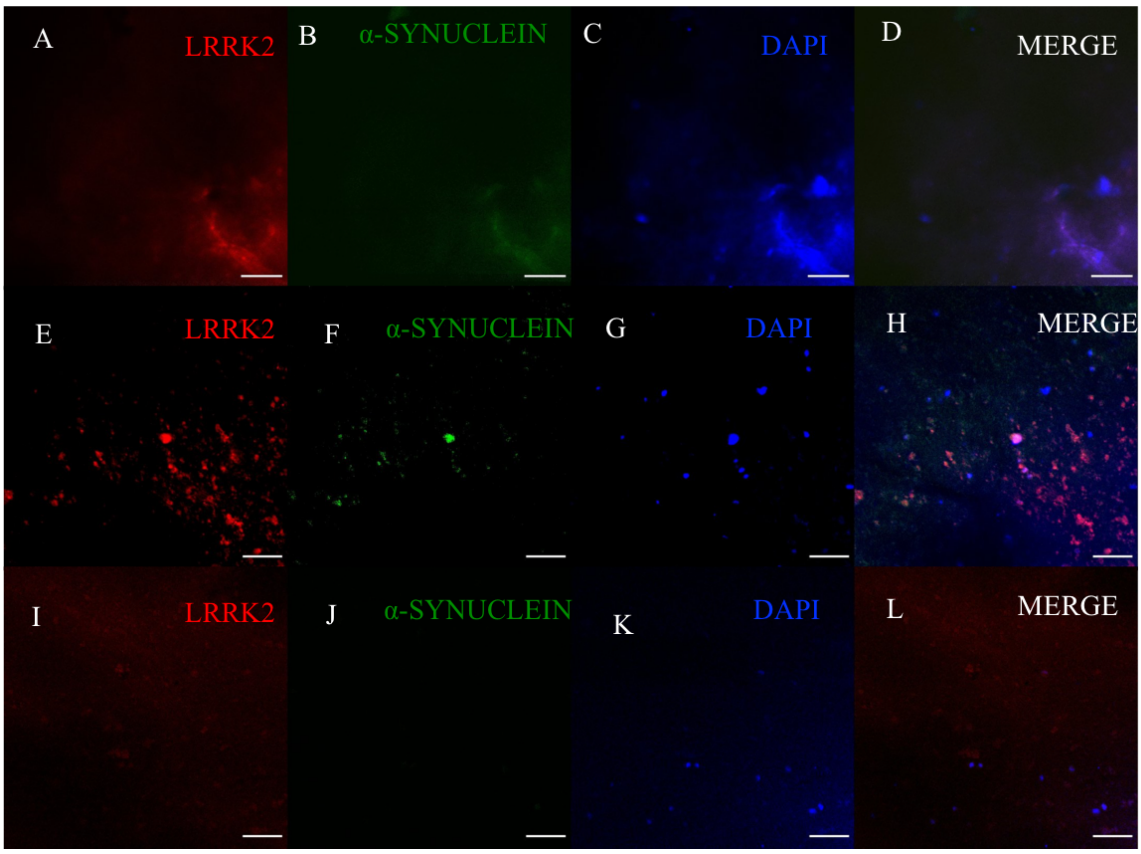

Figure 4.13 Immunocytochemistry of 3D bioprinted hiPSC-derived NPCs with soluble guggulsterone (A-D), guggulsterone microspheres (E-H), and control (I-L) stained for Leucine Rich Repeat Kinase 2 (LRRK2), alpha-synuclein, and 4′,6-diamidino-2-phenylindole (DAPI) on day 30 (Scale: 100um)

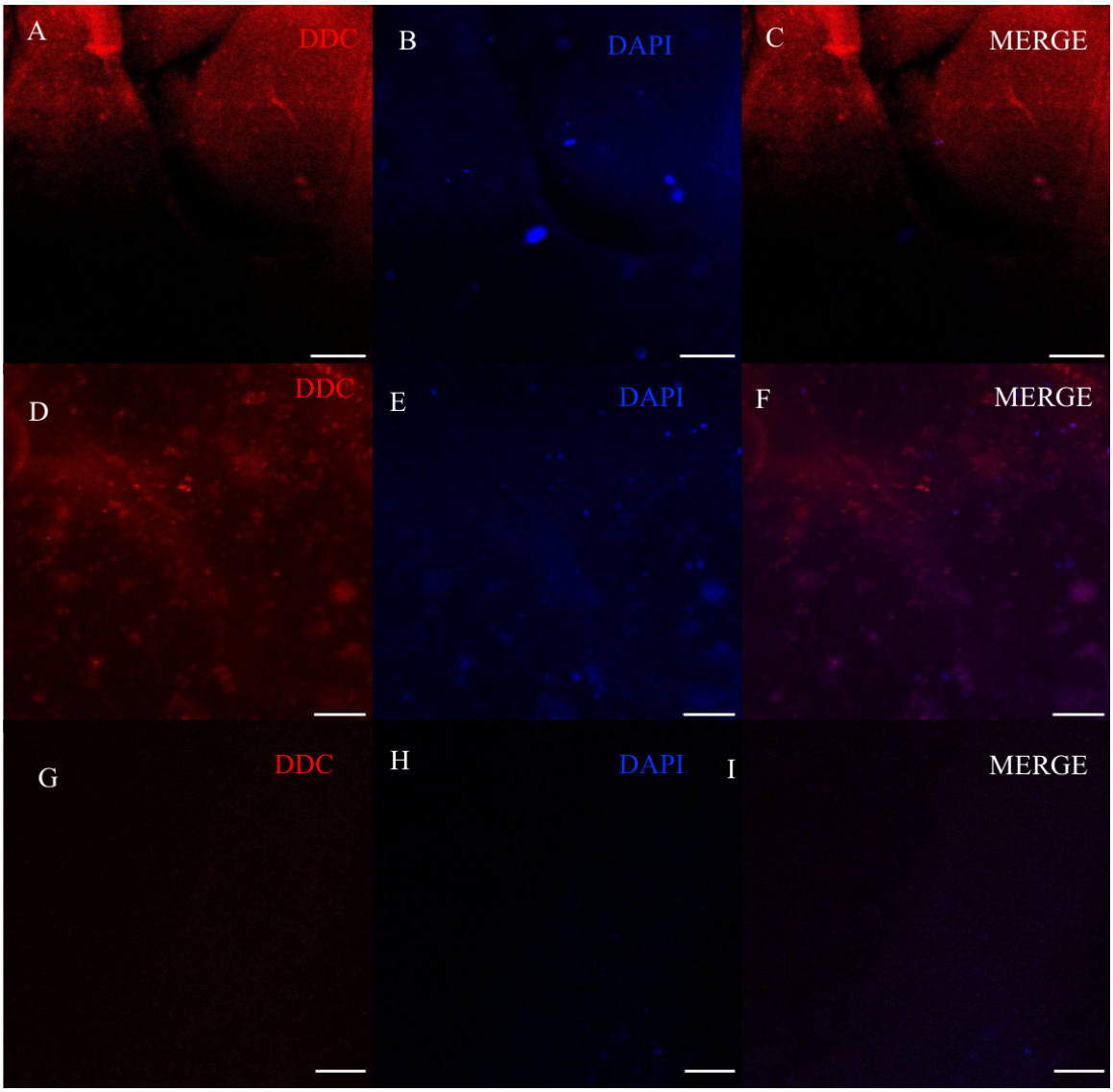

Figure 4.14 Immunocytochemistry of 3D bioprinted hiPSC-derived NPCs with soluble guggulsterone (A-D), guggulsterone microspheres (E-H), and control (I-L) stained for DDC (Dopa-decarboxylase) *and* 4′,6-diamidino-2-phenylindole (DAPI) on day 30 (Scale: 100um)

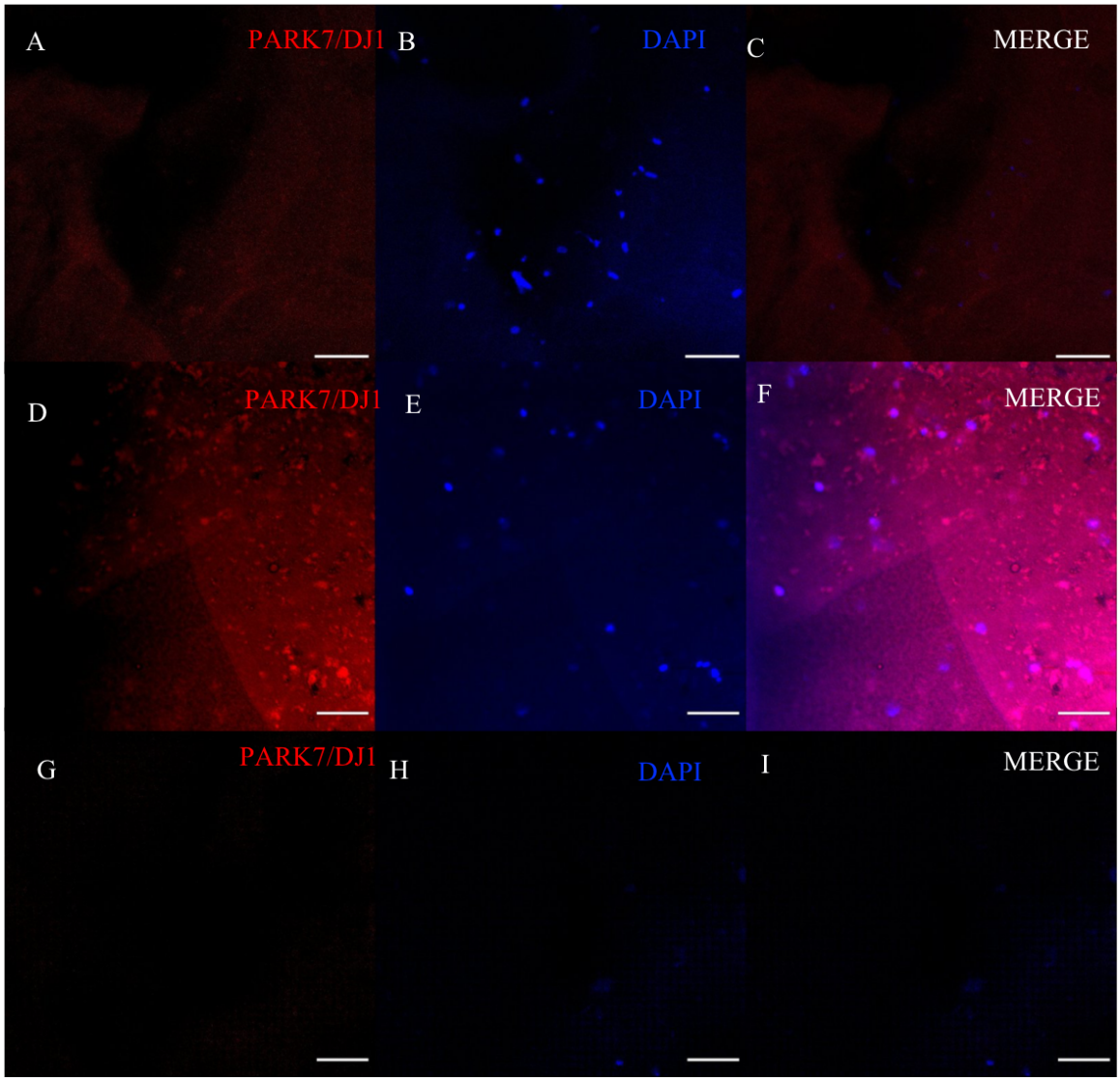

Figure 4.15 Immunocytochemistry of 3D bioprinted hiPSC-derived NPCs with soluble guggulsterone (A-D), guggulsterone microspheres (E-H), and control (I-L) stained for Parkinsonism Associated Deglycase (PARK7)/ Protein deglycase (DJ-1) and 4′,6-diamidino-2-phenylindole (DAPI) on day 30 (Scale: 100um)

4.5. Discussion

An appropriate human 3D cellular model of disease may provide a novel and convenient platform for investigating molecular pathways and screening therapeutic drugs [37]. Gonzalez et al. discovered guggulsterone as the most efficient inducer of DN differentiation, which replaces the complicated cocktail of molecular factors with a single component [68]. Guggulsterone may not stimulate a particular course that directs differentiation to a dopaminergic fate, but it may hinder another pathway that leads differentiation to another cell type. STAT3 is also involved in tumour cell proliferation and is constitutively activated in many human cancer cells. Guggulsterone has been explored as a cancer therapy medicine, and evidence suggests that it does so through suppressing STAT3 signalling [28, 70]. This simplified procedure produced ESC-derived DNs that released three times more dopamine *in vitro* than earlier studies while exhibiting conventional gene and protein profiles [68, 69]. A single emulsion approach was used to encapsulate guggulsterone into PCL microspheres and proved that guggulsterone may be released from these biodegradable microspheres in these bioprinted constructs over 30 days [28, 70].

The goal of the current study was to develop a novel bioprinted model to understand the pathogenesis of PD. Although PD is a progressive, chronic neurological disease, most *in vitro* studies have examined pathogenic mechanisms in 2D and 3D organoid models [2, 7]. Advances in disease modelling have been made in recent years, which have been made feasible because of 3D bioprinting technology, which allows for the creation of intricate tissue architecture [17, 25-28]. Furthermore, the ability to obtain hiPSCs from a given person enables a more targeted analysis of the processes that occur throughout disease

development. There are many approaches for generating DNs, however, the bulk of them do not take midbrain architecture into consideration [42]. In this work, we established for the first time that a 63-year-old Parkinson's disease patient's hiPSC-derived NPC could be bioprinted with drug-releasing microspheres and cultivated for 30 days. Before proceeding to pathological examination, cellular viability was evaluated at three different time periods. The immunocytochemistry revealed that after bioprinting on day 20, NPCs are orienting themselves toward becoming mature neurons and more than 90% PD-NPCs were viable in all three groups. Furthermore, misfolding and aggregation of alpha-synuclein (alpha-synuclein) with concurrent cytotoxicity is a feature of Lewy body. Alpha synuclein is a small protein that has been reported to be elevated in neurons of both familial and idiopathic Parkinson's disease patients. The development of Lewy bodies in bioprinted constructs was established by H and E findings. The application of the aforementioned approach also resulted in FOXA2-positive midbrain floor plate progenitors. FOXA2 is necessary for DA neuron growth *in vivo*, according to previous research. By day 20, FOXA2 was expressed in bioprinted structures with guggulsterone microspheres and TUJ1. Furthermore, on day 30, it is noticed that the protein levels of alpha synuclein and LRRK2 were higher in both guggulsterone microspheres and soluble guggulsterone, which may be related to the creation of Lewy bodies in the bioprinted constructs. Since LRRK2 is another protein connected to the aetiology of PD, and its presence in Lewy bodies has sparked speculation over whether LRRK2 and alpha-synuclein interact during the pathogenesis of PD. DJ-1 protein protects dopaminergic neurons from neurodegeneration in PD through numerous distinct pathways. Bioprinted tissues containing guggulsterone microspheres and those treated with soluble guggulsterone showed expression of mutation

DJ-1/PARK7. NURR1 has been linked to the maturation of early dopa progenitors into adult TH + neurons. In addition to its involvement in normal brain development, NURR1 loss has been linked to the development of DNs dysfunction in Parkinson's disease. Our sole guggulsterone microsphere group expressed more NURR1 than the other two groups. Due of DDC's critical role in neurotransmitter production, it is a significant target in the research of PD. Out of our three groups, exclusively guggulsterone microsphere expressed DDC. Thus, our findings revealed for the first time that a patient's bioprinted PD-NPCs may impact the establishment of complex midbrain structure. Similar findings were reported in a recent study by Smits et al., 2019, which focused on the effect of Parkinson's disease genetic background on organoid growth. To conclude, it is provided that a 3D bioprinted model of PD based on fibrin-based bioink with guggulsterone microspheres accurately mimics alpha-synuclein pathologies such as increased alpha-synuclein and Lewy body-like inclusions. Furthermore, bioprinted patient-specific tissues are a great technology for PD modelling. Patients' individual genetic features in PD may be replicated in a 3D model, allowing researchers to study the disease's pathology *in vitro.*

4.6. Conclusion

To conclude, the current work presents a new 3D bioprinted human cellular model of PD with alpha-synuclein phosphorylation buildup and Lewy body-like inclusions. The model is simple to construct, modify, and monitor, and it should be beneficial in researching PD processes and screening treatments for alpha-synuclein pathologies.

Chapter 4: Author's contribution

The scientific concept for this study purpose was designed by me (Ruchi Sharma, first author). I devised the experimental strategy, carried out and supervised the experimental procedures, and analysed the results. I completed the manuscript and sent it to the other authors and my supervisor for review, comments, and suggestions. After receiving their input, I modified and created the final draft for journal publication. I have included more particular information about each author's contribution to this publication below. I used the paid version of bio render to construct a schematic depiction of the culture, bioprinting, and maturation of PD-NPCs (figure 4.1). I have cultured and primed PD NPCs and prepared and characterized PCL microsphere (figure 4.2, 4.3). Cell viability (figures 4.4, 4.5, 4.6, and 4.7) was performed by me, and the second author (Perez Restan M.) and third author (Scheck K.) assisted me with the live and dead assays on day 1 and day 30. I have performed H and E staining to indicate the creation of Lewy bodies (figure 4.8). The second author assisted me in doing ICC. All the images (figure 4.9, 4.10, 4.11, 4.12, 4.13, 4.14, and 4.15) by confocal microscope have done and analyzed by me. Dr. Stephanie Willerth has provided suggestions and input into the experimental design, comments and supervision on the experimental analysis, and writing and editing the article at all phases of this investigation.

Chapter 5 Discussion and Conclusion

The ultimate objective of this research was to develop novel strategies for rapidly fabricating scalable brain tissue utilising sophisticated 3D bioprinting technology and to understand how morphogens released from bioprinted constructs differentiate hiPSC into mature neurons. My focus for this was on the development of neural tissues containing DNs from hiPSC-derived NPCs to mimic healthy brain tissue. Particularly, I investigated both healthy as well as diseased bioprinted models and also performed physical and mechanical properties analysis to validate the bioactive properties of microsphere-containing bioink. In this study, I bioprinted dome-shaped constructs with a diameter of 1 cm in a six-layered structure using hiPSC-derived NPCs encapsulated within guggulsterone microspheres and studied their charateristics. There are three distinct ways in which the research given here responded to objectives:

5.1 Discussion and conclusion of research objective 1

Research objective 1 was to bioprint healthy hiPSC-derived NPCs with drug-releasing microspheres and characterize their release in differentiated tissues. Drug-releasing microspheres in bioinks may boost cell differentiation efficiency while reducing medium changes.

In chapter 2, I focussed on bioprinting dome-shaped constructs containing NPCs. These dome-shaped structures were allowing for long-term cell growth in vitro, and also more effectively reflects the microenvironment in the brain. Here, I used a microfluidic-based Aspect Biosystems RX1 bioprinter to bioprint NPCs with guggulsterone-releasing microspheres to generate a complex brain tissue model, which are also called “mini- brain.”

Microspheres offered a cushion surrounding the cells, reducing shear stress during and after printing. This work showed that these microsphere-filled bioprinted constructs are excellent 3D environments for neural stem cells. Importantly, I showed that adding microspheres to printed structures improved cell survival. The enhanced viability on day 7 showed that cells acclimated to the scaffold microenvironment with microspheres, allowing them to proliferate. 3D-printed microsphere-based bioinks promoted neural differentiation into particular neuronal subtypes while preserving excellent cell viability. Overall, these findings pointed to the potential of this method to improve tissue regeneration in the future. Bioprinted 3D structures may be interesting for regenerating cell-specific tissues since poor cell survival is a key obstacle in transplanting. I showed that using microspheres to deliver guggulsterone, a bioactive small chemical, may help differentiate hiPSC-derived NPCs into DNs. This showed their significance as a tool for tissue engineering. Controlled guggulsterone release from microspheres may improve NPC survival and differentiation in bioprinted tissues.

Furthermore, increasing the efficacy of dopaminergic neurons in bioprinted brain tissues might be one of the next steps in research. These microspheres might be supplemented with retinoic acid and purmorphamine to further promote tissue development and maturation. 3D bioprinted brain tissues might also benefit from regulated distribution of additional signalling molecules.

5.2 Discussion and conclusion of research objective 2

Research objective 2 was to assess physicomechanical properties of bioink and bioprinted structures with drug-releasing microspheres

In this chapter, I investigated the physical and mechanical properties of the bioink and printed structures. The stiffness and porosity of the bioink that forms the microenvironment affect the differentiation of NPCs into adult phenotypes in bioprinted constructs. A fibrin-based bioink with or without microspheres promotes neuronal survival, proliferation, differentiation and maturation. The structures with microspheres were stiffer than those without. It had a high elastic modulus for a stiffer structure. These findings suggest that adding microspheres to bioprinted structures increases stiffness, which helps in long-term culture and, eventually, maturation of bioprinted brain tissues. The elastic moduli of the microsphere-filled bioprinted constructs were also 1 kPa, which is comparable to prior research. The indentation elastic moduli matched the rheometry elastic moduli. The viscoelastic characteristics were also determined, as extrusion via the bioprinter's nozzle relies on it. A good printing solution should be shear-thin under pressure, so it can readily flow through the nozzle and maintain the printed shape. Extrusion requires a greater pressure and that causes shear stress, which causes cell death. The bioink had great viscosity at low shear stresses and behaved like a solid. Moreover, slow degradation kinetics is required to regulate therapeutic compound release over time. I found that microspheres had no influence on swelling or porosity of bioprinted structures and those polymeric chains of biomaterials and microspheres may form certain physical interactions, such as chemical bonding. This increases crosslinking density and consequently strength and mechanical stability of the bioprinted constructions.

Composite hydrogel containing drug-releasing microspheres will control cell fate, enhance mechanical properties, and stimulate biological activities. In conclusion, I validated that adding microspheres to bioink boosted mechanical strength, decreased disintegration rate, and raised elastic modulus of bioprinted tissues, making them ideal for neural tissue engineering applications.

5.3 Discussion and conclusion of research objective 3

Research objective 3 was to bioprint patient-specific hiPSC-derived NPCs with drug-releasing microspheres and characterize their pathology in bioprinted tissues. The effect of bioprinting with guggulsterone microspheres was investigated in the PD-specific cell line "ATCC-DYS0530." This cell line has previously been employed for drug development, high-throughput screening, stem cell research, and toxicology [159]. DNs produced from hiPSCs have considerable potential for understanding disease processes underlying PD and testing drug effects. In chapter 4, I bioprinted disease-specific NPCs with guggulsterone microspheres for differentiating them to mature neurons with neurite defects. This is the first time 3D bioprinted model of PD containing guggulsterone microspheres have been created that may closely mimics alpha-synuclein pathology such increased alpha-synuclein and Lewy body-like inclusions. Also, bioprinted patient-specific tissues are an excellent PD modelling tool. I examined PD pathogenesis *in vitro* by replicating patients' genetic characteristics in a 3D model by investigating the different cellular markers. Conclusively, these 3D bioprinted hiPSC-based PD models derived from Parkinson's patients may provide fresh insights into their application as drug screening models.

5.4 Overall conclusion and future work

Overall conclusion

To conclude, my research showed that including drug-releasing microspheres into a novel bioink increases cell survival and differentiation, especially when bioprinting tissue from stem cell- derived progenitors, indicating that they have potential as a tool for tissue engineering. In this study, I demonstrated that the controlled release of guggulsterone from microspheres may improve the survival of NPCs present in bioprinted tissues as well as the differentiation of these cells into adult neural tissues.

I validated that by integrating tissue engineering, biomaterials, drug-delivery devices, and bioprinting, a framework can be created for the generation of neural tissues, which may be used as a tool for high-throughput drug screening for neurodegenerative disorders. Future research will focus on merging drug-releasing microspheres with other natural biomaterials to produce a more complicated bioprinted healthy brain tissue model with a high yield of neurons and glial cells. These have the potential to add value in cell treatments.

Future Work

With achievements from this thesis, some recommendations and suggested projects for future studies are given as follow:

Due to the size of bioprinted tissue, vascularization is critical. It is required for proper tissue function [17, 61]. A microvascular network is essential for oxygen transport, nutrition exchange, and ultimately, tissue cell viability. To overcome this issue, bioprinting of NPCs and endothelial cells can be done to form functional vascular networks. Previous research has suggested that NPCs and endothelial cells have a significant functional relationship and has shown spatial proximity between established neural and vascular networks [160] .

Moreover, it is always important to explore new hydrogels or other material types to simplify the process for other cell types to achieve the required cell functions in bioprinting. This thesis has validated the compatibility of fibrin-based bioink and microspheres with incorporated living cells as well as their physical and mechanical properties. However, new materials can be tested to create hydrogel to support both NPCs and endothelial cells [63, 127, 161]. Furthermore, the neuronal activity of 3D bioprinted diseased tissues may be analysed directly to determine the effects of L-DOPA.

The versatility of these bioprinted brain tissue allows widespread commercialized applications. BrainPrints are robust and replicable 3D structures that may last up to a month in culture. This fibrin-based bioink not only allows for long-term culture, but it also ensures cell viability and promotes neural development. The intricacy of BrainPrint's shape and microstructures might be employed as a therapeutic and drug-screening platform. The potential of these bioprinted brain tissues with innovative fibrin-based bioink will have a greater influence on 3D bioprinting in regenerative medicine and drug development [25, 28].

Bibliography

[1] S. Budday *et al.*, "Mechanical properties of gray and white matter brain tissue by indentation," *J Mech Behav Biomed Mater,* vol. 46, pp. 318-30, Jun 2015.

[2] E. G. Z. Centeno, H. Cimarosti, and A. Bithell, "2D versus 3D human induced pluripotent stem cell-derived cultures for neurodegenerative disease modelling," *Mol Neurodegener,* vol. 13, no. 1, p. 27, May 22 2018.

[3] A. H. Laperle *et al.*, "iPSC modeling of young-onset Parkinson's disease reveals a molecular signature of disease and novel therapeutic candidates," *Nat Med,* vol. 26, no. 2, pp. 289-299, Feb 2020.

[4] M. A. Cenci and A. Bjorklund, "Animal models for preclinical Parkinson's research: An update and critical appraisal," *Prog Brain Res,* vol. 252, pp. 27-59, 2020.

[5] P. Chlebanowska, A. Tejchman, M. Sulkowski, K. Skrzypek, and M. Majka, "Use of 3D Organoids as a Model to Study Idiopathic Form of Parkinson's Disease," *Int J Mol Sci,* vol. 21, no. 3, Jan 21 2020.

[6] K. Takahashi *et al.*, "Induction of pluripotent stem cells from adult human fibroblasts by defined factors," *Cell,* vol. 131, no. 5, pp. 861-72, Nov 30 2007.

[7] A. Chandrasekaran *et al.*, "Comparison of 2D and 3D neural induction methods for the generation of neural progenitor cells from human induced pluripotent stem cells," *Stem Cell Res,* vol. 25, pp. 139-151, Dec 2017.

[8] E. R. Aurand, K. J. Lampe, and K. B. Bjugstad, "Defining and designing polymers and hydrogels for neural tissue engineering," *Neurosci Res,* vol. 72, no. 3, pp. 199-213, Mar 2012.

[9] I. M. El-Sherbiny and M. H. Yacoub, "Hydrogel scaffolds for tissue engineering: Progress and challenges," *Glob Cardiol Sci Pract,* vol. 2013, no. 3, pp. 316-42, 2013.

[10] L. de la Vega, C. Lee, R. Sharma, M. Amereh, and S. M. Willerth, "3D bioprinting models of neural tissues: The current state of the field and future directions," *Brain Res Bull,* vol. 150, pp. 240-249, Aug 2019.

[11] S. R. Stott, E. Metzakopian, W. Lin, K. H. Kaestner, R. Hen, and S. L. Ang, "Foxa1 and foxa2 are required for the maintenance of dopaminergic properties in ventral midbrain neurons at late embryonic stages," *J Neurosci,* vol. 33, no. 18, pp. 8022-34, May 1 2013.

[12] S. K. Seidlits *et al.*, "The effects of hyaluronic acid hydrogels with tunable mechanical properties on neural progenitor cell differentiation," *Biomaterials,* vol. 31, no. 14, pp. 3930-40, May 2010.

[13] C. Benwood *et al.*, "Natural Biomaterials and Their Use as Bioinks for Printing Tissues," *Bioengineering (Basel),* vol. 8, no. 2, Feb 20 2021.

[14] J. Berg *et al.*, "Optimization of cell-laden bioinks for 3D bioprinting and efficient infection with influenza A virus," *Sci Rep,* vol. 8, no. 1, p. 13877, Sep 17 2018.

[15] J. Kajtez, F. Nilsson, A. Fiorenzano, M. Parmar, and J. Emneus, "3D biomaterial models of human brain disease," *Neurochem Int,* vol. 147, p. 105043, Jul 2021.

[16] H. Kim *et al.*, "Modeling G2019S-LRRK2 Sporadic Parkinson's Disease in 3D Midbrain Organoids," *Stem Cell Reports,* vol. 12, no. 3, pp. 518-531, Mar 5 2019.

[17] M. Cadena *et al.*, "3D Bioprinting of Neural Tissues," *Adv Healthc Mater,* p. e2001600, Nov 16 2020.
[18] F. Y. Hsieh and S. H. Hsu, "3D bioprinting: A new insight into the therapeutic strategy of neural tissue regeneration," *Organogenesis,* vol. 11, no. 4, pp. 153-8, 2015.
[19] A. Schwab, R. Levato, M. D'Este, S. Piluso, D. Eglin, and J. Malda, "Printability and Shape Fidelity of Bioinks in 3D Bioprinting," *Chem Rev,* vol. 120, no. 19, pp. 11028-11055, Oct 14 2020.
[20] N. Tasnim *et al.*, "3D Bioprinting Stem Cell Derived Tissues," *Cell Mol Bioeng,* vol. 11, no. 4, pp. 219-240, Aug 2018.
[21] R. M. Marton and S. P. Pasca, "Neural Differentiation in the Third Dimension: Generating a Human Midbrain," *Cell Stem Cell,* vol. 19, no. 2, pp. 145-146, Aug 4 2016.
[22] E. P. Canovic *et al.*, "Characterizing Multiscale Mechanical Properties of Brain Tissue Using Atomic Force Microscopy, Impact Indentation, and Rheometry," *J Vis Exp,* no. 115, Sep 6 2016.
[23] M. Robinson, K. P. Valente, and S. M. Willerth, "A Novel Toolkit for Characterizing the Mechanical and Electrical Properties of Engineered Neural Tissues," *Biosensors (Basel),* vol. 9, no. 2, Apr 1 2019.
[24] T. Zhang, K. C. Yan, L. Ouyang, and W. Sun, "Mechanical characterization of bioprinted in vitro soft tissue models," *Biofabrication,* vol. 5, no. 4, p. 045010, Dec 2013.
[25] E. Abelseth, L. Abelseth, L. De la Vega, S. T. Beyer, S. J. Wadsworth, and S. M. Willerth, "3D Printing of Neural Tissues Derived from Human Induced Pluripotent Stem Cells Using a Fibrin-Based Bioink," *ACS Biomater Sci Eng,* vol. 5, no. 1, pp. 234-243, Jan 14 2019.
[26] L. de la Vega, D. A. Rosas Gómez, E. Abelseth, L. Abelseth, V. Allisson da Silva, and S. Willerth, "3D Bioprinting Human Induced Pluripotent Stem Cell-Derived Neural Tissues Using a Novel Lab-on-a-Printer Technology," *Applied Sciences,* vol. 8, no. 12, 2018.
[27] L. De la Vega, L. Abelseth, R. Sharma, J. Triviño-Paredes, M. Restan, and S. M. Willerth, "3D Bioprinting Human-Induced Pluripotent Stem Cells and Drug-Releasing Microspheres to Produce Responsive Neural Tissues," *Advanced NanoBiomed Research,* 2021.
[28] R. Sharma, I. P. M. Smits, L. De La Vega, C. Lee, and S. M. Willerth, "3D Bioprinting Pluripotent Stem Cell Derived Neural Tissues Using a Novel Fibrin Bioink Containing Drug Releasing Microspheres," *Front Bioeng Biotechnol,* vol. 8, p. 57, 2020.
[29] V. Fantini *et al.*, "Bioink Composition and Printing Parameters for 3D Modeling Neural Tissue," *Cells,* vol. 8, no. 8, Aug 5 2019.
[30] D. Joung *et al.*, "3D Printed Stem-Cell Derived Neural Progenitors Generate Spinal Cord Scaffolds," *Adv Funct Mater,* vol. 28, no. 39, Sep 26 2018.
[31] M. Restan Perez, R. Sharma, N. Z. Masri, and S. M. Willerth, "3D Bioprinting Mesenchymal Stem Cell-Derived Neural Tissues Using a Fibrin-Based Bioink," *Biomolecules,* vol. 11, no. 8, Aug 21 2021.

[32] X. Zhou *et al.*, "Three-Dimensional-Bioprinted Dopamine-Based Matrix for Promoting Neural Regeneration," *ACS Appl Mater Interfaces,* vol. 10, no. 10, pp. 8993-9001, Mar 14 2018.
[33] M. M. Adil *et al.*, "Efficient generation of hPSC-derived midbrain dopaminergic neurons in a fully defined, scalable, 3D biomaterial platform," *Sci Rep,* vol. 7, p. 40573, Jan 16 2017.
[34] M. A. Cenci and A. R. Crossman, "Animal models of l-dopa-induced dyskinesia in Parkinson's disease," *Mov Disord,* vol. 33, no. 6, pp. 889-899, Jul 2018.
[35] P. S. Gungor-Ozkerim, I. Inci, Y. S. Zhang, A. Khademhosseini, and M. R. Dokmeci, "Bioinks for 3D bioprinting: an overview," *Biomater Sci,* vol. 6, no. 5, pp. 915-946, May 1 2018.
[36] Z. Zheng *et al.*, "3D Bioprinting of Self-Standing Silk-Based Bioink," *Adv Healthc Mater,* vol. 7, no. 6, p. e1701026, Mar 2018.
[37] S. Avazzadeh, J. M. Baena, C. Keighron, Y. Feller-Sanchez, and L. R. Quinlan, "Modelling Parkinson's Disease: iPSCs towards Better Understanding of Human Pathology," *Brain Sci,* vol. 11, no. 3, Mar 14 2021.
[38] S. Bolognin *et al.*, "3D Cultures of Parkinson's Disease-Specific Dopaminergic Neurons for High Content Phenotyping and Drug Testing," *Adv Sci (Weinh),* vol. 6, no. 1, p. 1800927, Jan 9 2019.
[39] S. Shimohama, H. Sawada, Y. Kitamura, and T. Taniguchi, "Disease model: Parkinson's disease," *Trends in Molecular Medicine,* vol. 9, no. 8, pp. 360-365, 2003.
[40] X. C. Zhen and H. Y. Chu, "Emerging novel approaches to drug research and diagnosis of Parkinson's disease," *Acta Pharmacol Sin,* vol. 41, no. 4, pp. 439-441, Apr 2020.
[41] T. Kim, J. J. Song, L. Puspita, P. Valiulahi, J. W. Shim, and S. H. Lee, "In vitro generation of mature midbrain-type dopamine neurons by adjusting exogenous Nurr1 and Foxa2 expressions to their physiologic patterns," *Exp Mol Med,* vol. 49, no. 3, p. e300, Mar 10 2017.
[42] S. V. Murphy and A. Atala, "3D bioprinting of tissues and organs," *Nat Biotechnol,* vol. 32, no. 8, pp. 773-85, Aug 2014.
[43] A. Poon *et al.*, "Modeling neurodegenerative diseases with patient-derived induced pluripotent cells: Possibilities and challenges," *N Biotechnol,* vol. 39, no. Pt B, pp. 190-198, Oct 25 2017.
[44] L. Smirnova *et al.*, "A LUHMES 3D dopaminergic neuronal model for neurotoxicity testing allowing long-term exposure and cellular resilience analysis," *Arch Toxicol,* vol. 90, no. 11, pp. 2725-2743, Nov 2016.
[45] S. H. Shahmoradian *et al.*, "Lewy pathology in Parkinson's disease consists of crowded organelles and lipid membranes," *Nat Neurosci,* vol. 22, no. 7, pp. 1099-1109, Jul 2019.
[46] J. M. Baena-Montes, S. Avazzadeh, and L. R. Quinlan, "alpha-synuclein pathogenesis in hiPSC models of Parkinson's disease," *Neuronal Signal,* vol. 5, no. 2, p. NS20210021, Jun 2021.
[47] L. Borgs *et al.*, "Dopaminergic neurons differentiating from LRRK2 G2019S induced pluripotent stem cells show early neuritic branching defects," *Sci Rep,* vol. 6, p. 33377, Sep 19 2016.

[48] I. Gonzalez-Casacuberta, D. L. Juarez-Flores, C. Moren, and G. Garrabou, "Bioenergetics and Autophagic Imbalance in Patients-Derived Cell Models of Parkinson Disease Supports Systemic Dysfunction in Neurodegeneration," *Front Neurosci,* vol. 13, p. 894, 2019.

[49] S. V. Precious *et al.*, "Dopaminergic Progenitors Derived From Epiblast Stem Cells Function Similarly to Primary VM-Derived Progenitors When Transplanted Into a Parkinson's Disease Model," *Front Neurosci,* vol. 14, p. 312, 2020.

[50] E. M. Hartfield *et al.*, "Physiological characterisation of human iPS-derived dopaminergic neurons," *PLoS One,* vol. 9, no. 2, p. e87388, 2014.

[51] F. Salaris and A. Rosa, "Construction of 3D in vitro models by bioprinting human pluripotent stem cells: Challenges and opportunities," *Brain Res,* vol. 1723, p. 146393, Nov 15 2019.

[52] M. Obinata, "The immortalized cell lines with differentiation potentials: their establishment and possible application," *Cancer Sci,* vol. 98, no. 3, pp. 275-83, Mar 2007.

[53] H. Xicoy, B. Wieringa, and G. J. Martens, "The SH-SY5Y cell line in Parkinson's disease research: a systematic review," *Mol Neurodegener,* vol. 12, no. 1, p. 10, Jan 24 2017.

[54] Y. C. Cheng *et al.*, "Generation of 2 induced pluripotent stem cell lines derived from patients with Parkinson's disease carrying LRRK2 G2385R variant," *Stem Cell Res,* vol. 28, pp. 1-5, Apr 2018.

[55] A. Cota-Coronado, J. C. Durnall, N. F. Diaz, L. H. Thompson, and N. E. Diaz-Martinez, "Unprecedented Potential for Neural Drug Discovery Based on Self-Organizing hiPSC Platforms," *Molecules,* vol. 25, no. 5, Mar 4 2020.

[56] E. Ferrari, A. Cardinale, B. Picconi, and F. Gardoni, "From cell lines to pluripotent stem cells for modelling Parkinson's Disease," *J Neurosci Methods,* vol. 340, p. 108741, Jul 1 2020.

[57] K. K. Bayram *et al.*, "Gene Expression of Mouse Hippocampal Stem Cells Grown in a Galactose-Derived Molecular Gel Compared to In Vivo and Neurospheres," *Processes,* vol. 9, no. 4, 2021.

[58] M. Hospodiuk, M. Dey, D. Sosnoski, and I. T. Ozbolat, "The bioink: A comprehensive review on bioprintable materials," *Biotechnol Adv,* vol. 35, no. 2, pp. 217-239, Mar - Apr 2017.

[59] E. O. Osidak, V. I. Kozhukhov, M. S. Osidak, and S. P. Domogatsky, "Collagen as Bioink for Bioprinting: A Comprehensive Review," *Int J Bioprint,* vol. 6, no. 3, p. 270, 2020.

[60] X. Hu *et al.*, "Modeling Parkinson's Disease Using Induced Pluripotent Stem Cells," *Stem Cells Int,* vol. 2020, p. 1061470, 2020.

[61] A. Elemoso, G. Shalunov, Y. M. Balakhovsky, A. Y. Ostrovskiy, and Y. D. Khesuani, "3D Bioprinting: The Roller Coaster Ride to Commercialization," *Int J Bioprint,* vol. 6, no. 3, p. 301, 2020.

[62] D. Warren, E. Tomaskovic-Crook, G. G. Wallace, and J. M. Crook, "Engineering in vitro human neural tissue analogs by 3D bioprinting and electrostimulation," *APL Bioeng,* vol. 5, no. 2, p. 020901, Jun 2021.

[63] Z. Zhao *et al.*, "Composite Hydrogels in Three-Dimensional in vitro Models," *Front Bioeng Biotechnol,* vol. 8, p. 611, 2020.

[64] L. Zhou *et al.*, "Lipid-Bilayer-Supported 3D Printing of Human Cerebral Cortex Cells Reveals Developmental Interactions," *Adv Mater,* vol. 32, no. 31, p. e2002183, Aug 2020.
[65] G. Jensen, C. Morrill, and Y. Huang, "3D tissue engineering, an emerging technique for pharmaceutical research," *Acta Pharm Sin B,* vol. 8, no. 5, pp. 756-766, Sep 2018.
[66] M. Thomas and S. M. Willerth, "3-D Bioprinting of Neural Tissue for Applications in Cell Therapy and Drug Screening," *Front Bioeng Biotechnol,* vol. 5, p. 69, 2017.
[67] L. De la Vega, K. Karmirian, and S. M. Willerth, "Engineering Neural Tissue from Human Pluripotent Stem Cells Using Novel Small Molecule Releasing Microspheres," *Advanced Biosystems,* vol. 2, no. 12, 2018.
[68] R. Gonzalez *et al.*, "Deriving dopaminergic neurons for clinical use. A practical approach," *Sci Rep,* vol. 3, p. 1463, 2013.
[69] M. Robinson *et al.*, "Optimizing Differentiation Protocols for Producing Dopaminergic Neurons from Human Induced Pluripotent Stem Cells for Tissue Engineering Applications," *Biomarker Insights,* vol. 10s1, 2015.
[70] A. Agbay, L. De La Vega, G. Nixon, and S. Willerth, "Guggulsterone-releasing microspheres direct the differentiation of human induced pluripotent stem cells into neural phenotypes," *Biomedical Materials,* vol. 13, no. 3, 2018.
[71] A. Agbay, L. De La Vega, G. Nixon, and S. Willerth, "Guggulsterone-releasing microspheres direct the differentiation of human induced pluripotent stem cells into neural phenotypes," *Biomed Mater,* vol. 13, no. 3, p. 034104, Feb 28 2018.
[72] S. J. Chinta and J. K. Andersen, "Dopaminergic neurons," *Int J Biochem Cell Biol,* vol. 37, no. 5, pp. 942-6, May 2005.
[73] N. Filipovic *et al.*, "Poly (epsilon-caprolactone) microspheres for prolonged release of selenium nanoparticles," *Mater Sci Eng C Mater Biol Appl,* vol. 96, pp. 776-789, Mar 2019.
[74] J. C. Gomez *et al.*, "Incorporation of Retinoic Acid Releasing Microspheres into Pluripotent Stem Cell Aggregates for Inducing Neuronal Differentiation," *Cellular and Molecular Bioengineering,* vol. 8, no. 3, pp. 307-319, 2015.
[75] W. Liu, M. A. Borrell, D. C. Venerus, W. F. Mieler, and J. J. Kang-Mieler, "Characterization of Biodegradable Microsphere-Hydrogel Ocular Drug Delivery System for Controlled and Extended Release of Ranibizumab," *Transl Vis Sci Technol,* vol. 8, no. 1, p. 12, Jan 2019.
[76] Y. J. Tan, X. Tan, W. Y. Yeong, and S. B. Tor, "Hybrid microscaffold-based 3D bioprinting of multi-cellular constructs with high compressive strength: A new biofabrication strategy," *Sci Rep,* vol. 6, p. 39140, Dec 14 2016.
[77] D. Chimene, K. K. Lennox, R. R. Kaunas, and A. K. Gaharwar, "Advanced Bioinks for 3D Printing: A Materials Science Perspective," *Ann Biomed Eng,* vol. 44, no. 6, pp. 2090-102, Jun 2016.
[78] B. A. G. de Melo, Y. A. Jodat, E. M. Cruz, J. C. Benincasa, S. R. Shin, and M. A. Porcionatto, "Strategies to use fibrinogen as bioink for 3D bioprinting fibrin-based soft and hard tissues," *Acta Biomater,* vol. 117, pp. 60-76, Nov 2020.
[79] J. Gopinathan and I. Noh, "Recent trends in bioinks for 3D printing," *Biomater Res,* vol. 22, p. 11, 2018.

[80] S. Heid and A. R. Boccaccini, "Advancing bioinks for 3D bioprinting using reactive fillers: A review," *Acta Biomater,* vol. 113, pp. 1-22, Sep 1 2020.
[81] "<Fibrin-based Bioinks New Tricks from an Old Dog.pdf>."
[82] T. Shen, Y. Dai, X. Li, S. Xu, Z. Gou, and C. Gao, "Regeneration of the Osteochondral Defect by a Wollastonite and Macroporous Fibrin Biphasic Scaffold," *ACS Biomater Sci Eng,* vol. 4, no. 6, pp. 1942-1953, Jun 11 2018.
[83] F. Hafezi *et al.*, "Bioprinting and Preliminary Testing of Highly Reproducible Novel Bioink for Potential Skin Regeneration," *Pharmaceutics,* vol. 12, no. 6, Jun 13 2020.
[84] N. S. Kajave, T. Schmitt, T. U. Nguyen, and V. Kishore, "Dual crosslinking strategy to generate mechanically viable cell-laden printable constructs using methacrylated collagen bioinks," *Mater Sci Eng C Mater Biol Appl,* vol. 107, p. 110290, Feb 2020.
[85] H. G. Sundararaghavan, G. A. Monteiro, B. L. Firestein, and D. I. Shreiber, "Neurite growth in 3D collagen gels with gradients of mechanical properties," *Biotechnol Bioeng,* vol. 102, no. 2, pp. 632-43, Feb 1 2009.
[86] D. Bociaga, M. Bartniak, J. Grabarczyk, and K. Przybyszewska, "Sodium Alginate/Gelatine Hydrogels for Direct Bioprinting-The Effect of Composition Selection and Applied Solvents on the Bioink Properties," *Materials (Basel),* vol. 12, no. 17, Aug 22 2019.
[87] F. E. Freeman and D. J. Kelly, "Tuning Alginate Bioink Stiffness and Composition for Controlled Growth Factor Delivery and to Spatially Direct MSC Fate within Bioprinted Tissues," *Sci Rep,* vol. 7, no. 1, p. 17042, Dec 6 2017.
[88] N. Mansouri, S. F. Al-Sarawi, J. Mazumdar, and D. Losic, "Advancing fabrication and properties of three-dimensional graphene–alginate scaffolds for application in neural tissue engineering," *RSC Advances,* vol. 9, no. 63, pp. 36838-36848, 2019.
[89] J. E. McBane, B. Vulesevic, D. T. Padavan, K. A. McEwan, G. S. Korbutt, and E. J. Suuronen, "Evaluation of a collagen-chitosan hydrogel for potential use as a pro-angiogenic site for islet transplantation," *PLoS One,* vol. 8, no. 10, p. e77538, 2013.
[90] N. Ashammakhi *et al.*, "Bioinks and bioprinting technologies to make heterogeneous and biomimetic tissue constructs," *Mater Today Bio,* vol. 1, p. 100008, Jan 2019.
[91] A. Parak, P. Pradeep, L. C. du Toit, P. Kumar, Y. E. Choonara, and V. Pillay, "Functionalizing bioinks for 3D bioprinting applications," *Drug Discov Today,* vol. 24, no. 1, pp. 198-205, Jan 2019.
[92] S. Budday, G. Sommer, G. A. Holzapfel, P. Steinmann, and E. Kuhl, "Viscoelastic parameter identification of human brain tissue," *J Mech Behav Biomed Mater,* vol. 74, pp. 463-476, Oct 2017.
[93] S. Cheng, E. C. Clarke, and L. E. Bilston, "Rheological properties of the tissues of the central nervous system: a review," *Med Eng Phys,* vol. 30, no. 10, pp. 1318-37, Dec 2008.
[94] S. Budday *et al.*, "Mechanical characterization of human brain tissue," *Acta Biomater,* vol. 48, pp. 319-340, Jan 15 2017.

[95] H. N. Kim and N. Choi, "Consideration of the Mechanical Properties of Hydrogels for Brain Tissue Engineering and Brain-on-a-chip," *BioChip Journal,* vol. 13, no. 1, pp. 8-19, 2019.
[96] D. B. MacManus, B. Pierrat, J. G. Murphy, and M. D. Gilchrist, "Dynamic mechanical properties of murine brain tissue using micro-indentation," *J Biomech,* vol. 48, no. 12, pp. 3213-8, Sep 18 2015.
[97] B. Rashid, M. Destrade, and M. D. Gilchrist, "Mechanical characterization of brain tissue in simple shear at dynamic strain rates," *J Mech Behav Biomed Mater,* vol. 28, pp. 71-85, Dec 2013.
[98] D. C. Stewart, A. Rubiano, K. Dyson, and C. S. Simmons, "Mechanical characterization of human brain tumors from patients and comparison to potential surgical phantoms," *PLoS One,* vol. 12, no. 6, p. e0177561, 2017.
[99] G. J. Her, H. C. Wu, M. H. Chen, M. Y. Chen, S. C. Chang, and T. W. Wang, "Control of three-dimensional substrate stiffness to manipulate mesenchymal stem cell fate toward neuronal or glial lineages," *Acta Biomater,* vol. 9, no. 2, pp. 5170-80, Feb 2013.
[100] J. Jang, T. G. Kim, B. S. Kim, S. W. Kim, S. M. Kwon, and D. W. Cho, "Tailoring mechanical properties of decellularized extracellular matrix bioink by vitamin B2-induced photo-crosslinking," *Acta Biomater,* vol. 33, pp. 88-95, Mar 2016.
[101] D. Lee, M. M. Rahman, Y. Zhou, and S. Ryu, "Three-Dimensional Confocal Microscopy Indentation Method for Hydrogel Elasticity Measurement," *Langmuir,* vol. 31, no. 35, pp. 9684-93, Sep 8 2015.
[102] S. Ali, I. B. Wall, C. Mason, A. E. Pelling, and F. S. Veraitch, "The effect of Young's modulus on the neuronal differentiation of mouse embryonic stem cells," *Acta Biomater,* vol. 25, pp. 253-67, Oct 2015.
[103] T. Hu *et al.*, "3D-printable supramolecular hydrogels with shear-thinning property: fabricating strength tunable bioink via dual crosslinking," *Bioact Mater,* vol. 5, no. 4, pp. 808-818, Dec 2020.
[104] N. D. Leipzig and M. S. Shoichet, "The effect of substrate stiffness on adult neural stem cell behavior," *Biomaterials,* vol. 30, no. 36, pp. 6867-78, Dec 2009.
[105] T. P. Prevost, G. Jin, M. A. de Moya, H. B. Alam, S. Suresh, and S. Socrate, "Dynamic mechanical response of brain tissue in indentation in vivo, in situ and in vitro," *Acta Biomater,* vol. 7, no. 12, pp. 4090-101, Dec 2011.
[106] A. Mazzocchi, S. Soker, and A. Skardal, "3D bioprinting for high-throughput screening: Drug screening, disease modeling, and precision medicine applications," *Appl Phys Rev,* vol. 6, no. 1, Mar 2019.
[107] L. Ouyang, R. Yao, Y. Zhao, and W. Sun, "Effect of bioink properties on printability and cell viability for 3D bioplotting of embryonic stem cells," *Biofabrication,* vol. 8, no. 3, p. 035020, Sep 16 2016.
[108] L. Yildirimer *et al.*, "Engineering three-dimensional microenvironments towards in vitro disease models of the central nervous system," *Biofabrication,* vol. 11, no. 3, p. 032003, Jun 6 2019.
[109] Z. Wu, X. Su, Y. Xu, B. Kong, W. Sun, and S. Mi, "Bioprinting three-dimensional cell-laden tissue constructs with controllable degradation," *Sci Rep,* vol. 6, p. 24474, Apr 19 2016.

[110] J. George, C. C. Hsu, L. T. B. Nguyen, H. Ye, and Z. Cui, "Neural tissue engineering with structured hydrogels in CNS models and therapies," *Biotechnol Adv,* vol. 42, p. 107370, Sep - Oct 2020.
[111] A. Panwar and L. P. Tan, "Current Status of Bioinks for Micro-Extrusion-Based 3D Bioprinting," *Molecules,* vol. 21, no. 6, May 25 2016.
[112] F. Gao, C. Ruan, and W. Liu, "High-strength hydrogel-based bioinks," *Materials Chemistry Frontiers,* vol. 3, no. 9, pp. 1736-1746, 2019.
[113] A. Tabet, S. Mommer, J. A. Vigil, C. Hallou, H. Bulstrode, and O. A. Scherman, "Mechanical Characterization of Human Brain Tissue and Soft Dynamic Gels Exhibiting Electromechanical Neuro-Mimicry," *Adv Healthc Mater,* vol. 8, no. 10, p. e1900068, May 2019.
[114] R. J. M. Riemens, D. L. A. van den Hove, M. Esteller, and R. Delgado-Morales, "Directing neuronal cell fate in vitro: Achievements and challenges," *Prog Neurobiol,* vol. 168, pp. 42-68, Sep 2018.
[115] Y. Zhang, W. Li, T. Laurent, and S. Ding, "Small molecules, big roles -- the chemical manipulation of stem cell fate and somatic cell reprogramming," *J Cell Sci,* vol. 125, no. Pt 23, pp. 5609-20, Dec 1 2012.
[116] E. A. Kiyotake, A. W. Douglas, E. E. Thomas, S. L. Nimmo, and M. S. Detamore, "Development and quantitative characterization of the precursor rheology of hyaluronic acid hydrogels for bioprinting," *Acta Biomater,* vol. 95, pp. 176-187, Sep 1 2019.
[117] Y. B. Lee *et al.*, "Bio-printing of collagen and VEGF-releasing fibrin gel scaffolds for neural stem cell culture," *Exp Neurol,* vol. 223, no. 2, pp. 645-52, Jun 2010.
[118] F. Salaris *et al.*, "3D Bioprinted Human Cortical Neural Constructs Derived from Induced Pluripotent Stem Cells," *J Clin Med,* vol. 8, no. 10, Oct 2 2019.
[119] W. Niu, T. Zang, L. L. Wang, Y. Zou, and C. L. Zhang, "Phenotypic Reprogramming of Striatal Neurons into Dopaminergic Neuron-like Cells in the Adult Mouse Brain," *Stem Cell Reports,* vol. 11, no. 5, pp. 1156-1170, Nov 13 2018.
[120] A. Sebastian-Serrano, A. Sandonis, M. Cardozo, F. M. Rodriguez-Tornos, P. Bovolenta, and M. Nieto, "Palphax6 expression in postmitotic neurons mediates the growth of axons in response to SFRP1," *PLoS One,* vol. 7, no. 2, p. e31590, 2012.
[121] C. Yu, W. Zhu, B. Sun, D. Mei, M. Gou, and S. Chen, "Modulating physical, chemical, and biological properties in 3D printing for tissue engineering applications," *Appl Phys Rev,* vol. 5, no. 4, Dec 2018.
[122] M. Chopin-Doroteo, E. A. Mandujano-Tinoco, and E. Krotzsch, "Tailoring of the rheological properties of bioinks to improve bioprinting and bioassembly for tissue replacement," *Biochim Biophys Acta Gen Subj,* vol. 1865, no. 2, p. 129782, Feb 2021.
[123] M. E. Cooke and D. H. Rosenzweig, "The rheology of direct and suspended extrusion bioprinting," *APL Bioeng,* vol. 5, no. 1, p. 011502, Mar 2021.
[124] N. Diamantides *et al.*, "Correlating rheological properties and printability of collagen bioinks: the effects of riboflavin photocrosslinking and pH," *Biofabrication,* vol. 9, no. 3, p. 034102, Jul 5 2017.

[125] N. Paxton, W. Smolan, T. Bock, F. Melchels, J. Groll, and T. Jungst, "Proposal to assess printability of bioinks for extrusion-based bioprinting and evaluation of rheological properties governing bioprintability," *Biofabrication,* vol. 9, no. 4, p. 044107, Nov 14 2017.

[126] J. Lee, S. J. Oh, S. H. An, W. D. Kim, and S. H. Kim, "Machine learning-based design strategy for 3D printable bioink: elastic modulus and yield stress determine printability," *Biofabrication,* vol. 12, no. 3, p. 035018, May 28 2020.

[127] E. M. Ahmed, "Hydrogel: Preparation, characterization, and applications: A review," *J Adv Res,* vol. 6, no. 2, pp. 105-21, Mar 2015.

[128] S. Moeinzadeh and E. Jabbari, "Gelation characteristics, physico-mechanical properties and degradation kinetics of micellar hydrogels," *Eur Polym J,* vol. 72, pp. 566-576, Nov 1 2015.

[129] C. Kayal, E. Moeendarbary, R. J. Shipley, and J. B. Phillips, "Mechanical Response of Neural Cells to Physiologically Relevant Stiffness Gradients," *Adv Healthc Mater,* vol. 9, no. 8, p. e1901036, Apr 2020.

[130] S. Chatelin, A. Constantinesco, and R. Willinger, "Fifty years of brain tissue mechanical testing: from in vitro to in vivo investigations," *Biorheology,* vol. 47, no. 5-6, pp. 255-76, 2010.

[131] S. J. Lee, M. A. King, J. Sun, H. K. Xie, G. Subhash, and M. Sarntinoranont, "Measurement of viscoelastic properties in multiple anatomical regions of acute rat brain tissue slices," *J Mech Behav Biomed Mater,* vol. 29, pp. 213-24, Jan 2014.

[132] J. A. van Dommelen, T. P. van der Sande, M. Hrapko, and G. W. Peters, "Mechanical properties of brain tissue by indentation: interregional variation," *J Mech Behav Biomed Mater,* vol. 3, no. 2, pp. 158-66, Feb 2010.

[133] R. Long, M. S. Hall, M. Wu, and C. Y. Hui, "Effects of gel thickness on microscopic indentation measurements of gel modulus," *Biophys J,* vol. 101, no. 3, pp. 643-50, Aug 3 2011.

[134] A. J. Engler, S. Sen, H. L. Sweeney, and D. E. Discher, "Matrix elasticity directs stem cell lineage specification," *Cell,* vol. 126, no. 4, pp. 677-89, Aug 25 2006.

[135] K. Saha *et al.*, "Substrate modulus directs neural stem cell behavior," *Biophys J,* vol. 95, no. 9, pp. 4426-38, Nov 1 2008.

[136] N. Diamantides, C. Dugopolski, E. Blahut, S. Kennedy, and L. J. Bonassar, "High density cell seeding affects the rheology and printability of collagen bioinks," *Biofabrication,* vol. 11, no. 4, p. 045016, Aug 22 2019.

[137] Y. Zhao, Y. Li, S. Mao, W. Sun, and R. Yao, "The influence of printing parameters on cell survival rate and printability in microextrusion-based 3D cell printing technology," *Biofabrication,* vol. 7, no. 4, p. 045002, Nov 2 2015.

[138] Z. Li, C. Ji, D. Li, R. Luo, G. Wang, and J. Jiang, "A comprehensive study on the mechanical properties of different regions of 8-week-old pediatric porcine brain under tension, shear, and compression at various strain rates," *J Biomech,* vol. 98, p. 109380, Jan 2 2020.

[139] S. Zhang *et al.*, "Fabrication of Microspheres from High-Viscosity Bioink Using a Novel Microfluidic-Based 3D Bioprinting Nozzle," *Micromachines (Basel),* vol. 11, no. 7, Jul 14 2020.

[140] M. Rizwan, S. W. Chan, P. A. Comeau, T. L. Willett, and E. K. F. Yim, "Effect of sterilization treatment on mechanical properties, biodegradation, bioactivity and printability of GelMA hydrogels," *Biomed Mater,* vol. 15, no. 6, p. 065017, Oct 3 2020.

[141] Q. Mao *et al.*, "Fabrication of liver microtissue with liver decellularized extracellular matrix (dECM) bioink by digital light processing (DLP) bioprinting," *Mater Sci Eng C Mater Biol Appl,* vol. 109, p. 110625, Apr 2020.

[142] L. Wei *et al.*, "An approach for mechanical property optimization of cell-laden alginate-gelatin composite bioink with bioactive glass nanoparticles," *J Mater Sci Mater Med,* vol. 31, no. 11, p. 103, Nov 2 2020.

[143] Z. Li *et al.*, "Tuning Alginate-Gelatin Bioink Properties by Varying Solvent and Their Impact on Stem Cell Behavior," *Sci Rep,* vol. 8, no. 1, p. 8020, May 22 2018.

[144] I. Noh, N. Kim, H. N. Tran, J. Lee, and C. Lee, "3D printable hyaluronic acid-based hydrogel for its potential application as a bioink in tissue engineering," *Biomater Res,* vol. 23, p. 3, 2019.

[145] L. Y. Daikuara, Z. Yue, D. Skropeta, and G. G. Wallace, "In vitro characterisation of 3D printed platelet lysate-based bioink for potential application in skin tissue engineering," *Acta Biomater,* vol. 123, pp. 286-297, Mar 15 2021.

[146] B. S. Kim, S. Das, J. Jang, and D. W. Cho, "Decellularized Extracellular Matrix-based Bioinks for Engineering Tissue- and Organ-specific Microenvironments," *Chem Rev,* vol. 120, no. 19, pp. 10608-10661, Oct 14 2020.

[147] C. W. Peak, K. A. Singh, M. a. Adlouni, J. Chen, and A. K. Gaharwar, "Printing Therapeutic Proteins in 3D using Nanoengineered Bioink to Control and Direct Cell Migration," *Advanced Healthcare Materials,* vol. 8, no. 11, 2019.

[148] A. H. Karoyo and L. D. Wilson, "Physicochemical Properties and the Gelation Process of Supramolecular Hydrogels: A Review," *Gels,* vol. 3, no. 1, Jan 1 2017.

[149] C. Yan and D. J. Pochan, "Rheological properties of peptide-based hydrogels for biomedical and other applications," *Chem Soc Rev,* vol. 39, no. 9, pp. 3528-40, Sep 2010.

[150] "<(692c) Engineering a Highly Elastic Protein-Based Bioink for Printing Complex Soft Tissues | AIChE.pdf>."

[151] M. L. Previtera, C. G. Langhammer, and B. L. Firestein, "Effects of substrate stiffness and cell density on primary hippocampal cultures," *J Biosci Bioeng,* vol. 110, no. 4, pp. 459-70, Oct 2010.

[152] K. P. Valente, S. S. Thind, M. Akbari, A. Suleman, and A. G. Brolo, "Collagen Type I-Gelatin Methacryloyl Composites: Mimicking the Tumor Microenvironment," *ACS Biomater Sci Eng,* vol. 5, no. 6, pp. 2887-2898, Jun 10 2019.

[153] W. Gross and H. Kress, "Simultaneous measurement of the Young's modulus and the Poisson ratio of thin elastic layers," *Soft Matter,* vol. 13, no. 5, pp. 1048-1055, Feb 7 2017.

[154] M. Galluzzi, C. S. Biswas, Y. Wu, Q. Wang, B. Du, and F. J. Stadler, "Space-resolved quantitative mechanical measurements of soft and supersoft materials by atomic force microscopy," *NPG Asia Materials,* vol. 8, no. 11, pp. e327-e327, 2016.

[155] A. L. Rutz *et al.*, "Employing PEG crosslinkers to optimize cell viability in gel phase bioinks and tailor post printing mechanical properties," *Acta Biomater,* vol. 99, pp. 121-132, Nov 2019.
[156] E. A. Lopez-Guerra and S. D. Solares, "On the frequency dependence of viscoelastic material characterization with intermittent-contact dynamic atomic force microscopy: avoiding mischaracterization across large frequency ranges," *Beilstein J Nanotechnol,* vol. 11, pp. 1409-1418, 2020.
[157] M. L. Previtera, M. Hui, D. Verma, A. J. Shahin, R. Schloss, and N. A. Langrana, "The effects of substrate elastic modulus on neural precursor cell behavior," *Ann Biomed Eng,* vol. 41, no. 6, pp. 1193-207, Jun 2013.
[158] Y. Shanjani, C. C. Pan, L. Elomaa, and Y. Yang, "A novel bioprinting method and system for forming hybrid tissue engineering constructs," *Biofabrication,* vol. 7, no. 4, p. 045008, Dec 18 2015.
[159] "<ACS-5001 Product Sheet - Neural Progenitor Cells Derived from ATCC-DYS0530 Parkinson's Disease.pdf>."
[160] "<pnas.0506020102.pdf>."
[161] U. A. Aregueta-Robles, P. J. Martens, L. A. Poole-Warren, and R. A. Green, "Tissue engineered hydrogels supporting 3D neural networks," *Acta Biomater,* vol. 95, pp. 269-284, Sep 1 2019.

Appendix

Supplementary Table One: Primer Assays used for Quantitative Polymerase Chain Reaction Analysis

Assays Purchased from Qiagen	Information
TH	QT00067221 QuantiTect Primer Assay
PAX6	QT00071169 QuantiTect Primer Assay
NR4A2 (NURR1)	QT00037716 QuantiTect Primer Assay
TUBB3	QT00083713 QuantiTect Primer Assay
LMX1B	QT00025746 QuantiTect Primer Assay
Primers purchased from Eurofins	**Sequences**
GAPDH	Forward Primer (5'-3') GGTCTCCTCTGACTTCAACA Reverse Primer (5'-3') AGCCAATTCGTTGTCATAC